

INFORMATION TO USERS

This manuscript has been reproduced from the microfilm master. UMI films the text directly from the original or copy submitted. Thus, some thesis and dissertation copies are in typewriter face, while others may be from any type of computer printer.

The quality of this reproduction is dependent upon the quality of the copy submitted. Broken or indistinct print, colored or poor quality illustrations and photographs, print bleedthrough, substandard margins, and improper alignment can adversely affect reproduction.

In the unlikely event that the author did not send UMI a complete manuscript and there are missing pages, these will be noted. Also, if unauthorized copyright material had to be removed, a note will indicate the deletion.

Oversize materials (e.g., maps, drawings, charts) are reproduced by sectioning the original, beginning at the upper left-hand corner and continuing from left to right in equal sections with small overlaps.

Photographs included in the original manuscript have been reproduced xerographically in this copy. Higher quality 6" x 9" black and white photographic prints are available for any photographs or illustrations appearing in this copy for an additional charge. Contact UMI directly to order.

ProQuest Information and Learning
300 North Zeeb Road, Ann Arbor, MI 48106-1346 USA
800-521-0600

UMI[®]

**THE INDEPTH MAGNETOTELLURIC EXPERIMENT
ON THE TIBETAN PLATEAU AND ITS IMPLICATIONS**

by

Shenghui Li

A dissertation submitted in partial fulfillment
of the requirements of the degree of

Doctor of Philosophy

University of Washington

2001

Program Authorized to Offer Degree: Geophysics Program

UMI Number: 3013994

UMI[®]

UMI Microform 3013994

Copyright 2001 by Bell & Howell Information and Learning Company.

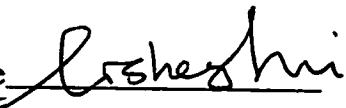
All rights reserved. This microform edition is protected against
unauthorized copying under Title 17, United States Code.

Bell & Howell Information and Learning Company
300 North Zeeb Road
P.O. Box 1346
Ann Arbor, MI 48106-1346

Doctoral Dissertation

In presenting this dissertation in partial fulfillment of the requirements for the Doctoral degree at the University of Washington, I agree that the Library shall make its copies freely available for inspection. I further agree that extensive copying of the dissertation is allowable only for scholarly purposes, consistent with "fair use" as prescribed in the U.S. Copyright Law. Requests for copying or reproduction of this dissertation may be referred to Bell and Howell Information and Learning, 300 North Zeeb Road, P.O. Box 1346, Ann Arbor, MI 48106-1346, to whom the author has granted "the right to reproduce and sell (a) copies of the manuscript in microform and/or (b) printed copies of the manuscript made from microform."

Signature



Date

June 8th, 2001

University of Washington

Graduate School

This is to certify that I have examined this copy of doctoral dissertation by

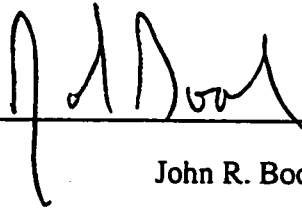
Shenghui Li

and have found that it is complete and satisfactory in all respects,

and that any and all revisions required by the final

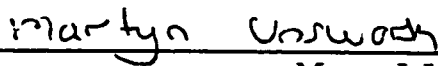
examining committee have been made.

Chair of Supervisory Committee:

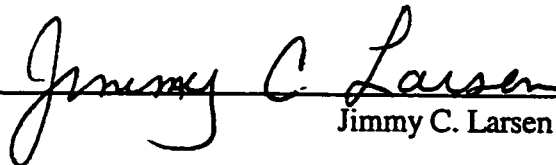


John R. Booker

Reading Committee:



Martyn J. Unsworth



Jimmy C. Larsen

Date:

June 8th, 2001

University of Washington

Abstract

**The INDEPTH Magnetotelluric Experiment
on the Tibetan Plateau and its Implications**

by Shenghui Li

Chairperson of the Supervisory Committee

Professor John R. Booker

Geophysics Program

This dissertation focus on the application of the magetotelluric method to tectonic studies on the Tibetan Plateau. The framework of this thesis composes three parts. The first part concentrates on magnetotelluirc data inversion in the presence of strong topographic or bathymetric distortions. A new approach is described to invert magnetotelluric data with strong topographic distortions and a few examples are shown to demonstrate the capability of this algorithm. The second part of this dissertation illustrates how magnetotelluirc data can be used to constrain the nature of the conductive middle crustal zone in southern Tibet. Seismic bright spots have been identified in the middle crust of southern Tibet, but the nature of these bright spots can not be resolved by seismic data alone. Using minimum conductance derived from magnetotelluric data, important thickness constraints are developed for the middle crutsal conductive zone. Combining these constraints with other geophysical data, the

seismic bright spots in southern Tibet may be best explained by a thin layer of aqueous fluid overlaying a thick partially molten system. Study of the electrical structures in central Tibet is presented in part three. High regional conductance is observed in central Tibet and the best candidate for the high conductance is partial melt. The dissertation ends with main conclusions from these studies.

TABLE OF CONTENTS

List of Figures	iv
Chapter 1: Introduction.....	1
1.1 The Tibetan Plateau.....	1
1.2 Previous works	3
1.3 Overview of this dissertation	5
Chapter 2: The Magnetotelluric method.....	11
2.1 The theory of MT	11
2.2 MT data collection and processing.....	13
2.3 Inversion of MT data.....	17
Chapter 3: Inversion of Magnetotelluric data in the presence of topography or bathymetry	24
3.1 Introduction	24
3.2 Calculating the MT responses of topography and bathymetry.....	25
3.3 Forward modeling examples	30
3.3.1 The TM responses of a simple topographic model	30
3.3.2 The MT responses of a bathymetric model	31
3.4 Inversion of MT data in the presence of topography and bathymetry	33

3.5 Inversion examples.....	35
3.5.1 Inversion of topographic data with noise	35
3.5.2 Coast model with a conductive structure	36
3.6 Conclusions	37
Chapter 4 Constraining the nature of the conductive middle crustal zone in souther Tibet.	45
4.1 Introduction	45
4.2 Regional geology, previous work.....	48
4.3 The 200-line magnetotelluric data.....	50
4.4 Constrained inversion of the 200 line MT data	52
4.5 Possible causes of high crustal conductivity in southern Tibet.....	58
4.5.1 Electrical conductivity of partial melt	59
4.5.2 Electrical conductivity of crustal saline fluids	61
4.5.3 Electrical conductivity of fluid bearing rocks	63
4.6 How much fluid is there in the middle crust of southern Tibet?.....	66
4.7 Three possible models for southern Tibet	69
4.7.1 Partial melt only	69
4.7.2 Pure melt layer.....	70
4.7.3 Poure melt over partial melt	71
4.7.4 model with only aquouse fluid	72
4.7.5 Water and partial melt	73

4.8 Conclusions and tectonic implications	74
Chapter 5 Resistivity structure of central Tibet and its implications.....	97
5.1 Introduction	97
5.2 Regional geology and previous work.....	99
5.3 The 500-line magnetotelluric data.....	101
5.4 Inversion of the 500 line MT data	104
5.5 Discussions	109
5.5.1 The resistivity structure of the northern Lhasa Terrane	109
5.5.2 The resistivity structure near the BNS.....	112
5.5.3 Partial melt in central Tibet?	113
5.6 Conclusions and implications.....	116
Chapter 6 Conclusions	130
Conclusions	130
Reference	132

LIST OF FIGURES

1.1	Topographic map of the Tibetan Plateau.....	8
1.2	Proposed models for the Tibetan Plateau	9
1.3	The INDEPTH MT experiment layout on the Tibetan Plateau	10
2.1	Magnetotelluric field site setup	19
2.2	Observed MT time series.....	20
2.3	MT data shown as apparent resistivity and phase	21
2.4	Electrical strikes on a regional map.....	22
2.5	A set of MT data can be fit by different models.....	23
3.1	Using FDA to calculate the auxiliary field on a flat earth.....	38
3.2	MT auxiliary field calculation on topography or bathymetry	39
3.3	PW2D and RRI TM responses over a ramp model	40
3.4	MT responses of a coast model.	41
3.5	Using the topography vector to define internal interface within the model	42
3.6	Inversion of a thin conductive layer under a ramp	43
3.7	Inversion of coast model with a conductive structure	44
4.1	Location map of Tibet 200 Line	78
4.2	Histograms of strike, shear and twist for single frequency data analysis.....	79
4.3	(a) 200 line MT data in Pseudosection form. (b) Model and MT responses.....	80
4.4	Observed MT data at site 220 and 240	81

4.5	I-D models and their MT responses.....	82
4.6	Conductivity models inverted from 200 line data.	83
4.7	Data misfit of constrained inversion.....	84
4.8	TE and TM responses of set of models with EW strike and observed data at site 220.....	85
4.9	TE and TM responses of set of models with EW strike and observed data at site 240.....	86
4.10	Static shift coefficients for 200 line data.	87
4.11	Model conductance for Tibet 200 line.....	88
4.12	Electrical conductivity of melts and saline fluid.	89
4.13	The Pressure-temperature-salinity critical curve.....	90
4.14	Conductivity of KCL solution as function of temperature and weight percentage.....	91
4.15	Bulk conductivity of fluid bearing rocks.....	92
4.16	Effect of solid rock conductivity on bulk conductivity	93
4.17	Three schematic models for southern Tibet	94
4.18	Thickness as function of porosity.....	95
4.19	Possible models for Damxung bright spots	96
5.1	Location map of INDEPTH MT surveys on the Tibetan Plateau.	118
5.2	Simplified tectonic map of central Tibet.	119
5.3	Pseudosections of INDEPTH 500 Line data.	120

5.4	Observed MT data and model reponses.	121
5.5	Geoelectrical strike of INDEPTH 500 Line data.	122
5.6	Reversed real induction vectors of INDEPTH 500 Line.....	123
5.7	(a) Resistivity model inverted from TM only data. (b). Resistivity model inverted from TE+TM data	124
5.8	Observed MT data and model reponses for model (a) in Figure 5.7.....	125
5.9	Observed MT data and model reponses for model (b) in Figure 5.7.	126
5.10	Constrained inversion models of INDEPTH 500 Line data.....	127
5.11	The model conductances of constrained inversions..	128
5.12	The inversion models of MT 200 and 500 Lines..	129

ACKNOWLEDGMENTS

Many thanks to my advisor Professor John R. Booker who provided me this opportunity and encouraged me through these years. Without his support for independent research and his encouragement, this work would not have been possible. Professor Martyn J. Unsworth has played a key role in the process of this study and this work could not be possible without his guidance and financial support.

Special thanks to Professor Stewart McCallum, Ken Creager, Jimmy Larsen and Sean Willett for serving as my supervise committee and their critical inputs have significantly improved this dissertation. I want to thank Ruth Ludwin for her help with my English writing and Lorien Gremore, Professor Steve Malone for their great computer support. I am lucky to have Paul Bedrosian as my colleague since he is always there to help, no matter what kind of problems I have.

Finally, I want thank my wife Baiping Wang and my family for their support and encouragement for this endeavor.

To my parents
and
whomever has encouraged me in my life

CHAPTER 1

INTRODUCTION

This dissertation focus on the application of the magnetotellurics (MT) method to the lithospheric study of the Tibetan Plateau. The MT experiment is an integral part of the International Deep Profiling of Tibet and the Himalaya (INDEPTH) project to promote the understanding of the geological structures and evolution of the Tibetan Plateau. The INDEPTH MT experiment is the largest MT project on the plateau and composes three summers of field campaigns in the harsh environment of Tibet. The main MT profile traverses the whole plateau and covers a distance of ~1000 km. Additionally, the INDEPTH MT experiment is the most densely deployed profile with most site spacings less than 10 km. With the most advanced instruments and processing techniques, the INDEPTH MT experiment provides detailed information about the electrical structures of the Tibetan lithosphere.

In the following sections, I first give a brief description of the Tibetan Plateau and then summarize previous works. To construct a roadmap for this dissertation, an overview of this work will be presented in the third section.

1.1 The Tibetan Plateau

The Tibetan Plateau is one of the most spectacular geographic features on the surface of the earth. The Himalayas extend for thousands of kilometers from west to

east and bound the southern margin of the Tibetan Plateau (Fig 1.1). The Tibetan Plateau is the largest and highest plateau on earth. With a mean elevation of 5 km above the sea level, this giant plateau covers an area about half the size of the conterminous United States. Because of its size and height, the Tibetan Plateau plays important roles in effecting the globe atmosphere circulation and may have significantly changed the global climate during its uplift.

Fascinated by this high plateau, many scientific expeditions have been made to Tibet. In the past century, our understanding of the plateau has been significantly improved. Now, it is well accepted that the Tibetan Plateau is a consequence of the collision between the India continent and Asia continent and this collision is still active today. A thick Tibetan crust has been identified by seismic studies on the plateau. Although the crust is thinner in the north than the south, a thickness of 60~70 km is generally accepted.

Despite what we have learned about the plateau, some of the first order questions are still under debate. For example, how did the Tibetan crust get thickened? And what mechanisms uplifted the plateau? Many tectonic models have been proposed to answer these questions. These models (Fig1.2) span the spectrum from underthrusting of the Indian plate [Argand, 1924] to distributed thickening of the Tibetan crust [Dewey and Burke, 1973]. Other suggested processes include fluid injection into the Tibetan lower crust [Zhao and Morgan, 1987], eastward extrusion of crust and mantle [Tapponnier *et al.*, 1982], and southward subduction of Asian lithospheric mantle [Willett and Beaumont, 1994].

1.2 Previous works

As early as 1896, Littledale made his first trip to Tibet and then Henning [1915] and Norin [1946] followed. Since then, many studies (mainly Chinese scientific expeditions) have been carried out on the plateau and these expeditions have made significant contributions to our knowledge of the plateau. In the early 1980s, joint international expeditions started to apply advance instruments and techniques to Tibet on much larger scales. In the following discussion, only three of the large-scale geophysical expeditions will be discussed since they are most related to this work.

The Sino-French scientific expedition in 1981 collected comprehensive geological and geophysical data in southern Tibet. The results of the geological studies were reported by Tapponnier et al. [1981]. Seismic, heat flow and MT results were reported by Hirn et al.[1984], Francheteau et al.[1984] and Pham et al. [1984]. In 1992, another Sino-French seismic expedition was made to Tibet and the main results were reported by Hirn et al. [1995].

A Sino-U.S project started in 1991 and extended to 1992. Using teleseismic data, this study concentrated on the velocity structure variations on the plateau. The results of this project were reported by McNamara et al. [1995,1997] and Owens and Zandt [1997].

These projects sample different areas of the plateau with some overlap and provide an invaluable opportunity to compare these results. Although there are differences, similar large-scale lithosphere structures have been identified. In southern Tibet, seismic data and deep earthquakes indicated a thick (~80 km) crust and a cold

mantle lid, while a thinner (~60 km) crust and warmer (> 800 °C) mantle has been suggested in northern Tibet.

Most recently, INDEPTH (International Deep Profiling of Tibet and the Himalayas) was initiated to substantiate previous studies and provide more detailed data for better constraining the lithosphere structures of the Tibetan Plateau. This group was composed of scientists from China, the United States, Canada, and Germany and applied advanced geological and geophysical approaches on a very large scale. So far, INDEPTH has completed three phases and more investigations are under way. INDEPTH I in 1992 included seismic and geological work, the main results of this phase was an image of the active zone by which India underthrusts southern Tibet [Zhao et al. [1993]. Phase II began in 1994 and extensive seismic and MT profiles were deployed. The main results of this phase were reported by Nelson et al. [1996]. Among these results, an abnormal middle crust has been identified by both seismic and MT data. The high seismic reflectivity and high electrical conductivity of this middle crustal layer strongly suggest the existence of fluids in the crust. Phase I and II of the Project INDEPTH concentrated on southern Tibet and most of the profiles were deployed along the ~N-S Yadong-Gulu rift. In 1998, INDEPTH phase III extended the profile ~400 km into the central Qiangtang Terrane in central Tibet. Along this profile, active and passive seismic (seismic reflection and broadband earthquake), magnetotelluric and surface geological data were collected. Results from these studies have been reported by Zhao et al. [2000], Huang et al. [2000], Hacker et al. [2000] and Wei et al. [2001].

1.3 Over view of this dissertation

Imaging the electrical structures of the Tibetan Plateau is the main focus of this dissertation. So far, 6 MT profiles have been deployed as a part of INDEPTH. Together, they extend ~1000 km and traverse the whole plateau. These MT profiles are shown in Figure 1.3 and some of the large-scale geological features are also shown. Not all of these MT data will be analyzed in this dissertation. The MT sites studied are shown as red reversed triangles (Figure 1.3). Three parts composed the frame of this work and they are based on three papers that are under preparation for submission.

Chapter 2 gives a brief introduction about MT theory and the process of data collection and processing. Since this work concentrates more on the application of MT to tectonic problems in Tibet, I try to provide only the very basic concepts so that readers can get a better understanding of this work. Also, in this section, I provide pointers to further discussion of MT for readers who want to learn more about this field.

Chapter 3 is devoted to the implementation of MT inversion in the presence of topography. In this chapter, a new version of the Rapid Relaxation Inversion (RRI) [Smith and Booker, 1989] is reported. This new version of RRI is capable of inverting MT data in the presence of strong topography and bathymetry. Synthetic examples are shown to illustrate the capabilities of this new program.

In Chapter 4, MT data collected on the Tibet 200 line are analyzed to address the nature of the middle crustal conductive layer in southern Tibet. In the southern

Lhasa Terrane, seismic reflection surveys have identified a number of seismic bright spots within the Yadong-Gulu rift system. Waveform analyses of these reflections suggest a fluid origin, but cannot distinguish unequivocally aqueous fluids from partial melt. Coincident magnetotelluric data imaged a major zone of low electrical resistivity with its top at the same depth as the bright spots (15-20 km). Magnetotelluric data are most sensitive to the depth to the top of a conductor and its total conductance (vertically integrated conductivity). Using constrained inversions, we show that the MT data require a crustal conductance in southern Tibet of ~6,000 Siemens. This high conductance is not restricted to grabens. To explain this unusually high regional conductance, we appeal to laboratory studies of the electrical conductivity of fluid-rock mixtures. If this conductance is due to partial melt, a range of melt fraction-thickness combinations could explain the 8000 S conductance. For example, with a melt fraction of 10% and melt conductivity of 10 S/m, the layer would need to be 15 km thick. Alternatively, saline, aqueous fluids could equally explain the conductance. Again, a wide range of porosity-thickness combinations will all give the same conductance. For example, with a porosity of 10%, and an aqueous fluid conductivity of 100 S/m, the layer would need to be 1.5 km thick. To distinguish between these two types of models, other petrological and geophysical information are needed. Seismic reflection data suggest that the top of the layer has an aqueous region, while passive source seismology has imaged a thick low velocity zone that is characteristic of a distributed, low melt fraction region. Thermal studies suggest that at the depths of the top of the conductor temperatures are too low for widespread

melting. However, at greater depth thermal conditions are high enough for melting to occur. In combination with the MT data, these data suggest that the low resistivity crust in southern Tibet can be best explained by a thin (~200 m) layer of saline fluids overlying a thick (>10 km) zone of partial melt.

In Chapter 5 of this work I present a detailed analysis of INDPETH MT data that span both the Lhasa and Qiangtang Terrane and address the question of whether partial melt exists beneath the Qiangtang Terrane. Using constrained inversion techniques, we estimate the minimum electrical conductance in the region of study. Although the conductance in the Qiangtang Terrane is lower than that of the Lhasa Terrane, the high lower crust temperature (>1000 °C) and high conductance (~4,000 S) strongly suggest the presence of partial melt. Finally, conclusions based on these studies are presented in Chapter 6.

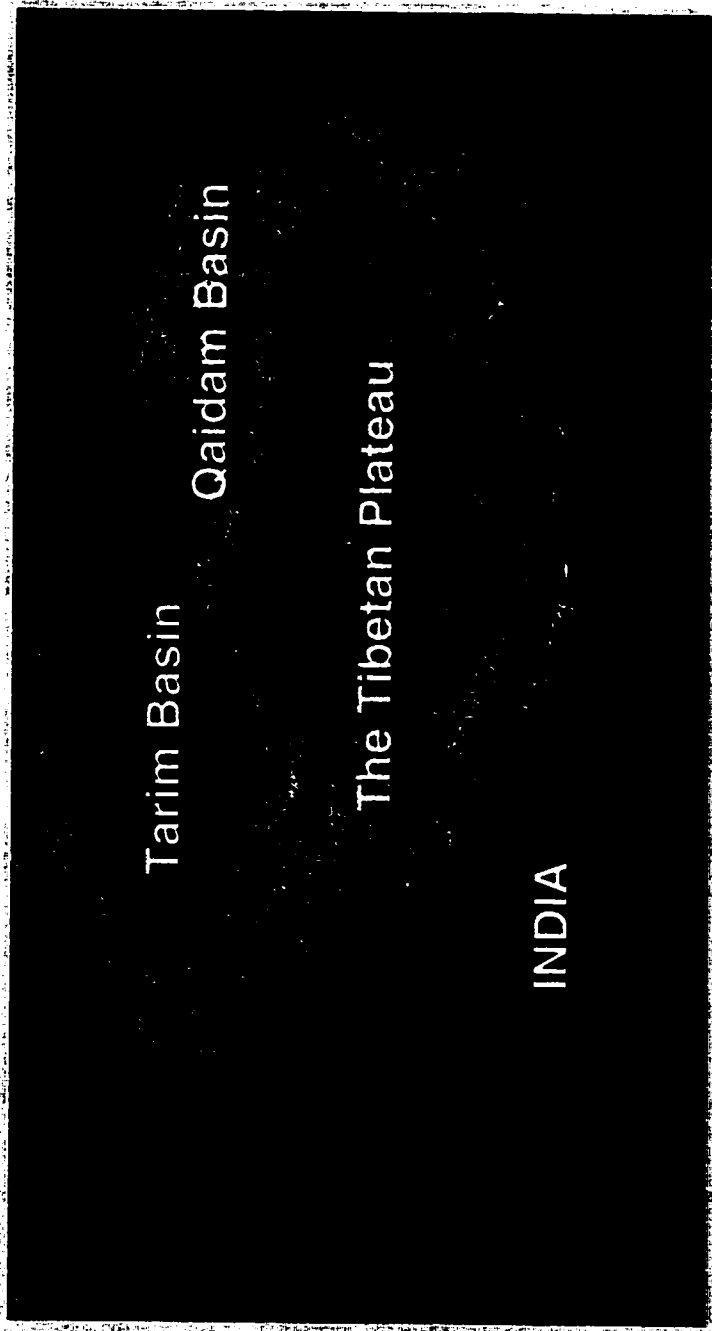


Figure 1.1 Topographic map of the Tibetan Plateau

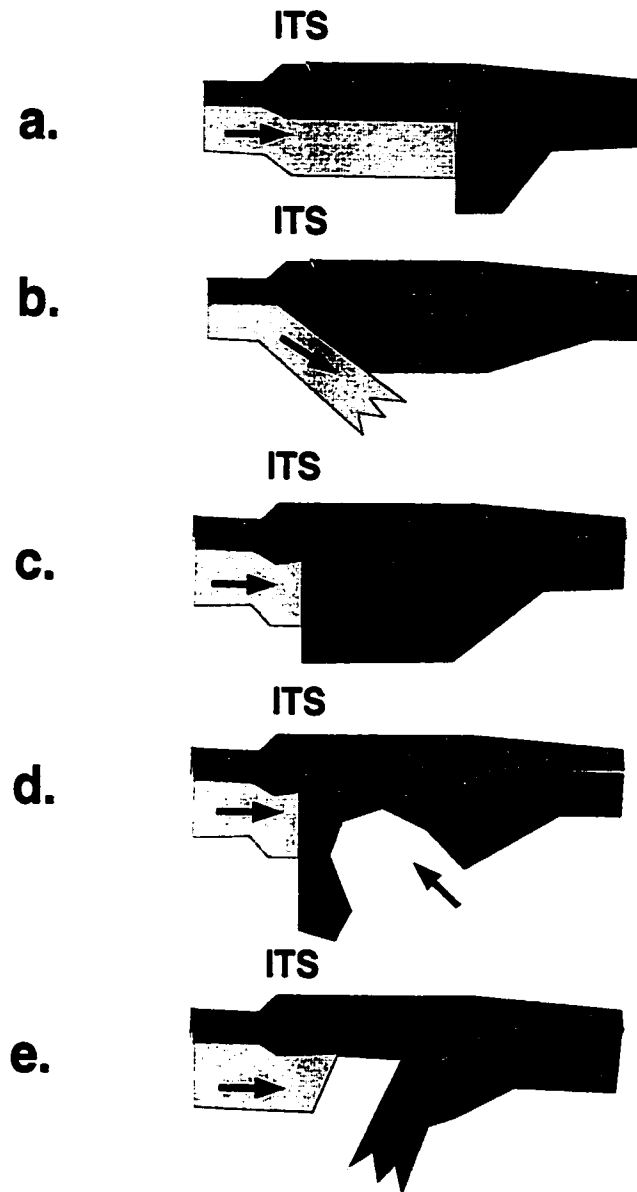


Figure 1.2 Proposed models for the Tibetan Plateau.

- a. Underthrusting model.
- b. The injection model.
- c. The distributed thickening model.
- d. The convective removal of lithospheric mantle model.
- e. The Asian subduction model.

(Modified from Willet and Beaumont, 1994)

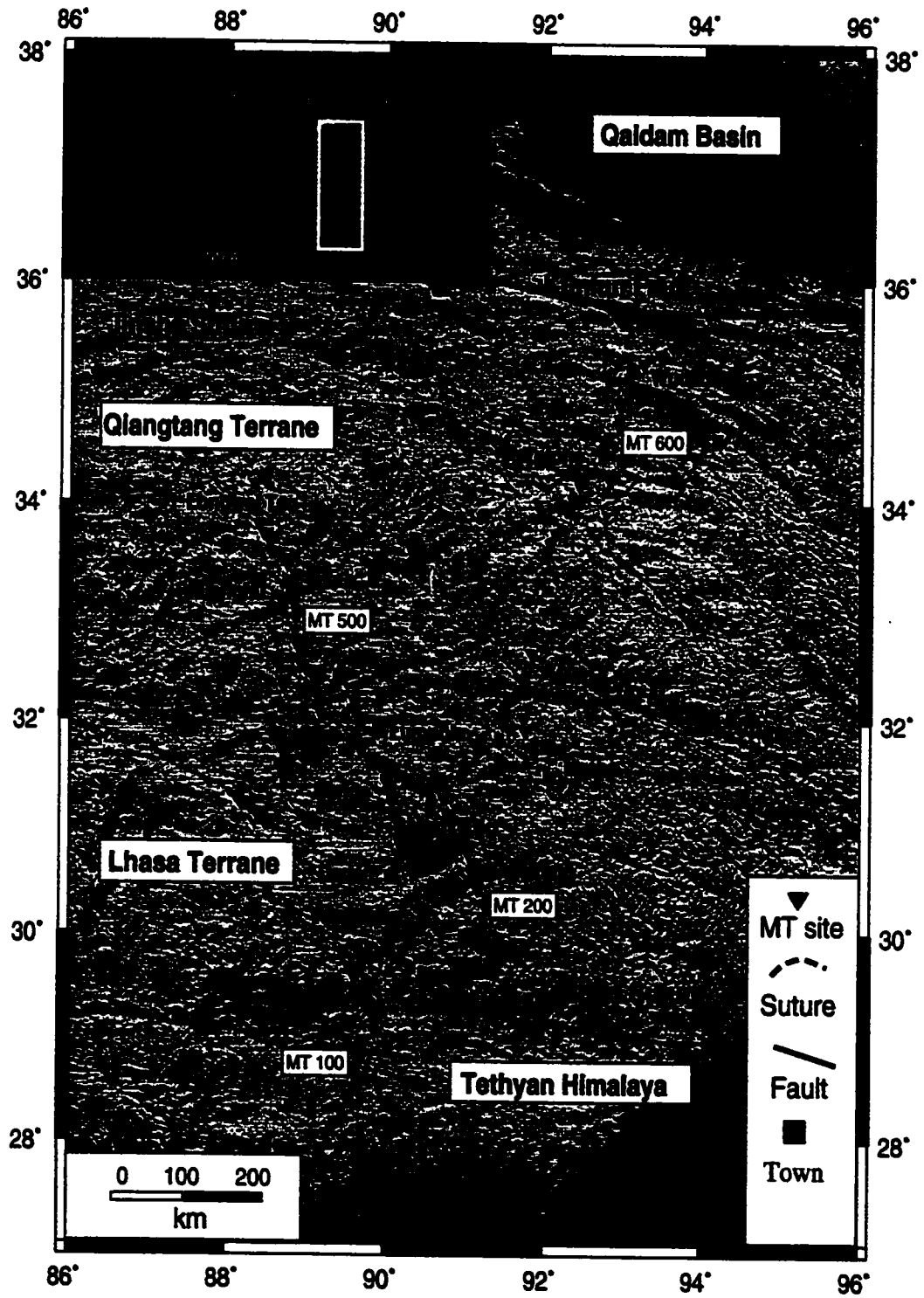


Figure 1.3 The INDEPTH MT experiment layout on the Tibetan Plateau

CHAPTER 2

THE MAGNETOTELLURIC (MT) METHOD

A brief introduction to the MT method will be presented in this chapter. The purpose of this introduction is to give readers the basic background needed for understanding this dissertation. A variety of books are available in this field. *The magnetotelluric sounding method* by A. A. Kaufman and G V. Keller and *The Electrical Methods in Geophysical Exploration* by M.S Zhdanov and G.V. Keller are two that provide a comprehensive view of the MT method and include reference to further work.

2.1 The theory of MT

The MT method was developed independently by Tikhonov [1950] and Cagniard [1953] and can be derived from the Maxwell's equations. When the EM frequency is sufficiently low and we can ignore ferromagnetism, the following equations are true:

$$\nabla \cdot \mathbf{E} = 0 \quad (2.1)$$

$$\nabla \cdot \mathbf{H} = 0 \quad (2.2)$$

$$\nabla \times \mathbf{E} = i\omega\mu_0\mathbf{E} \quad (2.3)$$

$$\nabla \times \mathbf{E} = \sigma \mathbf{E} \quad (2.4)$$

where \mathbf{E} and \mathbf{H} are the vector electric and magnetic fields, ω is the radian frequency, μ_0 is the permeability of free space σ is the conductivity. Throughout this dissertation I

will often use resistivity $\rho=1/\sigma$ instead of conductivity. In writing these equations we have used the isotropic form of Ohm's law:

$$j = \sigma E \quad (2.5)$$

Note that the current density j is always conserved because electrons can not be created or destroyed. This implies that the component of that j perpendicular to an interface is always conserved. If σ changes across an interface, the perpendicular component of E must change which means there will be charges on such an interface.

In the 2-D case, we can assume that σ , H and E are constant in the X direction and the above equations can be separated into two independent modes (or polarizations). When the currents are flowing along the X or strike direction, the equations for the Transverse Electric (TE) mode can be written as:

$$\frac{\partial^2 E_x}{\partial y^2} + \frac{\partial^2 E_x}{\partial z^2} = -i\omega\mu_0\sigma E_x \quad (2.6)$$

$$\frac{\partial E_x}{\partial z} = -i\omega\mu_0\sigma H_y \quad (2.7)$$

Similarly, when the currents are flowing in the Y direction, or perpendicular to the strike, we have the equations of the Transverse Magnetic (TM) mode:

$$\frac{\partial}{\partial y} \frac{1}{\sigma} \frac{\partial H_x}{\partial y} + \frac{\partial}{\partial z} \frac{1}{\sigma} \frac{\partial H_x}{\partial z} = -i\omega\mu_0 H_x \quad (2.8)$$

$$\frac{\partial H_x}{\partial z} = \sigma E_y \quad (2.9)$$

Now, applying proper boundary conditions, a uniform source and a numerical approximation such as a finite difference approximation, the above equations can be transformed to a sparse linear system. Solving these linear equations, the MT impedances of a model with known conductivity values can be computed. This is the process of forward modeling and more detail discussions of different algorithms are presented in next chapter.

2.2 MT data collection and processing

Although some elements are common to all MT fieldwork, detailed implementation of the site setup can be quite different depending on the purpose of the study and the instruments used. In this section, I describe briefly the MT data collection and processing used in the INDEPTH MT experiment.

Note that the equations (2.8) and (2.9) involve a relation between the horizontal electric and magnetic fields in perpendicular directions. Thus, MT involves measuring the relation between these orthogonal horizontal fields. In the frequency domain this relationship can be written as:

$$\begin{pmatrix} E_x \\ E_y \end{pmatrix} = \begin{pmatrix} Z_{xx} & Z_{yy} \\ Z_{yx} & Z_{yy} \end{pmatrix} \begin{pmatrix} H_x \\ H_y \end{pmatrix} \quad \text{or} \quad \underline{e} = \underline{Z} \underline{h} \quad (2.10)$$

where \underline{Z} is the MT impedance tensor. \underline{Z} has, in general, 4 complex elements which vary with frequency. In the 2-D case with X along strike, the diagonal elements are zero, Z_{xy} corresponds to the TE mode and Z_{yx} corresponds to the TM mode. Note that the diagonal elements are not zero if the coordinate system is not aligned with the strike or the Earth is 3-D.

MT uses naturally generated EM signals and no active power sources are needed. The long periods signals are generated in Earth's Magnetosphere, while short period (< 1 s) signals are from thunderstorms worldwide. To measure these signals, electrical field and magnetic field sensors are needed. Two types of MT system were used in Tibet. Long period MT data (20-20,000 s) were collected with 15 Long period Recording MT Systems (LRMT) built by Phoenix Geophysics following the design of the Geological Survey of Canada's LiMS systems. Broadband MT data (from 1000 Hz to 100 s) were collected using two MT-24 systems. Since both systems are band-limited, using both systems at the same site gives the widest bandwidth. A typical LRMT site setup is shown in Figure 2.1.

To get precise long period ($>1,000$ s) data, a LRMT site needs to be occupied for about two weeks while a MT-24 system only records for about 24 hours. The raw data recorded by LRMT and MT-24 are time series, a 5 minutes time series is shown in Figure 2.2. While these systems are quite reliable, many things can go wrong when collecting data in the field. So checking the quality of the time series is essential before moving the instrument to the next site. Although some time series problems can only be identified after processing, obvious problems, such as missing data or noisy channels, should be identified by any field crew. If necessary, the measurement needs to be repeated at the same site, since a poor site will not only waste time and money, it can also affect the following data interpretation. If possible, MT sites should be always remote referenced and these simultaneously multi-sites measurements will provide a means to conceal uncorrelated noises (Gamble et al., 1978). Typically, true MT signals

are coherent but noise are not, so data from a remote site can effectively reduce signal bias.

Various codes exist for time series processing and a comparative study of these techniques is reported by Jones et al. [1989]. Basically time series processing involves computing the transfer functions in the frequency domain between the electric and magnetic field components. As Jones' comparison makes clear, this needs to be done using robust techniques. Ordinary least squares performs very poorly because these are often many non-Gaussian outliers. These transfer functions are the MT impedance tensor elements. The magnitude of the impedance is commonly converted to apparent resistivity:

$$\rho_{ij} = \frac{1}{5f} |Z_{ij}|^2 \quad (2.11)$$

where ρ_{ij} has the unit $\Omega.m$, f is frequency (Hz) and Z_{ij} is in $mv/km/nT$. The apparent resistivity would be the true Earth resistivity if it was a half space. Figure 2.3 shows MT data collected at a site in southern Tibet. In this Figure, phase is the phase of the complex impedance. Only the off-diagonal elements are shown.

Geological targets are never truly 2-D, but 2-D may be a realistic regional approximation. A major advance in MT of the last decade has been development of techniques to determine regional electrical strike and estimate and remove the distorting effect of smaller scale, possibly 3-D structures [Bahr, 1988, Groom and Bailey, 1989, Groom and Bailey, 1991, Chave and Smith, 1994, Smith, 1995, McNeice and Jones, 2000]. All existing algorithms assume that the electrical field of the regional

2-D structure may be distorted by local 3-D (or 2-D with different strike) bodies. Groom et al.[1991] and Chave et al.[1994] also consider a further complication in which the local body may also distort the magnetic field. The data in Figure 2.3 show clear evidence of electric field distortion. At periods > 100 s the phase data for the two polarizations are identical within their errors. However, the two apparent resistivity curves are parallel, but offset by one order of magnitude. This offset is called static shift because it is due to accumulation of electric charges when electric currents flow in the direction of resistivity gradients and would exist even at zero frequency. Static shift should be zero for the TE mode, but for real data, there is almost always some variations of resistivity along strike. So it often has some static shift. The static (sometimes called Galvanic) response is part of the TM mode as one can see from the left side of equation (2.8). So, one can not tell from the data in Figure 2.3 whether the TM ρ offset is due to large scale 2-D structures or local 3-D structures. However, with the information in the diagonal elements and adjacent sites, it is possible to separate these possibilities.

The process of determining regional strike is called impedance tensor decomposition because in all cases it involves writing the measured impedance in the form of distortion and rotation matrices times the regional 2-D impedance. In this study, I used the implementation of Smith [1995] and McNeice and Jones [2000] and the results were very similar. The detailed analysis of strike will be presented in Chapter 4 and 5. A sample strike map is shown in Figure 2.4.

2.3 Inversion of MT data

While we can calculate the MT responses of a known conductivity model, more often we need to find a conductivity model based on a set of observed MT data. This is the process of inversion. Inverse theory itself is an independent subject. Again, because MT inversion is not the target of this study, I will only give a short explanation. The book, *Geophysical Inverse Theory* by Robert Parker covers broad applications in geophysics. Although many MT inversion algorithms exist, three 2-D algorithms are widely used in the MT community. Occam's inversion algorithm was developed by deGroot-Hedlin and Constable [1990] and has gained popular usage because it explicitly calculates 2-D sensitivity (Frechet Derivatives) and uses exact smoothing criteria. Smith and Booker [1991] developed a much faster inversion algorithm called the Rapid Relaxation Inversion (RRI) which is also widely used due to its speed and efficiency but which uses sensitivity and smoothing criteria that only approach the fully 2-D forms at convergence. Another MT inversion algorithm (Non-linear Conjugate Gradient, NLCG), described by Rodi and Mackie [2001], is closer to RRI in speed but closer to Occam in its use of 2-D sensitivities and smoothing criteria

As with most inversions, MT inversion has a non-uniqueness problem. Given a set of MT data, many models can be found that give an adequate fit to the observed data. It is therefore necessary to add a side condition such as minimum model roughness to the inversion. Such side conditions, if carefully chosen, can be very helpful in interpreting the resulting model. However, it should still be recognized that the model

is just one of many possibilities. To illustrate that a given set of MT data can be fit by multiple conductivity models, an example is shown in Figure 2.5.

Sensitivity analysis in which specific model elements are perturbed is usually very helpful in validating the conductivity structures in a MT model. Inverting the same data using different inversion algorithms can also help to test if some features of the model are required by different inversions. In this study, I used both the RRI and NLCG algorithms because of their numerical efficiency. Both allow any part of the model to be fixed during inversion steps and can be used to constrain the minimum model conductance required by the data. Inversion is more a model space exploration than a simple mechanical operation. An inversion process usually involves tedious, lengthy work to extract features that are common to all the possible models. Known features of the target from additional geophysical or geological considerations can be very useful in constraining the conductivity structures. A good example can be found in Nong [1994]. To illustrate

While the MT model generated from an inversion algorithm is non-unique, the vertically integrated conductivity or model conductance is usually a stable feature. Due to this fact, the model conductance has been heavily used in this dissertation and has provided important constraints on some real problems in Tibet. Many examples will be presented in Chapter 4 and 5 to demonstrate that the model conductance can be used to address tectonic problems on the plateau.

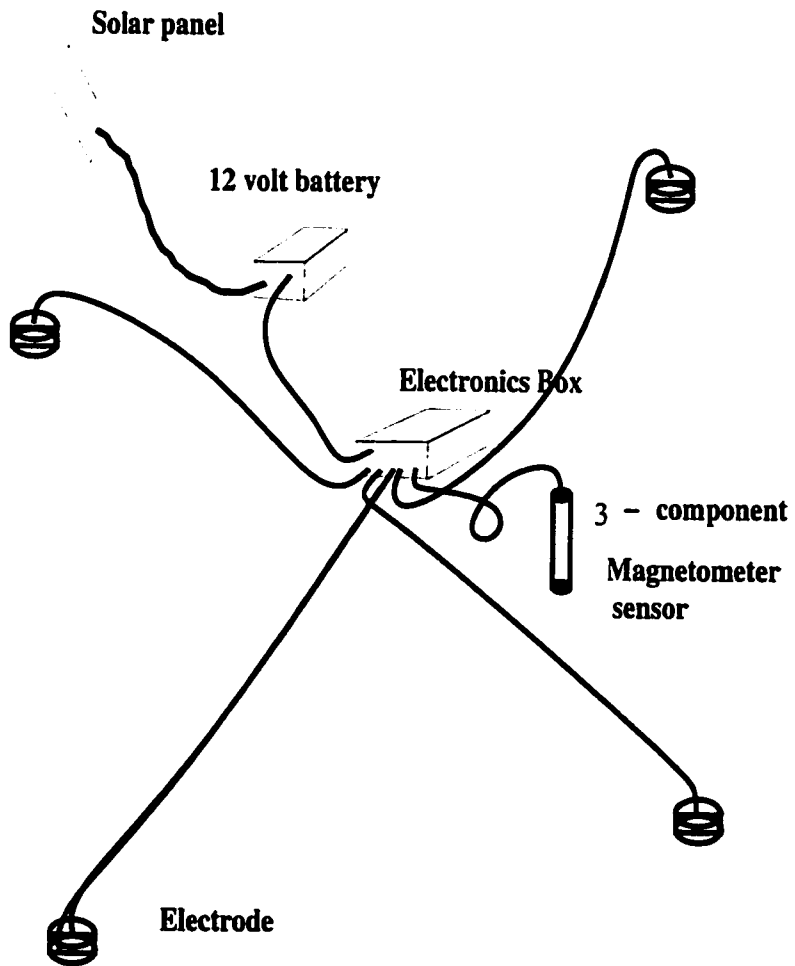


Figure 2.1 Magnetotelluric Site Setup

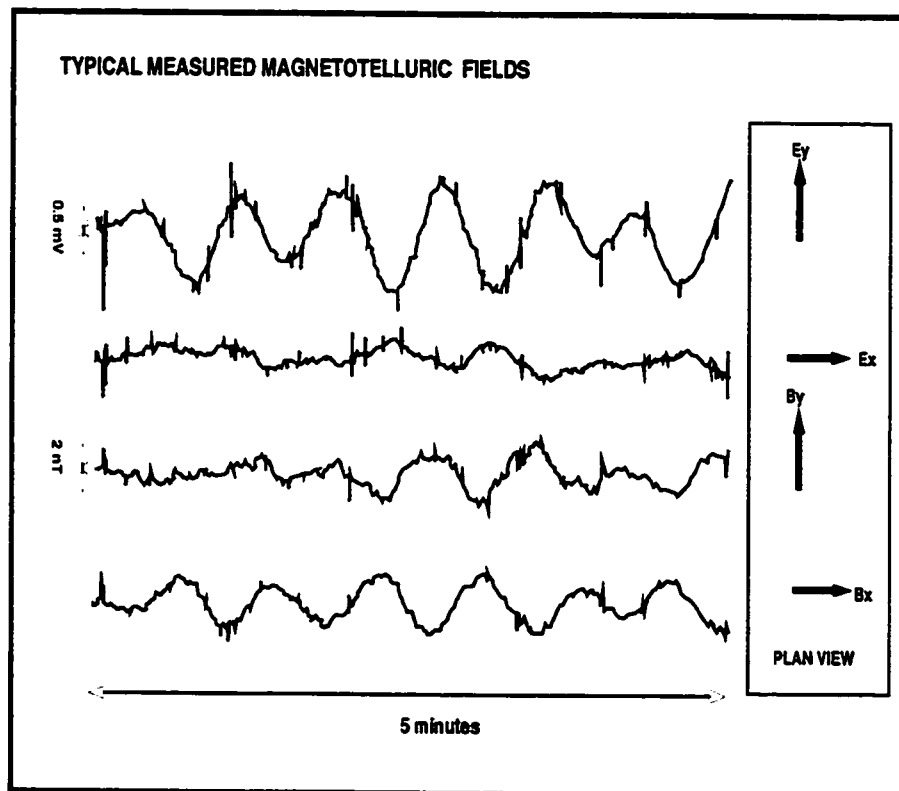


Figure 2.2 Observed MT time series

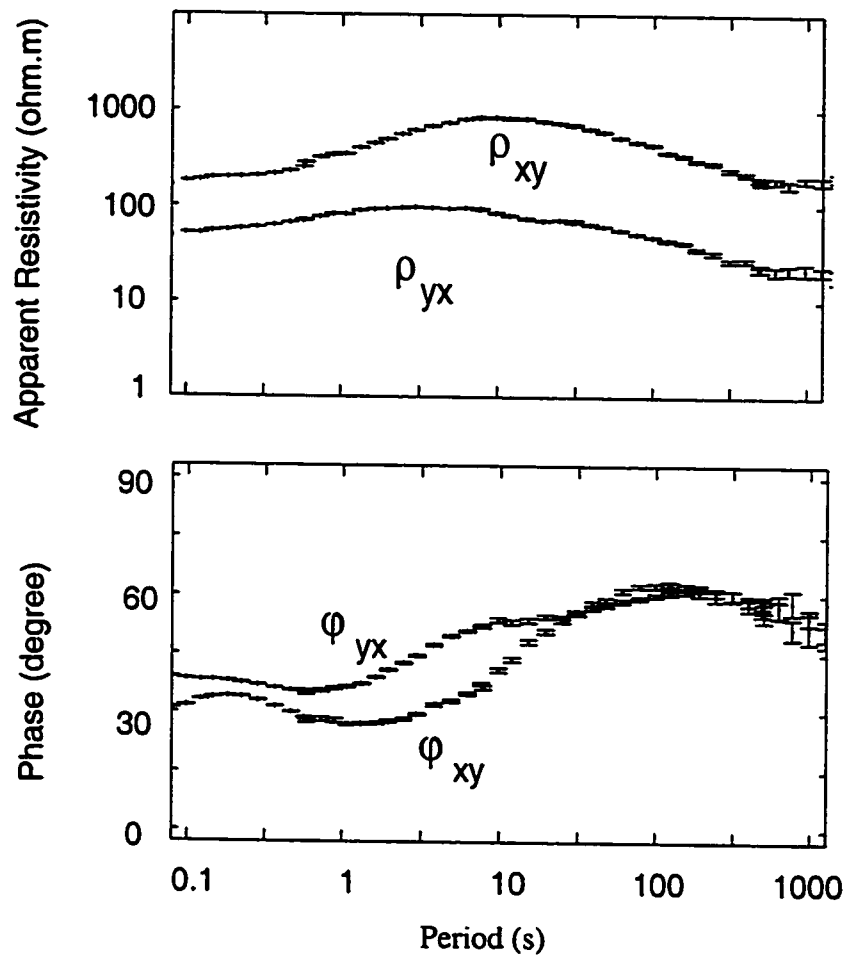


Figure 2.3 Apparent resistivity and phase data on a MT site in central Tibet. x -- North y -- East.

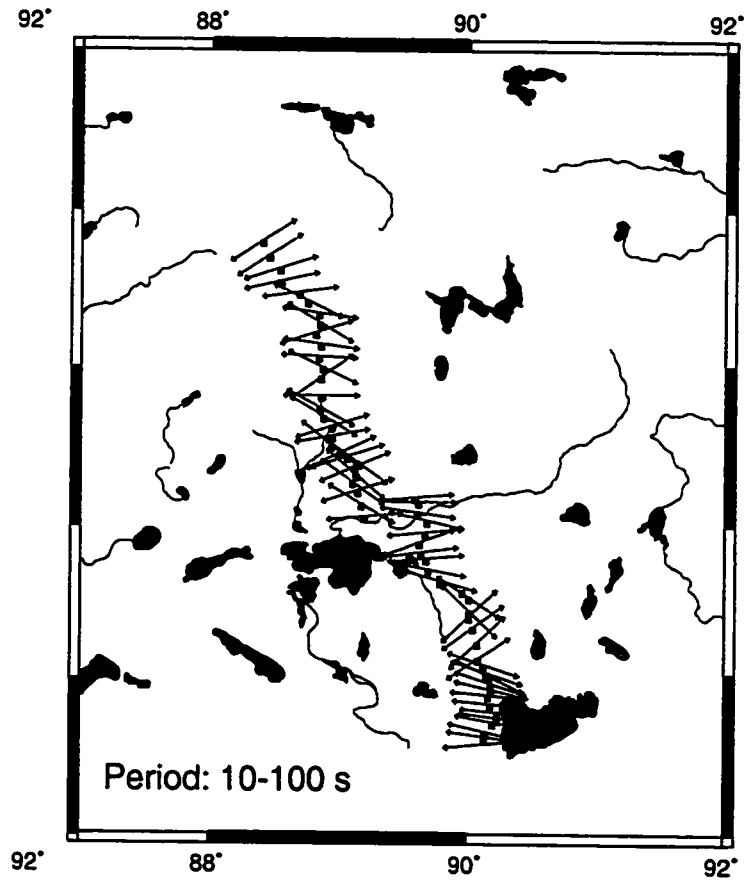


Figure 2.4 Electrical strikes on a regional map.

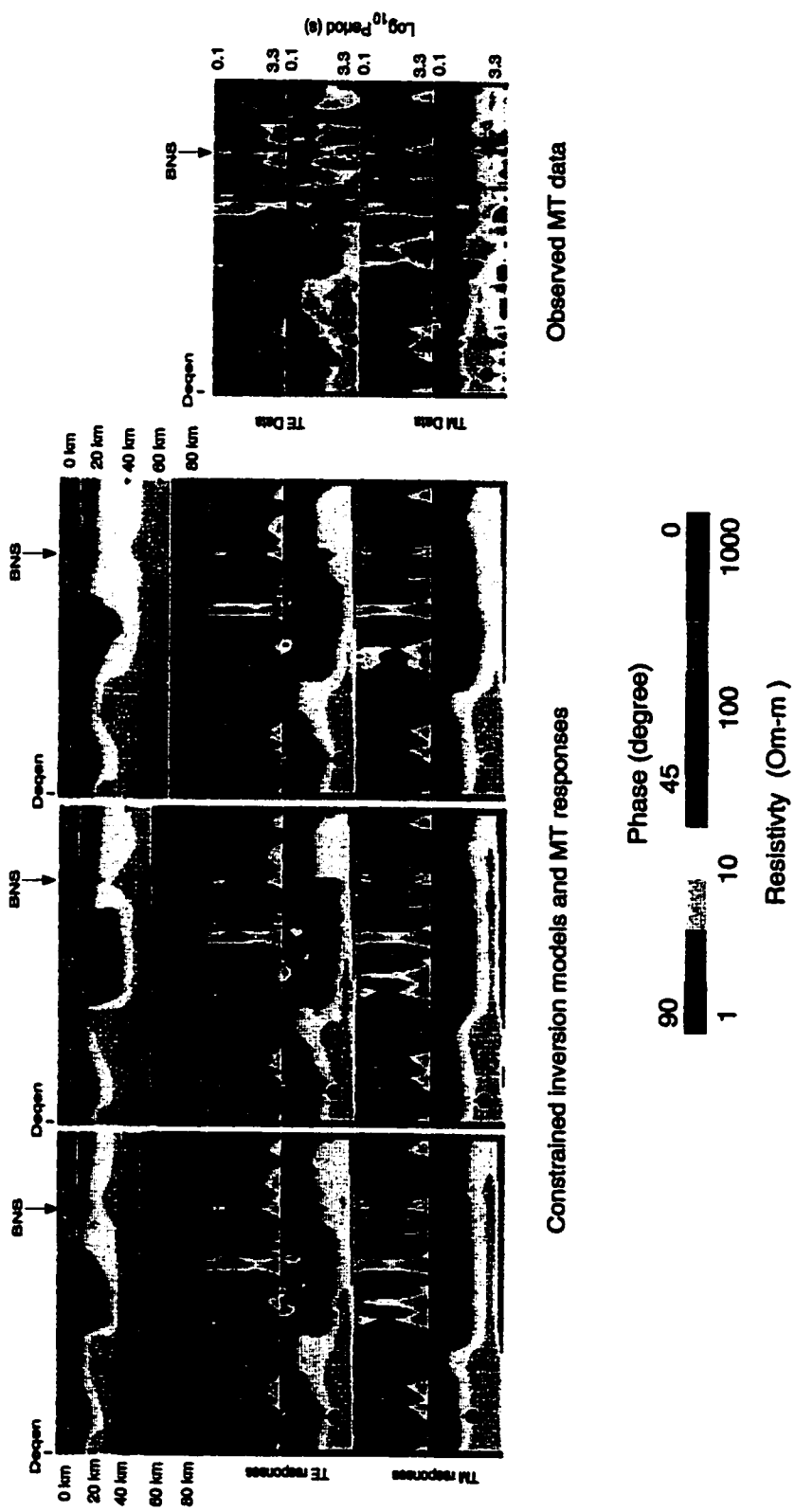


Figure 2.5 A set of MT data can be fit by different models

CHAPTER 3

INVERSION OF MAGNETOTELLURIC DATA IN THE PRESENCE OF BATHYMETRY AND TOPOGRAPHY

3.1 Introduction

Ideally, MT data should be collected on a flat or near flat surface to avoid topographic distortions. However, some regions of interest have very strong topography or bathymetry. Examples include tectonic studies in mountainous areas (Schwarz et al., 1984, Kurtz et al., 1986) and the study of mid-ocean ridges (Evans et al., 1999) where bathymetric distortion can be very strong and cannot be ignored. To reduce or even eliminate the distortion associated with topography, many approaches have been proposed (Fox et al., 1980, Holcombe et al., 1984). Jiracek et al. (1986) proposed a distortion tensor approach that assumes the topographically distorted subsurface response can be represented by the product of a distortion tensor and the undistorted subsurface response. Under this assumption, the undistorted subsurface response can be recovered by calculating the distortion coefficients and applying the inverted distortion tensor to the measured MT data. After this correction, the data can be interpreted as if they were collected on a flat surface. A few synthetic examples are reported by Chouteou and Bouchard [1988] and their calculation showed that this technique can be effective in reducing topography distortions.

In order to use the distortion tensor approach, one needs to compute the distortion coefficients. This requires knowledge of the sub-surface resistivity. Usually, a uniform half-space is assumed. This means that the distortion tensor is only an approximation and limits its application in real MT experiments.

Instead of correcting the topographically or bathymetrically distorted MT data, we will incorporate the topographic or bathymetric response directly into the inversion. To invert MT data in the presence of topography or bathymetry, we need a high precision forward modeling approach and an inversion algorithm which can properly handle the various discontinuities within the model. In the following discussion, we will first discuss calculating MT responses to a sufficient accuracy using a Finite Difference Approximation (FDA) and then discuss the strategies to overcome the inherent difficulties when inverting MT data in the presence of topography or bathymetry.

3.2 Calculating the MT responses of topography and bathymetry.

Many approaches exist for calculating the MT response in the presence of strong topography (Aprea et al., 1997, Wannamaker et al., 1986, Redding et al., 1984, Ngoc, 1980, Word, 1967). Wannamaker et al. (1986) studied the MT response of a 2-D earth with topography using a Finite Element (FE) method and compared their calculations with other approaches. The close agreement of Wannamaker's program (PW2D) and an analytic solution of a simple hemicylindrical model indicated that PW2D is a good candidate for computing MT responses of a 2-D model including topography.

Finite Difference Approximation (FDA) is simpler to implement but has been thought to be less accurate when discontinuities are present in the model. Aprea et al. (1997) showed that a new FDA can accurately calculate MT responses of models with arbitrary 2-D topography and with internal discontinuities. Using a range of models, they demonstrated that their FDAs yield results that differ by less than 1% from the FE approach of Wannamaker et al (1986). This new FDA is used in our program to calculate the model responses.

The detailed description of the new FDA is presented by Aprea et al. [1997]; here we will briefly go over the basic steps. In the case of 2-D, the MT response can be separated into two modes. For electric currents flowing along strike (TE mode), the 2-D MT governing equations (2.1-2.4) can be reduced to:

$$\nabla \cdot \nabla E_x = -i\omega\mu_0\sigma E_x \quad (3.1)$$

$$\frac{\partial E_x}{\partial z} = -i\omega\mu_0\sigma H_y \quad (3.2)$$

For electric currents flowing perpendicular to the strike (TM mode), the 2-D MT governing equations can be reduced to:

$$\nabla \cdot \rho \nabla H_x = -i\omega\mu_0 H_x \quad (3.3)$$

$$\frac{\partial H_x}{\partial z} = \sigma E_y \quad (3.4)$$

Integrating equation (3.1) and (3.3) over a rectangular cell surrounding a node and extending halfway to the adjacent nodes, we obtain the following equations using Gauss' Theorem:

$$\oint \left(\hat{n} \bullet \nabla E_x \right) dl = -i\omega\mu_0 \int_A E_x \sigma dA \quad (3.5)$$

$$\oint \left(\hat{n} \bullet \rho \nabla H \right) dl = -i\omega\mu_0 \int_A H_x dA \quad (3.6)$$

where the left side integral is around the edge and the right side is over the same area of the cell.

These equations can then be approximated using an FDA approach. If the conductivity is continuous within the small rectangular cell, a five point approximation can be used. However, this approximation will not yield accurate results when a discontinuity exists within the cell. To improve the FDA accuracy, Aprea et al. (1997) introduced the concepts of “effective conductivity” and “effective resistivity”, which are essentially weighted means of the conductivity or resistivity of surrounding nodes. This modification to the FDA significantly improves the accuracy of the fields within the model, but accurate auxiliary fields (H_y for the TE mode and E_y for the TM mode) at the interface where the measurement is made are still needed.

The auxiliary fields are calculated from the following equations:

$$\frac{\partial E_x}{\partial z} = -i\omega\mu_0 \sigma H_y \quad (3.7)$$

$$\frac{\partial H_x}{\partial z} = \sigma E_y \quad (3.8)$$

which are usually approximated using a three-point approximation which does not

cross the earth-air (or earth-seawater) interface where the derivatives are discontinuous. For the TM mode (Figure 3.1a) equation (3.8) can be approximated as:

$$\sigma E_y = \frac{(H_1 - H_0) \bullet (h_2 + h_1)}{h_1 \bullet h_2} - \frac{(H_2 - H_0) \bullet h_1}{(h_1 + h_2) \bullet h_2} \quad (3.9)$$

and for the TE mode (Figure 3.1b), equation (3.7) can be approximated by:

$$-i\omega\mu H_y = \frac{(E_{-2} - E_0) \bullet h_{-1}}{(h_{-2} + h_{-1}) \bullet h_{-2}} - \frac{(E_{-1} - E_0) \bullet (h_{-2} + h_{-1})}{h_{-1} \bullet h_{-2}} \quad (3.10)$$

For a flat earth-air interface in the TM mode, this calculation is straightforward. Only the three nodes beneath the surface are used since the H field above is a constant. However, one has two choices in calculating the auxiliary field for the TE mode: using three nodes below the surface as in the TM mode or using three nodes above the surface. Usually, the later method is used since the E field in the air satisfies the Laplace equation and can be better approximated by a polynomial than the E field in the earth.

The method discussed above works on a flat earth, however, this approach fails in the presence of topography or bathymetry. To illustrate this, we will use a simple trapezoid hill (Figure 3.2) as an example. At the top of the hill, the model is flat and the method discussed above can be used. When any of the MT sites fall on the slope of the model, the auxiliary field cannot be calculated by equation (3.7) or (3.8) because the auxiliary field may not be perpendicular to the primary fields. For example, the

auxiliary field on an earth-seawater interface in the TM mode has two components; one is along the interface and another is perpendicular to the interface.

Based on the study of Wannamaker et al. (1986) on effects of different magnetic sensor orientations, we assume that the magnetic sensor is always horizontal. This is, in any case, the easiest situation to achieve in practical data collections. With a horizontal magnetic sensor, we only need to compute the horizontal auxiliary field component in the TE mode and equation (3.7) will be valid in this case. If the interface is earth-air, we can still use equation (3.10). When the interface is earth-seawater, then the three nodes in the earth should be used since the earth is less conductive than seawater and the E field in the Earth varies more slowly and is thus more accurately approximated by a three point approximation. For the TM mode, calculation of the auxiliary E field is more complicated than for the TE mode because the electric field may not be horizontal or even along the interface. In the case of topography, the currents flow along the air-earth interface, so only the H field derivative normal to the slope is needed to calculate the auxiliary field. As shown in Figure 3.2, PW2D and RRI use different nodes in computing the auxiliary field. In PW2D, when the vertical and horizontal derivatives of the H field are calculated, a simple projection approach is used to obtain the auxiliary field in the direction normal to the slope. Instead of using the three horizontal nodes on one side of the interface, RRI uses three nodes along the slope. This allows one to use centered a difference formula that produces a more accurate result.

If the model contains only topography, the air is an insulator and the currents do not cross the interface. However, when the model contains bathymetry, the currents can cross the interface into the seawater. It is then necessary to use both the field derivatives along the slope and in the vertical direction to compute the auxiliary field normal to the slope.

Although we rarely put any MT sites on a topographic corner, for completeness we need to find a way to define the MT response there. PW2D uses the same approach on a corner as it uses on a slope, with the exception that on a corner, the tangential is defined to be perpendicular to a line which bisects the angle of the corner. RRI defines the field gradient as the derivative along a path around the corner and uses the vertical nodes and interface nodes adjacent to the corner to calculate the auxiliary field.

3.3 Forward modeling examples

3.3.1. The TM responses of a simple topographic model.

To test our forward algorithm, a simple ramp model is constructed (Figure 3.4 e). The slope of the ramp is ~30 degrees and the resistivity of the model is a uniform 1000 $\Omega \cdot m$ under the ramp. To generate a strong topographic response, we use 1000 Hz and 100 Hz in our forward calculation. We are presenting TM responses only because TE responses of many models have been investigated by Aprea et al (1997). Due to the high frequencies, we use a relatively fine mesh on the slope: 10 meters between vertical nodes and 17 meters between horizontal nodes.

In Figure 3.4, the top two plots (a and b) are calculated apparent resistivity curves for both 1000 Hz and 100 Hz and the lower two (c and d) are phase curves. The magnitudes and the wavelength of the topographic responses are frequency dependent. The apparent resistivity response at 1000 Hz is weaker in magnitude and spatially narrower than that of the 100 Hz. On the other hand, the phase response at 1000 Hz has stronger magnitude and is spatially narrower. The first order feature of these plots is that the results from PW2D and the RRI agree very well. The good agreement between these two programs indicate that the RRI and PW2D have almost identical accuracy in computing the MT responses of topography. While these two programs give very close results at most of the sites, they differ with respect to each other significantly at the topographic corners where the response is not well defined. For this case, there is no obvious basis to choose one code over the other at the corner.

3.3. 2. The MT responses of a bathymetric model.

While MT responses of 2-D topography is a well studied subject (Reddig et al., 1984, Wannamaker et al., 1986), the MT response of 2-D bathymetry is less investigated. Here we construct a model to imitate a rather drastic ocean coast (Figure 3.5(a)). The bathymetry slope consists a series of straight segments that approximate rounded corners. The maximum slope is 45 degrees. Beneath the slope is a uniform 100 O.m earth. Both TE and TM responses at periods of 100 seconds and 1000 seconds are calculated using both PW2D and RRI. Phases and resistivities for this model are shown in Figure 3.5 (b c d e).

As we expect, the longer period responses are less affected by the bathymetry than the short period. The TE resistivity and phase curves are shown in Figures 3.4b and 3.4c. The TE phase curves are above 90 degrees in the ocean and gradually decrease up the slope, reaching the half space value of 45 degrees on the land. The TE resistivity curves behave differently than the phase curves. The 100 second curve has a peak about 1.5 km from the coast and has only 1/10 of the Earth resistivity far away from the coast. This is the result of a strong electric current flowing in the seawater near the coast. This current has two effects: it represents a non-uniform source for an MT measurement on the seafloor and there will be an image current flowing in the seafloor.

The TM response of the model is significantly different from that of TE (Figure 3.4d and 3.4e). TM resistivity has much larger variations than TE resistivity and there is a very big discontinuity at the corner where the ocean meets with the land. The calculated TM resistivity on land near the coast is several orders of magnitude higher than the real earth. This large resistivity variation is primarily due to the galvanic response at the coast. When the current flows from the sea to the land, it must be continuous while there will be a discontinuity in electric field that will cause the accumulation of charges. This phenomenon can be considered a static shift due to a large-scale 2-D structure (the coast). The TM phase curves vary smoothly, have a smaller variation than TE phase and there is no corner-related discontinuity. Although we see very good agreement in results from both programs, there is an exception at the

node just to left of the coast. There is an offset in all TE and TM responses at this node and the offset in TM is larger. However, comparing to the adjacent nodes, RRI responses are smoother than PW2D responses. So, we conclude that in this case the auxiliary field computation used in RRI is more accurate than that used in PW2D.

3.4 Inversion of MT data in the presence of topography or bathymetry

A few modifications need to be made in order to use RRI to invert MT data in the presence of topography and bathymetry. First, we need to start the inversion at the air-earth or water-earth interface since the structure above the interface is fixed. Second, the roughness of the model should not include the earth-air or earth-seawater discontinuities.

To start the inversion at the air-earth or water-earth interface, we need to define the topography or bathymetry. A topography vector (Figure 3.5) can be used for this purpose. This vector has as many elements as model columns and these elements define the location of the interface. For example, if the i th element of the vector is 5, then the location of the interface on the i th column of the model mesh is the 5th row. Because sea level is, by default, flat, one can tell whether an interface node is earth-air or earth-water by examining if this interface is above or below sea level.

Figure 3.5 shows how the topography vector is used to define a water-earth interface. Given any two numbers, (3,6) for example, we can uniquely identify a node. Using the convention that column numbers increase monotonically, we can define the water-earth interface by a vector (0, 1, 2, 3, 3, 3, 3, 3, 3). Using such a simple vector,

we can define any discontinuity within the model. In designing the model mesh, we recommend putting all the MT sites on model nodes. In previous RRI versions, MT responses were computed on model nodes and then interpolated to a site if the site was not on a node. If the model contains topography or bathymetry, then the interpolation becomes 2-D and may incur extra computation errors. On the other hand, designing a mesh with sites on mesh nodes is relatively simple.

In the previous versions of RRI, the vertical structure beneath each site is first updated, then the whole model is updated by horizontally interpolating the values underneath these sites to all the nodes. Since each site inversion is 1-D, it is trivial to invert conductivity on the nodes beneath the site and compute their roughness. However, the interpolation step requires some care. When two adjacent sites are at different depth or height, the nodes above the lower site cannot be properly updated if a simple horizontal interpolation is used.

To overcome this problem, we used a two-step strategy. First, after inversion, we replace the air or seawater values above each site with the resistivity at the interface and then do the routine horizontal interpolation. After the interpolation, we restore the air and seawater nodes to their proper values. Thus the resistivity of the air or seawater does not come into the interpolation. Instead, the horizontal interpolation at each interface site depends on the resistivity values of adjacent sites on the interface.

3.5 Inversion examples

3.5.1. Inversion of topographic data with noise.

The model and its MT responses are shown in Figure 3.6 (b). This ramp has a slope of about 30 degrees. This is much stronger than likely in a real MT survey. We insert a thin, conductive layer under the ramp. The layer is designed to be parallel to the topography so that we can test whether the sites on the slope can recover the slope in the conductive layer. Random errors with a standard deviation of 5% in resistivity and 1.5 degrees in phase were added to the calculated data.

Although we believe our program can accurately calculate responses of a model with 2-D topography and internal discontinuities, we actually used PW2D to generate MT responses used as input to the inversion. Using the same program for both forward modeling and inversion can miss systematic errors.

As we can see from the calculated data, the TE response of this model is relatively simple while the TM response is more complicated. This again, shows that topography tends to have a stronger TM response than TE. 16 sites were used with only 4 sites are on the slope. The minimum distance between the sites are about 100 meters. We used 16 frequencies ranging from 100 Hz to 0.001 Hz.

The program inverts TE and TM data simultaneously and the inverted model fits the data to a normalized (wrt added error) rms misfit 1.7. The inverted model and its response are shown in Figure 3.6 (a). We see that the conductive layer in the inverted model mimics the structure in the model used to generate the data. However,

the depth transition of the conductive layer is spread out of a wider horizontal distance and the apparent slope is somewhat less than the true slope. The layer conductivity is also smeared out vertically. Both of these effects are the result of finite resolution of the inversion. It is interesting to point out that the vertically integrated conductivity (conductance) of the layer in the inverted model (42 S) is almost identical to the conductance of the true layer (40 S). This supports the technique we will use in Tibet—that conductance of a 2-D layer can be reliably extracted.

3.5.2. Coast model with a conductive structure.

The model used to generate the MT data is shown in Figure 3.7. The model consists of ocean, land and a conductive structure. Among the 21 MT sites, 11 of them are on ocean floor and 10 are on land. Data are computed at 9 periods ranging from 100 seconds to 10,000 seconds. We also added random noise to our data with a standard deviation of 5% in resistivity and 1.5 degrees in phase. The computed resistivity and phase are shown in Figure 3.7.

A TE mode inversion started from a 10 Ohm-m half space with the bathymetry is shown in Figure 3.7. 15 inversion iterations are performed followed by 20 smoothing iterations. The inverted model fits the noisy data to a normalized rms misfit of 1.5. We also tried starting from a 100 Ohm-m half space. In early iterations, spurious deep structures developed which could not be smoothed out in later iterations. This highlights one of the problems inherent in RRI (and other linearized inversions): if the starting model is too far away from the real model, RRI may be trapped in a local

minimum. Finally, a joint TE and TM inversion produced essentially the same structure as TE alone. This is probably due to the fact that the true model used to generate the data has a stronger TE signature.

3.6 Conclusions

In practice, situations arise that require MT surveys to be carried out either in mountainous regions or on the ocean floor in the presence of strong bathymetry. MT data from these regions can be highly distorted and ignorance of such distortion can lead to serious problems in data inversion. One may either generate false structures or even be unable to fit the data. To handle the distortion caused by the presence of topography or bathymetry, we have shown how to incorporate topography and bathymetry response into the inversion. Our FDA and auxiliary field calculation give accurate MT responses in the presence of strong 2-D topography or bathymetry and our inversion approach works satisfactorily with noisy data generated from known models.

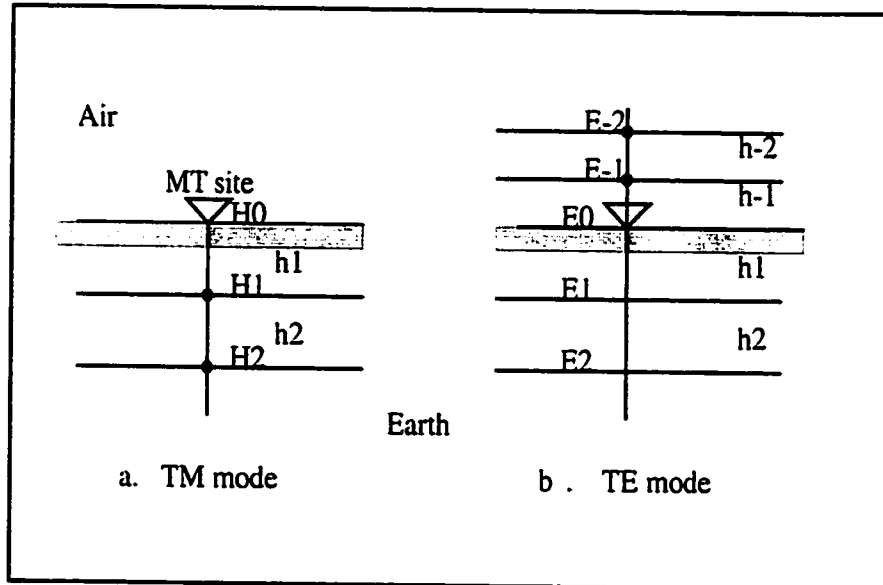


Figure 3.1 Using FDA to calculate the auxiliary field on a flat earth
 In TM mode, three nodes beneath the interface are used.
 In TE mode, three nodes above the interface are used.

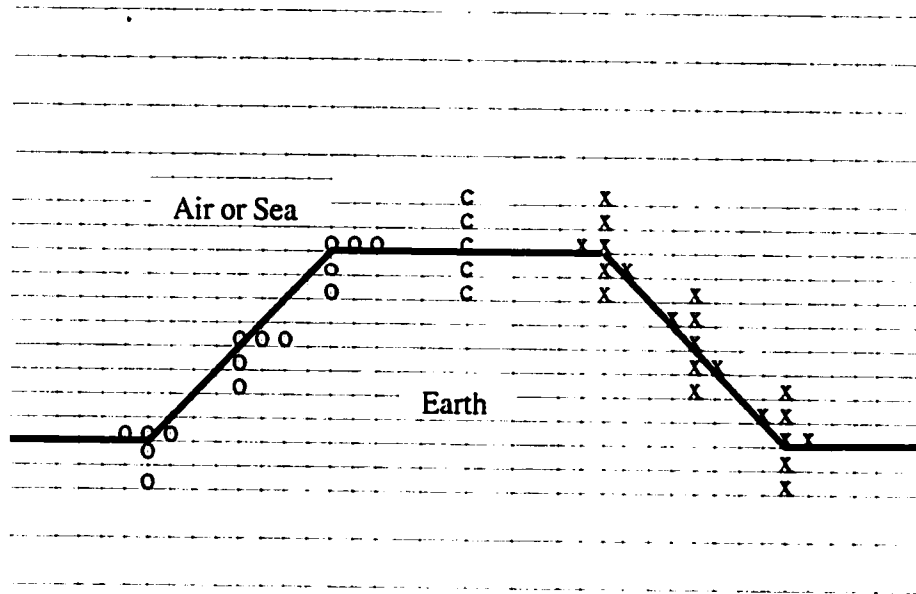


Figure 3.2. MT auxiliary field calculation on topography or bathymetry

o ---- nodes used in PW2D x---- nodes used in new RRI

c ---- nodes used by both program.

For earth-air interface, RRI uses three nodes above interface in TE .
and three nodes below the interface in TM .

For earth-sea interface, RRI uses three nodes below interface in TE .
and three nodes below the interface in TM .

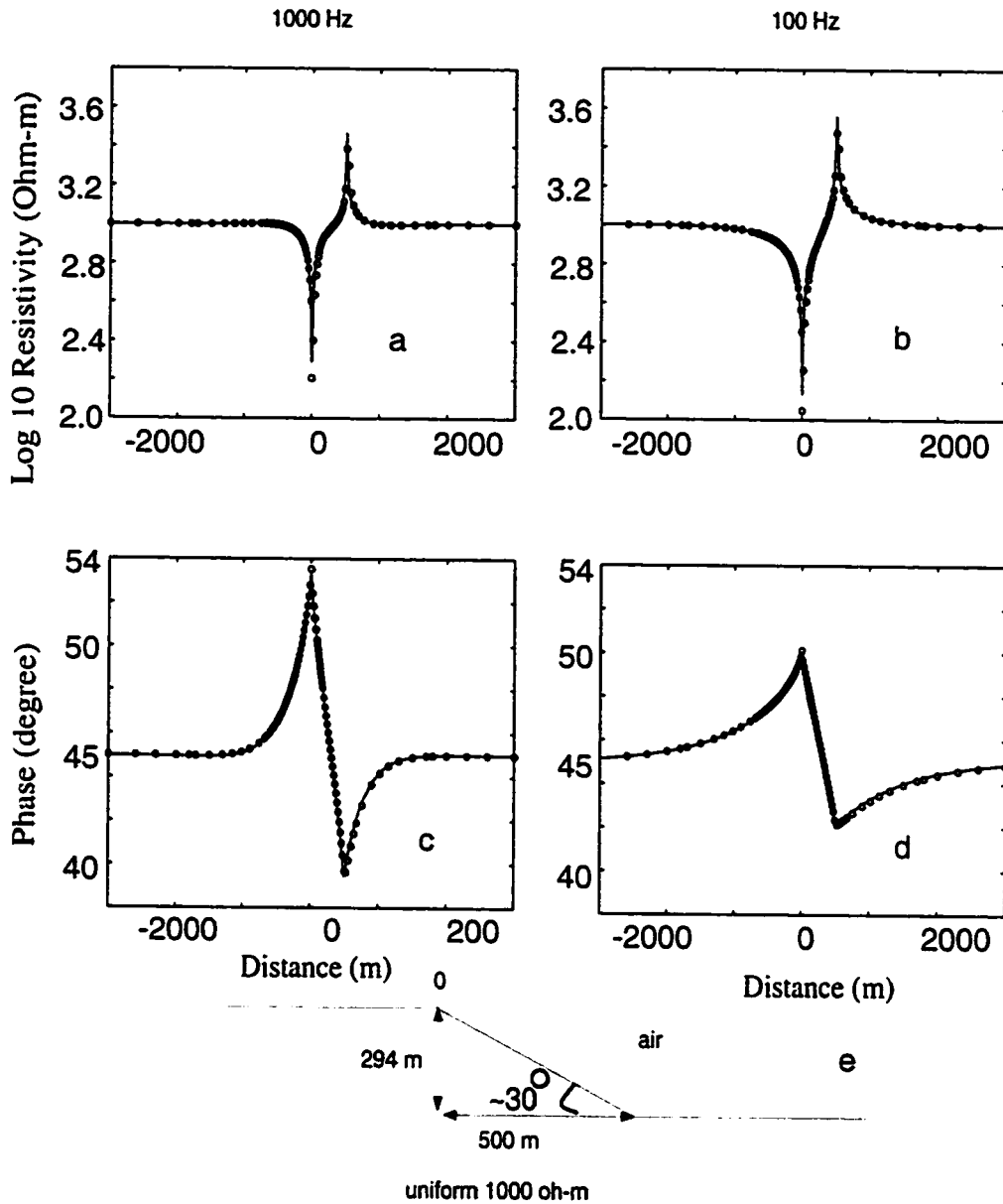


Figure 3.3 PW2D and RRI TM responses over a ramp.

o — PW2D — RRI.

- a. apparent resistivity response at 1000 Hz
- b. phase response at 1000 Hz
- c. apparent resistivity response at 100 Hz
- d. phase response at 100 Hz

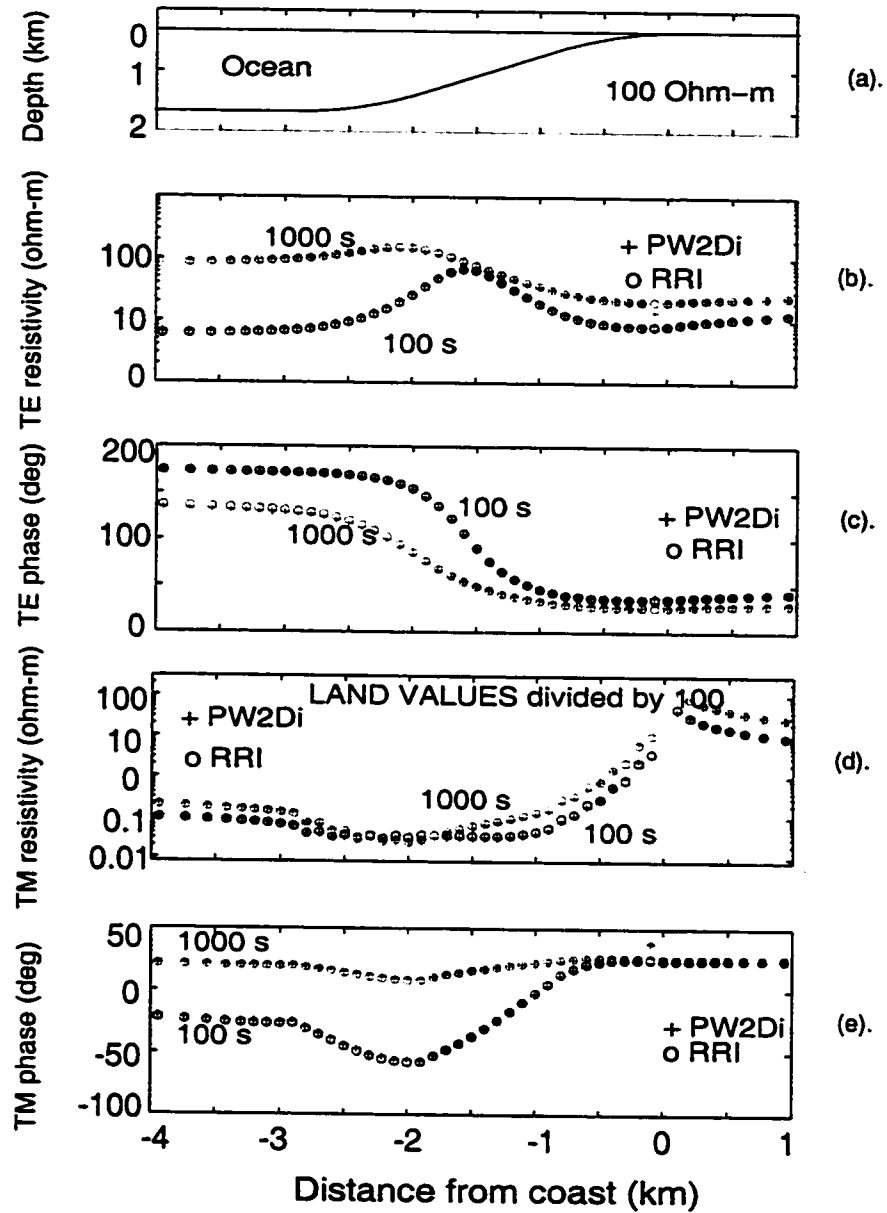


Figure 3.4 MT responses of a coast model shown in (a)
 (b). TE resistivity response. c. TE phase response.
 (d). TM resistivity response. e. TM phase response.

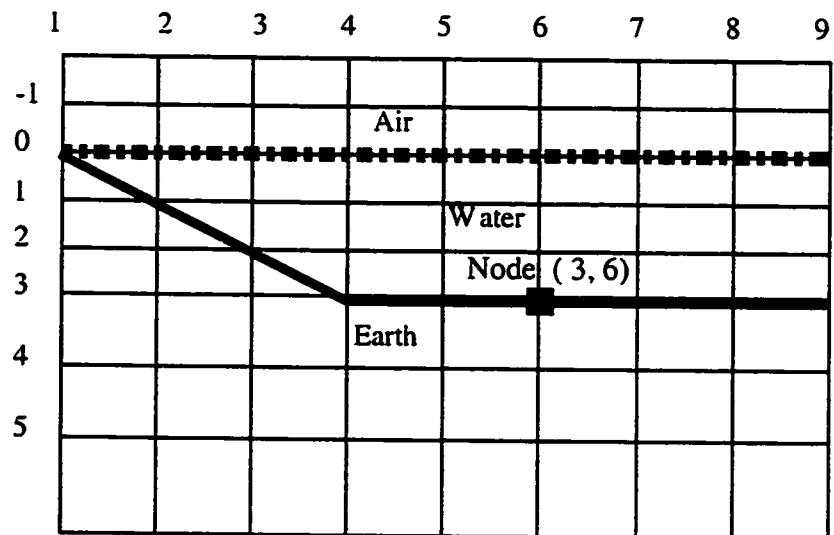


Figure 3.5. Using the topography vectors to define internal interface within the model

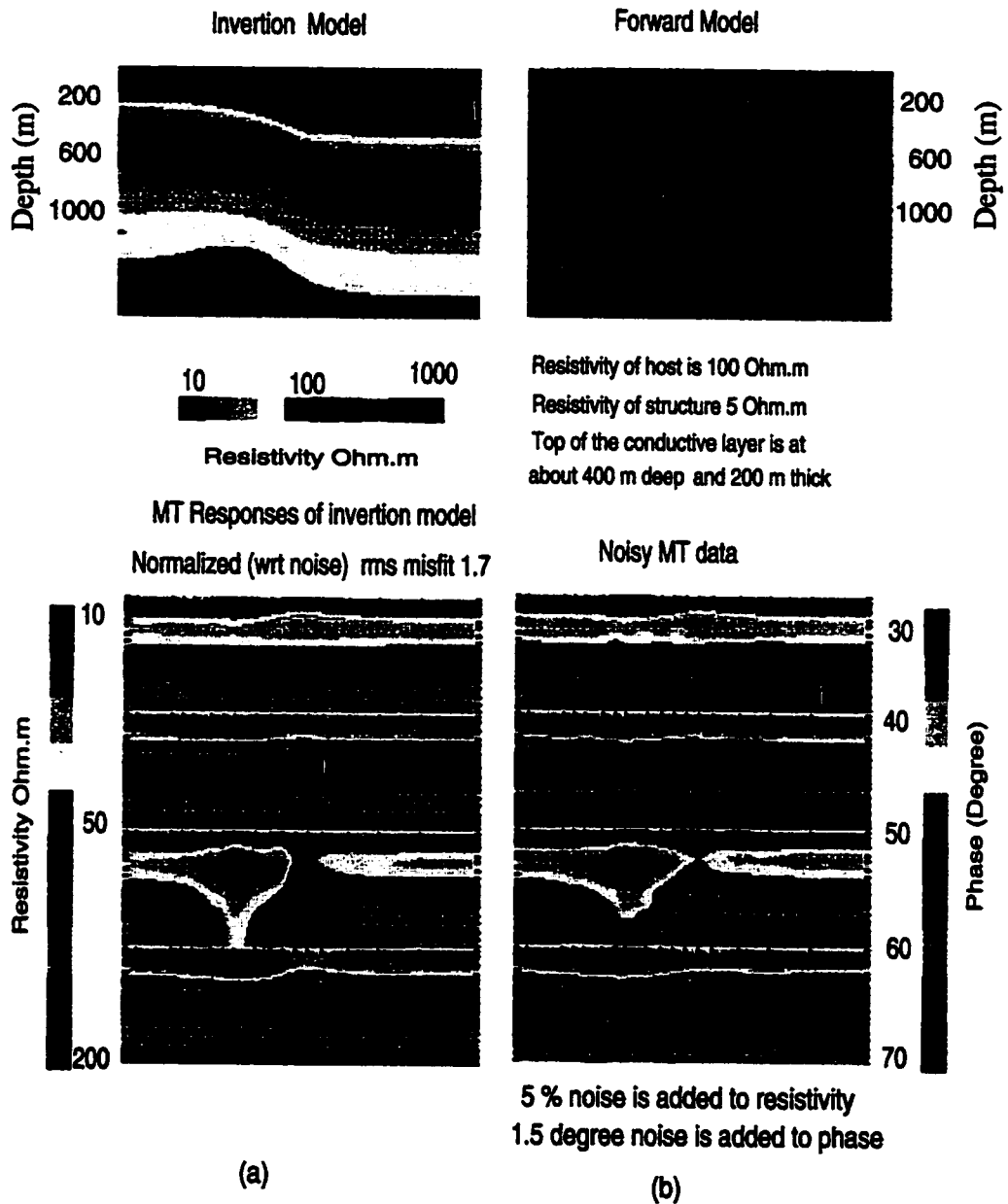


Figure 3.6. Inversion of a thin conductive layer under a ramp.

(a) inversion model and its MT responses.

(b) model and its MT responses with noise.

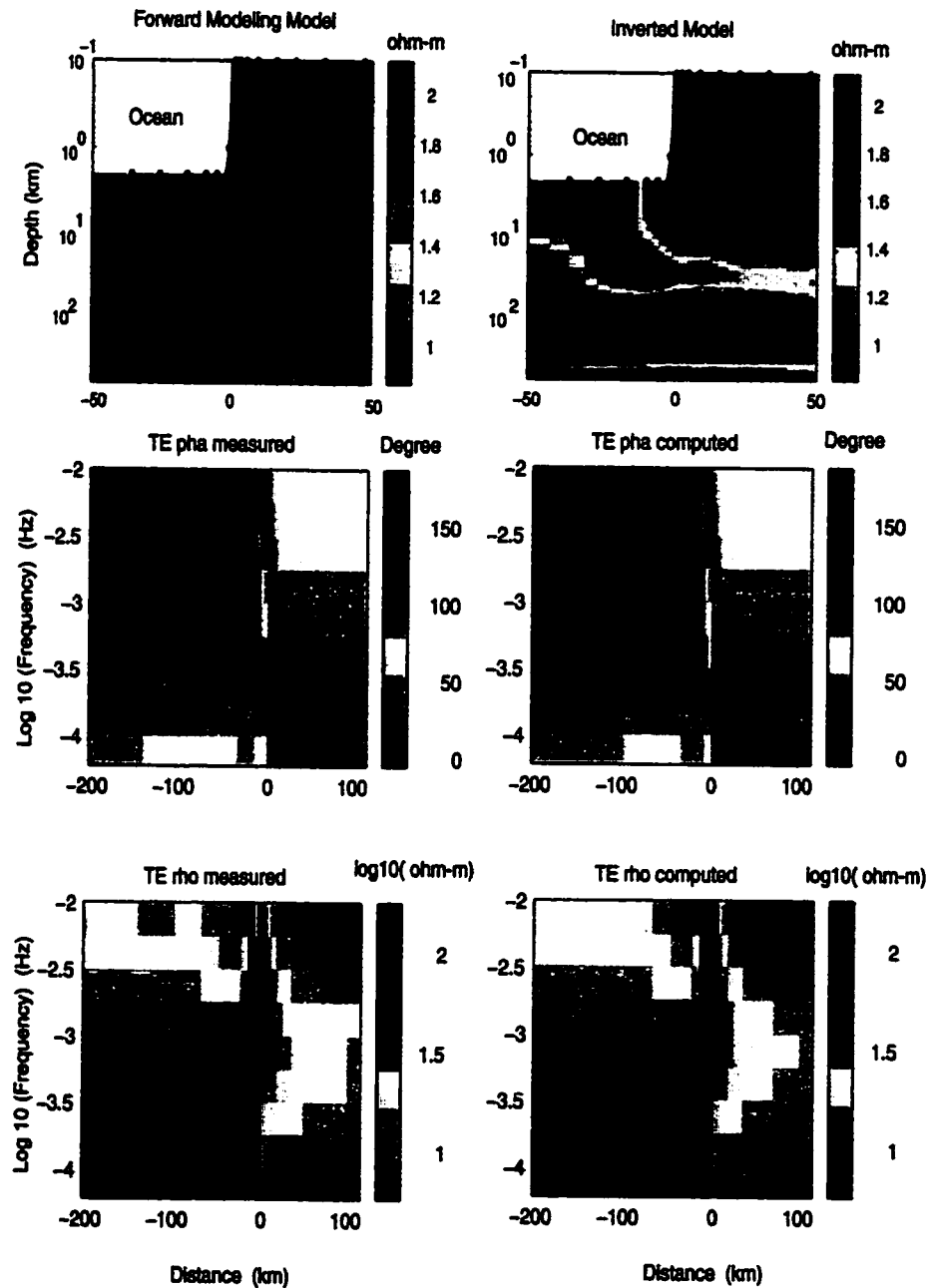


Figure 3.7 Inversion of a coast model with a conductive structure

CHAPTER 4

CONSTRAINING THE NATURE OF THE MIDDLE CRUSTAL CONDUCTIVE ZONE IN SOUTHERN TIBET

4.1 Introduction

The India-Asia continent-continent collision has created one of the most spectacular topographic features on the surface of the Earth – the Tibetan Plateau. The Tibetan Plateau has an area about half the size of the conterminous United States with a mean elevation above 5 km, and represents a key location for understanding the processes of mountain building and plateau formation during continent-continent collisions. Although our understanding of the geological structure and history of the Tibetan Plateau has significantly improved in the last two decades, many first order structural questions are still under debate. Numerous models have been proposed to explain the tectonic processes that have thickened the crust; these span the spectrum from underthrusting of the Indian plate [Argand, 1924] to distributed thickening of the Tibetan crust [Dewey and Burke, 1973]. Other suggested processes include fluid injection into the Tibetan lower crust [Zhao and Morgan, 1987], eastward extrusion of crust and mantle [Tapponnier *et al.*, 1982], and southward subduction of Asian lithospheric mantle [Willett and Beaumont, 1994].

The INDEPTH (International Deep Profiling of Tibet and the Himalayas) project was initiated in 1992 to improve our knowledge of geological structure and evolution

of the Tibetan Plateau. The INDEPTH corridor in southern Tibet extends from south of the High Himalaya to the center of the Lhasa Block (Figure 4.1) Along this profile active and passive seismic (seismic reflection and broadband earthquake), magnetotelluric and surface geological data have been collected. Nelson *et al.* [1996] synthesized the available data to 1995 and concluded that the middle crust beneath southern Tibet is partially molten. The evidence for partial melt included: high heat flow [Franchetaeu *et al.*, 1984], prominent seismic bright spots at a depth of 15-20 km [Brown *et al.*, 1996], low electrical resistivity [Chen *et al.*, 1996], strong P- to -S conversion shown by seismic wide-angle seismic data, and low crustal velocity [Kind *et al.*, 1996]. In addition to regional partial melt, INDEPTH-II seismic data suggested that the bright spots in southern Tibet may represent local accumulations of magma [Brown *et al.*, 1996].

More recent analyses of INDEPTH and other seismic data give alternative views of the composition and degree of melting in the Tibetan crust. A passive seismic study in Tibet [Owens and Zandt, 1997] found low to normal crustal Poisson's ratio in the southern plateau, which is inconsistent with a thick, extensively melted middle crust. In addition, Makovsky and Klemperer [1999] showed that detailed analysis of the wide-angle reflection data could be taken to indicate that the bright spots may be due to a thin layer of aqueous fluid. Although the existence of aqueous fluid does not necessarily preclude partial melt in the middle crust, it may constrain the thermal state at the depth of the bright spots.

The presence (or otherwise) of partial melt in the crust has important implications for the rheology of the Tibetan crust. A thermally weakened and partially molten crust can behave like a fluid and provides a simple explanation for both the flatness of the Tibetan Plateau [Fielding *et al.*, 1994] and a mechanism for uplift [Zhao and Morgan, 1987]. The nature of the bright spots and the possible existence of a layer of partial melt also have fundamental implications for the thermal state of the crust in southern Tibet. For example, if the seismic bright spots are due to aqueous fluids, then the temperature at the depth of the bright spots must be lower than the melting temperature (650°C) of wet granite. If one can conclude there is no partially molten layer underneath southern Tibet, then roles played by models requiring a fluid lower crust need to be reconsidered.

In this study, we will show how magnetotelluric data can constrain the nature and quantity of the fluids that cause both seismic reflectivity and high conductivity in the Tibetan crust. Using a constrained inversion we estimate the minimum electrical conductance in the region of study. This minimum conductance is then used to develop thickness constraints on the mid-crustal fluid zone. Combining the thickness constraints with other geophysical data, we examine the various models that have been proposed for the mid-crustal zone in southern Tibet and determine if they are consistent with the MT data. We first give some background information about the study region and then present detailed analyses of the MT data. In conclusion, we suggest that the middle crust conductive zone in southern Tibet is unlikely to be

explained by either partial melts or aqueous fluid alone. The bright spots in southern Tibet are most likely a concentration of aqueous fluid overlying a thick, widely distributed layer of partial melt.

4.2 Regional geology, previous work and the Yangbajian-Damxung Graben

The Yangbajian-Damxung Graben is part of the Yadong-Gulu rift, formed by ongoing east-west extension in southern Tibet [Armijo *et al.*, 1986]. The Nyainqentanghla range (Figure 4.1) extends for 100 km NE-SW on the northwestern margin of the graben. Exposed surface rocks include orthogneiss in the Nyainqentanghla Range, Cenozoic volcanic rocks and the Gangdese batholith southwest of the graben and Carboniferous-Permian sedimentary strata at the northeast portion of the graben [Pan and Kidd, 1992]. On the eastern edge of the Nyainqentanghla range, Pan and Kidd [1992] identified a ductile shear deformation zone, named the Nyainqentanghla Shear Zone (NSZ). A thermochronological study of the NSZ suggested that the footwall rocks of the NSZ had been uplifted ~17 km since ~8 Ma ago [Harrison *et al.*, 1995]. The activation of the NSZ has also been suggested to coincide with the time when rapid uplift of the Tibetan plateau occurred and may have strengthened the monsoon at about 8 Ma [Harrison *et al.*, 1995; Molnar *et al.*, 1993]. Within the graben a number of geothermal phenomena have been identified, including the largest geothermal system in Tibet at Yangbajian [Hochstein and Regnaud-Lieb, 1998]. The INDEPTH seismic reflection profiles in the graben showed seismic bright spots, whose high amplitude and negative polarity strongly

suggest the presence of a fluid phase within the middle crust [Brown *et al.*, 1996, Makovsky *et al.*, 1996]. Magnetotelluric data on a profile that crossed the graben (200-line, Figure 4.1) showed a conductive mid-crustal zone that extended outside the graben [Chen *et al.*, 1996]. Although the nature of the conductive zone is unclear, the unusually high conductivity on a large spatial scale indicates that a well-connected regional electrical current path must exist.

The nature of the fluid inferred from the seismic data is still under debate, with partial melt and aqueous fluids as the candidates. The presence of each fluid has different implications for the thermal state of the crust, and consequently for the likely processes that thickened the crust [Nelson *et al.*, 1996; Makovsky and Klemperer, 1999]. If the observed bright spots are magma bodies, then partial melt and a high-temperature ($>650^{\circ}\text{C}$) middle crust are expected. This hot middle to lower crust may then be weak enough to behave rheologically as a fluid layer, as in geodynamic models such as the continental injection model [Zhao and Morgan, 1987; Royden *et al.*, 1997]. On the other hand, an aqueous source for the bright spots would constrain the thermal state of the crust at the depth of the bright spots to be lower than 650°C . Although the existence of aqueous fluid does not exclude the existence of partial melt, the seismic bright spots and high electrical conductivity can be equally explained by aqueous fluid alone. MT is inherently sensitive to the presence of interconnected fluids. However, determining what fluid is causing the high conductivity requires additional geophysical and petrological data.

4.3 The 200-line magnetotelluric data

Magnetotelluric (MT) data were collected on two profiles in southern Tibet in 1995, and initial interpretations are described in Chen *et al.* [1996]. The 100-line extended from center of the High Himalaya to near Yangbajian, and the 200-line extended from east of Lhasa, across the Yangbajian-Damxung Graben to Nam Tso (Figure 4. 1). The location of the 200-line was chosen specifically to ascertain if there are differences in crustal electrical conductivity within and outside the Yadong-Gulu rift system. Two types of MT system were used in the survey; long period MT data (20-20,000 s) were collected with Long period Magnetotelluric System (LiMS) designed by the Geological Survey of Canada, and broad band MT data (from 320 Hz to ~1000 s) were collected using two Phoenix V5 systems. Long period sites were located roughly 20 km apart. Broadband data were collected at all long period sites, and also at intermediate sites to provide a more detailed image of shallow electrical structure. The shallow structure must be well defined in order to image faithfully the deeper structure. The long period data were remotely referenced, but the broadband data were not remotely referenced and thus may be subject to bias.

The first stage in analyzing these data is to determine an appropriate geoelectric strike direction for interpretation. These were first calculated using the tensor decomposition technique of McNeice and Jones [2001], and a summary of the results is shown in Figure 4.2. Although the shear and twist are statistically stable and cluster around zero (undistorted), the strike varies significantly. A possible interpretation of this result is that the electrical structure below the shallow structure

is totally uniform and does not have a strong preferred strike. We shall see that subsequent data are consistent with this. It is clear that a consistent geoelectric strike for the 200 line can not be clearly defined from the data themselves and constraints from geological data are required.

The regional strike of structures on the Plateau is roughly EW, while the Yangbajian-Damxung graben trends North-East. To investigate the effect of strike on the inversions, we consider two possible strikes throughout the following analysis, one east-west and the other northeast-southwest and we look for conductivity modes that are independent of the choice of strike. For reference, we will call the east-west strike the Zangbo strike since it is parallel to the Zangbo suture and the regional structure of accreted terranes. The northeast-southwest geoelectric strike is termed the Graben strike. With a geoelectric strike, MT data can be presented in two separated modes. The transverse magnetic (TM) mode has electrical currents flowing across strike while electrical currents flow along the strike in the transverse electric (TE) mode.

The observed MT data in Zangbo coordinates are shown in pseudosection form in Figure 4.3a. The short period data ($T < 10$ s) exhibit relatively high values of apparent resistivity and low phases. This implies that the shallow structures are resistive. At longer periods ($T > 10$ s), the phases increase and the apparent resistivities decrease, indicating an increase in conductivity with depth across the whole profile. Two typical sites are shown in Figure 4.4. Site 220 is south of Damxung while site 240 is located within the graben. Differences between TE and

TM modes indicate that these data are multi-dimensional, since a 1-D earth produces MT responses that are identical at all azimuths.

4.4 Constrained inversion of the 200 line MT data

Inversion of magnetotelluric data yields a subsurface resistivity model that is non-unique in a number of aspects. However, a quantity that can be stably determined for a layer of relatively high conductivity is the conductance of a layer, which is defined by

$$C = \int_{D_1}^{D_2} \sigma(x) dx$$

and represents the integrated conductivity in Siemens (S) between depth D_1 and D_2 .

Weidelt (1985) shows that one can construct conductance bounds from the MT impedances, and that these conductance bounds are tight even though the associated 1-D models vary quite widely. This is demonstrated in Figure 4.5 where three 1-D resistivity models are shown. Each model has a 10 km thick upper layer and a 100 Ω m half space at the base. In each model the conductance of the middle layer is 8000 S, but the individual thickness and conductivity of the layer vary. The MT responses of these models are shown in Figure 4.5 (b) and 4.5 (c). From 0.01 to 10 s the apparent resistivity responses of these models are identical. At periods greater than 10 s, small differences in apparent resistivity and phase can be discerned between the three models. To first order, the MT response of different 1-D models with the same conductance is the same. While extension to 2 and 3 D has not been examined rigorously, it is unlikely that the situation will differ greatly if the conductive layer is

nearly horizontal. So, given a set of MT data, inversions may find different models that can fit the data, but a stable model conductance should be expected.

In the context of constraining the nature of the proposed crustal fluid, the minimum conductance required by the data can provide important insights. If we can obtain the minimum conductance and the maximum overall conductivity of the rock-fluid mixture, then we can then estimate the minimum thickness of a layer containing fluids.

The minimum conductance is the lower bound on the model conductance that is required by a given set of data. For MT data of limited bandwidth and containing finite errors, it may not be possible to sense the bottom of a conductor. This leads to a problem if the inverse algorithm used to construct the model uses a maximum smoothness constraint to make the model unique, because the algorithm will simply extend such a conductor to infinite depth. Vertically integrating such a model would clearly lead to a conductance that is too large. To get around this problem, we replace the model below some depth with resistive material. If it is true that the data can not sense the bottom of the conductive layer, then the deep resistive region will not change the data misfit. However the conductive layer conductance will be lower. By moving the top of the deep resistor upward until we can no longer fit the data, we find the shallowest conductor bottom permitted by the data and hence the minimum conductance. We call this process constrained inversion.

In each of the following inversions, we have used an error floor of 2.86 degrees for all phase data (which is equivalent to a 10% error in apparent resistivity) and 20% for apparent resistivity data. Data errors smaller than this floor level are raised up to the floor value. This is needed for several reasons. First, if the MT data have standard errors that are optimistically small, trying to fit these small errors will result in a model with spurious details [Parker, 1980]. Even when data have accurate statistical errors, failure to choose a correct strike and possible un-corrected 3-D distortions result in optimistic error estimates. Finally, MT data usually have some frequency bands that have smaller data errors. In the absence of an error floor, the inversion will more heavily weight the frequency band with smallest errors, ignoring data in other bands. Hence, with an error floor, a better overall fit to the frequency dependence of the data will generally be obtained. Apparent resistivity data are more susceptible to near-surface distortions (i.e. static shift) than phase data. So we set a lower error floor for phase data.

Due to its speed and convenient features for constraining the model, we used the inversion algorithm of Smith and Booker [1991]. To invert for the minimum conductance required by the data, a low conductivity (0.001 S/m, $\rho=1000 \Omega.m$) half space was added to the starting model at a depth of 100 km. The conductivity below this depth was fixed, and thus the inversion algorithm is forced to place all the conductive structure required by the data above this depth. This process was then repeated with the progressively shallower resistive basement. In each inversion, both

TE and TM mode data were fit. The inversions were then repeated with the geoelectric strike in the alternative NE-SW direction. We started inversion from a 1-D layered model (a conductive layer over the resistive basement) and allowed 15 inversion steps followed by 20 smoothing steps. At this point, the misfit has converged to the set goal and the object function measuring model roughness is decreasing very slowly. Thus the models do not have exactly the minimum structure required for the given misfit, but are close. Specifically, they are close enough that an integrated property such as conductance should differ very little from that of the true minimum structure model. The models derived from these inversions for both the Graben and Zangbo strikes are shown in Figure 4.6. In Figure 4.3b, a model and its MT responses in pseudosection form are shown. Except for site 250 on the north side of the Nyainqentangulha, the model produces a reasonably good match to the observed data. Note that the shallow structures are very similar to the model presented by Chen *et al.* [1996] even though the model is fixed to 0.001 S/m below 40 km.

To illustrate how well the data are fit by these models, the overall normalized r.m.s. misfit for the models as a function of resistive basement depth is shown in Figure 4.7. When the resistive basement begins at a depth greater than 20 km, the misfit is almost insensitive to the depth of the basement. However, when the basement is moved up to 15 km, the misfit increases significantly. This indicates that the inversion algorithm can no longer fit the data when the basement is shallower

than 20 km. This is also illustrated in Figure 4.8 and 4.9 where the fit to the data is shown at sites 220 and 240. Note that the data can be adequately fit when the depth to basement is greater than 20 km. The fit is very much degraded when the basement is moved up to 15 km. Figure 4.10 shows the static shift coefficients for models with the resistive basement imposed at differing depths. The static shift coefficient curves for different models are roughly parallel and the static shift coefficients at the same site become more positive as the resistive basement is moved upwards. The model with the basement at 15 km has the most positive static shift coefficients and they are significantly more positive than that of the model with a basement at 20 km. When the basement is deeper than 30 km, the average static shift coefficients are close to zero and the static shift for different basement depths are very close. Thus we see that there is a trade-off between the basement depth and the average static shift when the basement is shallower than 30 km. While a non-zero average static can not be excluded, it implies either aliasing of static shifts to zero spatial frequency or a structure whose scale is larger than the survey, which will shift all sites in a consistent way. Again, neither possibility can be ruled out. However, the fact that we get an average static shift near zero when the basement is deeper than 30 km strongly suggests that the biased static shifts for shallower basement depths are entirely due to a basement that is too shallow. This again requires that the bottom of the conductor is most likely deeper than 30 km.

For the models shown in Figure 4.6, a number of features are common to all the models:

- (1) The upper crust is resistive except for localized conductive structures beneath the graben.
- (2) All the models have a conductive middle crust.
- (3) The maximum conductivity of this layer increases as the depth to basement becomes shallower than 50 km.

There are several immediate conclusions: the existence of a conductive middle crust is not dependent on choice of electrical strike. This conductive crust extends across the entire profile and is, if anything, stronger outside the Damxung Graben. The minimum depth of the bottom of this conductor is 20 km. However, two considerations suggest that the bottom of the conductor is significantly deeper than 20 km. First, a 20 km basement results in a conductor top that is much shallower than the 15 km depth of the seismic bright spots at Damxung. A resistive basement at 30 km or deeper results in a conductor top that coincides with the seismic bright spots. Second, as discussed above, static shifts with a mean significantly different from zero are required by the inversion when the basement is shallower than 30 km.

The integrated conductances above the basement for each model in Figure 4.6 are shown as a function of position in Fig 4.11. Note first that the absolute minimum conductance for all models occurs when the basement is 50 km deep. Note also that the maximum conductance for all models occurs when the basement is 20 km deep.

These two observations again support the conclusion that the bottom of the crustal conductor is significantly deeper than 20 km.

At Damxung (0 km), where the seismic bright spots are observed, the minimum conductance is 6,270 S, but could be as high as 30,000 S. In order to constrain the lower bound on the thickness of a conductive layer, we will only consider the minimum conductance of these models.

This crustal conductance is unusually high. In stable continental regions a lower crustal conductance of 20-2,000 S is typical [Jones, 1992]. To gain a sense of perspective of these high conductances, 2 km of seawater has a conductance of 6,000 S.

4.5 Possible causes of high crustal conductivity in southern Tibet

High electrical conductivity in the crust can be explained by several mechanisms including the presence of saline fluids, graphite, partial melt and ore minerals [Jones, 1992]. Graphite is sometimes found at mid-crustal depths [Frost *et al.*, 1989a]. Ore minerals may also play an important role in enhancing crustal conductivity. Nover *et al.* [1998] show that connected networks of carbon and ilmenite are responsible for the enhanced crustal conductivity near the very deep drill hole in Germany. However, maintaining connected networks of thin graphite film or ore minerals over 100's of kilometers in a tectonically active area seems unlikely. Thus, fluids are the most probable cause of the elevated conductivities in Tibet. INDEPTH seismic data also give evidence for the existence of fluids [Ross *et al.*, 2001; Makovsky and

Klemperer, 1999]. However, the nature of the fluid is difficult to determine. Can rocks containing partial melt and/or aqueous fluids reasonably explain the observed 6,000 S conductance in southern Tibet? To address this question, we will review the present knowledge to the electrical conductivity of liquid-rock mixtures.

4.5.1 Electrical conductivity of partial melts

Owing to the abundance and high mobility of ions, a molten rock is a good electrical conductor. Direct studies of the electrical conductivity of a molten rock are difficult to make, but consistent results have been obtained by a number of studies. Lebedev and Khitarov [1964], Waff and Weill [1975] and Tyburczy and Waff, [1983] showed that the electrical conductivity of the melt depends on its temperature, pressure, the amount of structurally bound and free water and oxygen fugacity.

Temperature is one of the dominant factors in the process of melting and this is associated with a large increase in conductivity. For dry rocks of various compositions, melting begins around 1200°C, and the conductivity of dry melt is typically in the range 1-10 S/m [Tyburczy and Waff, 1983]. The conductivity increases with temperature and decreases with pressure, but even under the most favorable conditions (1400 °C and 0 Kbar), the melt conductivity is below 10 S/m [Tyburczy and Waff, 1983]. In contrast, water saturated rocks will begin to melt at lower temperatures. Lebedev and Khitarov [1963] showed that in the presence of free water, granite begins to melt at about 650 °C. Again, the melt conductivity increases with temperature and typical conductivities are in the range 1-20 S/m, slightly higher

than for dry melting (Figure 4.12). One possible reason for this may be the breakdown of the water in the melt, hence improving the exchange of ions and conductivity [Burnham, 1975]. In contrast to dry melts, the conductivity of a wet melt appears to increase with pressure [Lebedev and Khitarov, 1963]. Burnham and Davis [1971] suggest that this pressure dependence is due to the high compressibility and activation volume for hydrous melting. Realizing that silicic melts are never truly dry or water saturated, Wannamaker [1986] examined the conductivity of water under-saturated melt and concluded that conductivity of melts is ~ 1 S/m when the melt is shallower than 8 km and can reach 10 S/m at greater depths (>25 km) in the presence of adequate water.

In order to estimate the possible melt conductivity in southern Tibet, the most important parameters are the temperature and water content of melt at a depth of 15-20 km. Thermal gradients are poorly defined in this region. Heat flow measurements give evidence of high gradients, and Francheteau *et al.* [1984] suggest that the 600° C isotherm could be in the depth range 10-25 km in southern Tibet. Direct evidence for temperature as a function of depth comes from the thermal history of rocks exhumed in the footwall of the Nyainqentangula Shear Zone. Harrison *et al.* [1995] showed that temperatures were at 600–700°C at a depth of ~ 17 km. Geological studies of Himalayan granites suggest that crustal anatexis occurred in the presence of water [Scaillet *et al.*, 1995; Debon *et al.*, 1986 and Guillot *et al.*, 1995]. Geodynamic modeling and earthquake studies give indirect information of temperature at depth

[Henry *et al.*, 1997, Chen and Molnar, 1983] and suggest temperatures at depths of 15-20 km could be as low as $\sim 400^{\circ}\text{C}$.

These lines of evidence suggest that temperatures in the mid-crust are too low for dry melting, but hydrous melting is possible. We conclude that a range of melt conductivity 1-10 S/m is to be expected (Figure 4.12).

4.5.2 Electrical conductivity of crustal saline fluids

Saline fluids are also good electrical conductors. Laboratory studies show that the electrical conductivity of a NaCl solution is strongly dependent on both pressure and temperature [Quist and Marshall, 1968, Sourirajan and Kennedy, 1962]. Figure 4.13 shows the variation of the critical point temperature as a function of pressure and salinity for a NaCl solution. The critical point for a liquid is defined as the pressure-temperature conditions at which gases and liquids can coexist. Given a minimum pressure required to keep a solution as a liquid, the conductivity of the solution will be independent of the pressure only when the temperature is lower than the critical temperature. Critical temperature and pressure are also functions of NaCl salinity. Below 0.1 molar concentration of NaCl, the critical properties of the fluid are similar to those of pure water. When the concentration of NaCl is higher than 0.1 molar, the critical temperature and pressure increase rapidly with increasing NaCl concentration. The temperature at which this behavior begins is 380°C . Below this temperature, the conductivity of the solution is relatively independent of the pressure.

Above this temperature, the conductivity value is strongly affected by the pressure [Olhoeft, 1981].

Given that geothermal brines have a lower temperature than the wet granite melting temperature, 650 °C can be considered the highest critical temperature for geothermal fluids. The critical pressure and salinity for this temperature are 110 MPa and ~25% in weight percent. So, for a solution with ~25 wt% NaCl concentration, the conductivity of the fluids will be independent of pressure because the fluid temperature must be lower than the melting temperature of the wet granite. The NaCl concentration of crustal fluids vary in a wide range, from a few weight percent to ~40 wt% [Jones, 1992], but very high concentration of salt (> 30 wt%) will lower the conductivity of the solution as it approaches the conductivity of the molten salt [Nesbitt, 1993]. In order to estimate a reasonable upper bound for the conductivity of the aqueous fluid, we will consider the 25 wt% salt concentration solution, since this is the highest salt concentration reported.

Although NaCl is the most abundant salt in crustal fluids, considerably more conductivity data for KCl solutions is available. Based on the available data, these two salt solutions have very similar conductivity values. Figure 4.14 shows conductivity of KCl solution as function of temperature and weight percentage. At the highest temperatures (500 °C) and KCl contents (24.7 wt%), the conductivity of the solution is ~100 S/m. Increasing the temperature above this value has a small effect on the conductivity, because the conductivity curve is flat above 200 °C. Increasing salt

concentration initially increases the electrical conductivity of the fluids, but no significant change should be expected at higher salinity than 25 wt%. Also, note that the conductivity of fluids may decrease when the salt concentration is higher than 30 wt% [Nesbitt, 1993]. Thus a reasonable upper bound for the saline fluid is ~ 100 S/m. It should be remembered that this is an upper bound and lower salinities, with correspondingly lower conductivities are equally possible.

4.5.3 Electrical conductivity of fluid bearing rocks

The overall conductivity of a fluid saturated rock depends on

- (a) The conductivity of the fluid,
- (b) The conductivity of the host rock,
- (c) The amount of fluid, and
- (d) The geometrical distribution of the fluid (*i.e.* its inter-connectivity).

In the previous two sections, we have discussed (a) for the case of the fluid being partial melt or aqueous fluids. The conductivity of the host rock is typically much lower than the fluid [Zhdanov and Keller, 1994]. We will show that this has little effect on the overall resistivity of a rock containing fluids. Our knowledge of (c) and (d) for crustal conditions is limited and based on indirect means and must be deduced from other related data (*e.g.*, seismic velocities and rock samples). The inter-connectivity is a key parameter since different fluid distributions can exist inside the solid rock texture. When the fluid is in isolated pockets, the bulk conductivity of the rock is controlled by the solid rock conductivity. As soon as a connected fluid

network is formed, electric current can flow along the conductive fluid paths and the overall conductivity of the rock will increase. The difference in bulk conductivity due to different fluid connectivity can be several orders of magnitude [Watanabe and Kurita, 1993]. Given the fluid conductivity and volume fraction, and the conductivity of the solid rock, several models can be used to calculate the bulk conductivity of the rock. Archie's Law [Archie, 1942] is an empirical expression relating fluid conductivity and porosity to bulk conductivity. Other models include the Hashin-Shtrikman (H-S) upper and lower bounds [Hashin and Strikman, 1962] and the modified brick-layer model [Macdonald, 1987]. While these models use different parameters to simulate the bulk conductivity of two-phase mixtures, they are all based on relatively simple parallel and series models [Maxwell, 1881]. For the H-S upper bound, the fluid is everywhere interconnected and the matrix and fluid are connected as parallel resistors and conductors. The overall conductivity of the circuit is dominated by the most conductive element. For the H-S lower bound, the fluid is separated by a resistive matrix. This formation is similar to a circuit where conductors and resistors are connected in series and the overall conductivity is dominated by the resistive elements. A comprehensive study of molten rock conductivity with different melt geometries and connectivity was reported by Schmeling [1986].

What degree of inter-connectivity should we expect for aqueous fluids and partial melt? Studies of fluid connectivity [Mibe et al., 1998 and Minarik et al., 1995]

show that both aqueous fluid and melt can form interconnected channels at very low fluid fraction. Roberts and Tyburczy [1999] showed that melt is typically found in tubes along grain boundaries and interconnects at relatively low melt fractions. Thus the bulk conductivity of the rock in their study was close to the Hashin-Shtrikman upper bound. The dihedral angle of aqueous fluids is an important factor in controlling the inter-connectivity of crustal fluids. When this angle is higher than 60° , fluids tend to isolate from each other. So connected fluids need a dihedral angle lower than 60° . Laboratory studies of dihedral angles for aqueous fluids [Watson and Brennan, 1987] indicate that increasing the amount of solute will decrease the dihedral angle to $\sim 40^\circ$ for quartz. Given the high concentration of the salt we consider in this study, a dihedral angle lower than 60° and inter-connected fluids networks are expected. Petrologic studies of the dihedral angle [Holness, 1998] also support aqueous fluid interconnection for a wide range of pressure and temperature conditions in middle and lower crustal rocks. Thus we use the Hashin-Shtrikman upper bound to estimate the bulk conductivity for fluid bearing rocks.

Figure 4.15 shows the relationship between the bulk conductivity and fluid fraction when the fluid is inter-connected. It shows melt with a conductivity of 3 S/m and 10 S/m, and aqueous fluids with 30 S/m and 100 S/m respectively. When the fluid fraction is small, the overall conductivity of the rock is heavily affected by solid rock conductivity even though a small amount of fluid can significantly increase the overall conductivity [Watanabe et al., 1993]. However, as the fluid fraction increases,

the bulk conductivity increases rapidly and the curves for different fluid conductivities separate. When the fluid fraction is higher than 5%, the bulk conductivity is close to a linear function of fluid fraction and the fluid conductivity becomes dominant. To investigate the effect of solid rock conductivity, a simple test is conducted. Figure 4.16 shows two different solid rock conductivities and a single fluid conductivity. When the fluid fraction is less than 5%, the solid rock conductivity has some effect on bulk resistivity. However, when the fluid fraction is higher than 5%, the effect of the solid rock conductivity is negligible.

4.6 How much fluid is there in the middle crust of southern Tibet?

In the previous section, we have shown that to compute the bulk conductivity of a rock, we need to quantify the fluid conductivity, its degree of interconnectivity and the fluid fraction. We have shown that estimates of these first two quantities can be made in the laboratory. Although theoretical and experimental studies [Schmeling, 1985 and Watanabe and Kurita, 1994] can provide guidelines for the relationship between fluid fraction and seismic velocity and electrical conductivity, the percentage of fluids *in situ* can only be determined from field data, and is one of the goals of our survey. Before determining the amount of fluid consistent with the MT data, we will review the possible fluid fractions determined by other means to gain an idea of the permissible range. Using geobarometric analysis, Scaillet *et al.* [1995] suggested that the High Himalayan Gangotri Leucogranite was emplaced into the cool country rock from a zone with 5~7% melting at a temperature of 700-800 °C.

Geophysical measurements also provide important information about the existence of fluid and their volume fractions. Studies on the effect of water and melt on seismic velocity [Watanabe, 1993] indicate that these two fluids can be clearly characterized by their compressive velocity, V_p . In principle, the fluid fraction and type of fluid can be deduced from a careful measurement of V_p and V_s . When the model proposed by Watanabe [1993] is applied to southern Tibet, the low seismic velocities ($V_p=3.0\pm 0.8$ km/s and $V_s=1.6 \pm 0.8$ km/s) and $V_p/V_s \sim 0.5$, suggest a fluid fraction of $\sim 15\%$ and possibly favor the existence of free water [Makovsky and Klemperer, 1999]. The reflection coefficients estimated by Ross *et al.* [2001] also suggest a high fluid fraction. The large reflection coefficients (-0.4 to -0.6) are best explained by $\sim 15\%$ free water or pure melt. Another parameter that can be used to quantify the amount of fluid in the crust is Poisson's ratio, which varies between 0.25 and 0.5. A low ratio (<0.3) can have a variety of composition implications [Zandt and Ammon, 1995]. Because pure fluid has a Poisson's ratio of 0.5, an increase of the bulk Poisson's ratio (>0.3) may indicate the existence of fluid in the crust [Owens and Zandt, 1997]. The low-to-normal Poisson's ratio in southern Tibet seems to contradict the hypothesis of widespread partially molten middle crust [Owens and Zandt, 1997], but it is quite possible that a thin partially molten layer may exist beneath southern Tibet. Nelson *et al.* [1999] showed that a 20 km thick, 10% partial melt layer can be sandwiched by a relatively low Poisson's ratio upper crust and a normal Poisson's ratio lower crust, and still give a normal average for the whole crust.

Fluid fraction can also be estimated from the electrical conductivity of the Earth. Given the bulk conductivity of a fluid bearing rock, if we know the fluid and solid rock conductivity, then fluid fraction can be estimated. Application of this approach can be found in Schilling et al. [1997] and Partzsch et al. [2000]. In general, the conductivity of rocks deep in the crust can not be directly measured except for samples from deep drilling holes. So the conductivity information in the deep crust is more often obtained from modeling and inversions of MT data collected on the surface of the Earth. For a set of MT data, model conductivity can vary significantly. Therefore, the fluid fraction estimation based only on model conductivity may be unreliable. Using a conductivity of 0.3 S/m, Partzsch et al. [2000] estimate 4 to 9 vol% melt for the Tibetan Plateau and similarly, Schilling et al. [1997] argue for 14 to 27 vol% melt for the Western Cordillera of the Andes of Chile and Bolivia based on the 1 S/m conductivity in their MT model. The local value of resistivity in an MT model strongly depends on the resolution of the inversion. Finite resolution smooths out the peaks and valleys. This makes it hard to know the actual conductivity value although integrated properties (such as conductance) may be well determined. So, we suggest that estimation of fluid fraction based on electrical conductivity of a model should be used with care. Other information, such as seismic data, should be included in order to achieve a reliable fluid fraction estimation.

4.7 Three possible physical models for southern Tibet

An infinite number of possible conductivity models exist to explain our data and to detail all of them is impossible. We are choosing instead to discuss a range of physical models that can explain a bound on all the conductivity models. As discussed above, fluids are almost certainly responsible for the high electrical conductivity observed by the MT surveys in southern Tibet. Therefore, three possible physical models are considered (Figure 4.17). The high conductivity could be due to (a) partial melt, (b) aqueous fluids or (c) a combination of partial melt and aqueous fluids. These physical models have also been suggested by INDEPTH seismic data [Nelson *et al.*, 1996; Ross *et al.*, 2001; Makovsky and Klemperer *et al.*, 1999]. In the following discussion, we will calculate what combinations of porosity, thickness and fluid are required in cases (a)-(c) to explain the minimum conductance of 6,000 S. The consistency of each model with other geological and geophysical data will be discussed. Note that depth-dependent porosity and/or salinity is possible, but our data can not resolve this information. So, in all the physical models we discuss below, a uniform porosity or salinity has been assumed within a fluid-containing layer.

4.7.1 Partial melt only

To account for the minimum conductance of 6,000 S, a layer of partial melt can have a range of porosity-thickness combinations. This is illustrated in Figure 4.18, where it can be seen that as the fluid (melt or saline fluid) fraction rises, the thickness of the layer decreases. For example, if the layer comprised 10% melt with 10 S/m

conductivity then it would need to be ~9 km thick. Note that in the above calculations, we have assumed that the melt has the upper limit of the range of permissible conductivity values. Thus this thickness is a lower bound for a 10% partial melt. Figure 4.18 also shows the same information, but with the melt conductivity lowered to 3 S/m. Here we can see that if there is 10% partial melt, a layer of 30 km is required to produce the minimum conductance of 6,000 S. Lowering the percentage of partial melt requires a thicker layer and a thinner layer is required if the percentage is increased. Because of the physics of the MT method (Figure 4.5), data error and site sparseness, MT cannot distinguish between models of equal conductance (*i.e.* a high melt fraction – thin layer gives the same observed response as a thick, lower melt fraction layer). Thus, other geophysical observations are needed to discriminate among possibilities. For instance, if the partial melt is coincident with the seismic low velocity zone observed by Kind et al. [1996], then it would be about 20 km thick. This would imply a ~ 4% partial melt for 10 S/m melt or 14 % for 3 S/m melt. If we assume a 10 % partial melt, then the melt conductivity must be lower than 10 S/m or the true conductance must be at least a factor of two higher than the lower bound.

4.7.2 Pure melt layer

However, the previous model cannot explain the observed large seismic reflection coefficient and low P- wave velocity associated with seismic bright spots [Ross et al., 2001 and Makovsky et al., 1999]. The observed high conductance in

southern Tibet could also be generated by a thin layer with a higher melt fraction, or even a completely molten layer. If we allow for pure melt with the maximum permitted conductivity of 10 S/m, a 600 m thick layer is required to produce 6,000 S conductance. Although a thin layer of high fraction melt can account for the MT data and seismic reflections, complete melting requires a temperature in excess of 900 °C [Murase, *et al.*, 1973]. Various lines of evidence suggest this temperature is unlikely to occur at a depth of 15 km [Chen and Molnar, 1983; Henry, *et al.*, 1997; Ross, *et al.*, 2000] and would not be able to produce the thick mid-crustal low velocity zone discussed in the context of the last model. Thus it is unlikely that the MT conductance can be explained by a thin, high fraction melt layer alone.

4.7.3 Pure melt over partial melt.

A composite model with pure melt over partial melt is observed in seismic studies of mid-ocean ridges [Navin *et al.*, 1998]. Seismic waveform modeling [Ross *et al.*, 2001] shows that a 37 m thick layer of pure melt over a 185 m partial melt layer (Figure 4.19, model 1) could produce the measured reflection coefficient in southern Tibet. However, this model has a conductance of just 600 S if the melt has a conductivity of 10 S/m. With 3 S/m melt, the conductance is only 200 S. Clearly additional melt at greater depths is needed to produce the minimum 6,000 S conductance.

4.7.4 Model with only aqueous fluid.

Alternatively, a layer of water-saturated rock could explain the high conductance in southern Tibet. Using an upper bound fluid conductivity of 100 S/m, the fluid fraction-thickness combinations consistent with 6000 S are also shown in Figure 4.18. Note that with the higher conductivity of the saline fluid, a thinner fluid layer is required to explain a specified conductance (*i.e.* a lower porosity or reduced thickness). For example, with 10% porosity, a layer only 0.9 km can produce 6000 S conductance. With a lower fluid conductivity of 30 S/m, the layer increases to 3 km. (see Figure 4.18).

A thin water saturated layer can explain both the observed MT and seismic reflection data [Ross *et al.* 2001; Makovsky and Klemperer, 1999]. It is also consistent with studies that suggest lower crustal temperatures in southern Tibet. These include the study by Chen and Molnar [1983] that showed earthquakes to a depth of 15 km. If this depth corresponds to the brittle-ductile transition, a temperature of 350° C can be inferred. Thermal modeling also suggests a temperature of this order at the depths of the bright spots [Henry *et al.*, 1997 and Ross *et al.*, 2001]. However, a thin layer of aqueous fluids is inconsistent with the INDEPTH passive seismic data [Kind *et al.*, 1996] that detected an ~20 km thick low velocity zone. It is of course possible that an aqueous layer would have a porosity that varies with depth. Ross *et al* [2001] showed that one such model (Figure 4.19, model 3) that gave a good match to the observed seismic reflection amplitudes and waveforms.

Assuming that the aqueous fluid has a conductivity of 100 S/m, then model 3 has a total conductance of only ~2000 S. With a lower fluid conductivity of 30 S/m, the conductance is only ~500 S. Clearly additional conductance is again needed to satisfy the MT data. This could be either a zone of lower porosity aqueous fluids or partial melt below the high porosity layers in model 3.

4.7.5 Water and partial melt

The MT data are consistent with both models (a) and (b) in Figure 4.17. However, as already discussed, (a) and (b) are both inconsistent with various other aspects of the geophysical and geological data in southern Tibet. Is a model with a combination of partial melt and aqueous fluids the optimal solution? Seismic data give some support for this interpretation. Makovsky and Klempner [1999] showed that the bright spots have amplitude-versus-offset characteristics consistent with an aqueous layer. However, the waveform study of Ross *et al.*, [2001] showed that a thin layer of water over partial melt (Figure 4.19, Model 2) can also produce the measured reflection amplitudes. Model 2 has a maximum conductance of ~2,000 S and model 3 has a maximum conductance of 1450 S, much less than the minimum conductance of 6,000 S. Thus, at least an additional 4,000 S of conductance are required to satisfy the MT data. The MT data are consistent with either partial melt or aqueous fluids below the thin layer in Model 2 and 3. However, other data suggest that partial melt is a more plausible explanation. This includes geological observations that imply that widespread crustal melting generated the granites now exposed in the Himalaya [Le

Fort, 1987; Debon *et al.*, 1986; Scaillet *et al.*, 1995]. The geophysical data that support widespread melting include the seismic observations listed above, and the satellite magnetic data modeled by Alsdorf and Nelson [1999]. A pronounced satellite magnetic low is identified on the Tibetan Plateau and a hot, partially molten crust has been suggested to be responsible. In addition, the geothermal phenomena in the Himalayan Geothermal belt [Hochstein and Regenaer-Lieb, 1998] and the associated high heat flow also favor melting as a heat source since the large scale of this belt (>1000 km) made deep circulation of surface a unlikely candidate.

4.8 Conclusions and tectonic implications

Based on the INDEPTH magnetotelluric data and other available geophysical data, we argue that a model with a thin (~200 m) 10-15% porosity aqueous fluid layer overlying a thick (>10 km) ~10% partial melt layer is preferred to explain the high crustal conductance in southern Tibet. The data that favor the saline fluid layer include wide-angle reflection data [Makovsky and Klemperer, 1999] and the upper crustal low temperature inferred by a number of studies [Chen and Molnar, 1983; Henry *et al.*, 1997 and Ross *et al.*, 2001]. The thick partial melt layer at depth is consistent with the passive seismic data [Kind *et al.*, 1996]. Note that these porosity estimates are mainly based on geophysical data and more investigations are necessary to provide detail geological explanations. For example, is the 10% partial melt sustained over a long geological time or it is recharged continuously? What is the origin of the aqueous fluids? One possibility is that they are derived from the cooling

of the deeper partially molten system. When wet crustal melts from the deep crust rise up to a depth where the temperature approaches the solidus, they crystallize. Then a phase rich in free water can separate from the saturated melt and collect above the cooling melt layer [Jahns, 1982].

Additional insight into the cause of the high crustal conductance in southern Tibet can be derived from comparison with other tectonically active areas. Worldwide, large-scale, high crustal conductances are often found in active orogens. For instance, observations of extremely high crustal conductance have been reported in both the Andes [20,000 S, Echtermacht *et al.*, 1997; Brasse *et al.*, 2000] and the Pyrenees [30,000 S, Pous *et al.*, 1995]. These authors also attribute the high conductance to partial melting. High conductances are also found in extensional environments; For instance, Wannamaker *et al* [1997] reports a very uniform conductor that underlies the Eastern Great Basin (Nevada and Utah) and attributed this to aqueous fluids overlying partial melting.

In this study, we have shown that study of crustal conductance may be used to address the nature of the proposed fluid in Tibet. We have shown that the regional conductance beneath the 200-line is at least 6,000 S, and near the Damxung Graben it can be as high as 30,000 S. If this were due to just 10% partial melt, a thickness range of 8 km to more than 30 km is possible (given that true conductance may be higher than 6,000 S and melt conductivity could range from 3 to 10 S/m). Alternatively, this conductance could be due to a layer of 10% aqueous fluids with a

thickness that varies from 0.9 km to at least 3 km (with 6,000 S and 30-100 S/m fluids). Finally, based on the available geophysical data and thermal models of southern Tibet, we suggest that the high conductance in southern Tibet may be best explained by a thin layer of saline fluids overlying a thick partially molten zone.

The layer conductance that we have accounted for by a zone of fluids shows significant lateral variations. This could be due to changes in (a) the porosity within the layer, (b) the layer thickness (c) the degree of interconnection or (d) the conductivity of the fluid. Changes due to (d) are less likely than (a)-(c) since fluid composition depends on the subsurface geology, rather than pressure or temperature. Thus, lateral changes in the conductance have the potential to determine where more fluid is present, or alternatively where the fluid is most effectively connected.

The widespread distribution of fluids is important since fluids can dramatically alter the rheology of a rock. When the melt fraction is close to a critical melt fraction (20%-55%) [Renner *et al.*, 2000], the rock loses significant strength [Renner *et al.*, 2000]. The presence of partial melt at much lower melt fractions also has mechanical effects, and is typified by enhanced creep rates and slow deformation [Cooper and Kohlstedt, 1986]. Aqueous fluids can also weaken a rock and enhance creep rates through a range of mechanisms [Etheridge *et al.*, 1984; Tullis *et al.*, 1996]. A weakened layer in the mid or lower crust is required in geodynamic models that account for lithospheric deformation through crustal flow [Royden *et al.*, 1997; Clark and Royden, 2000]. Thus, observations of a pervasive layer of crustal fluids in

southern Tibet show, in principle at least, that large crustal flow could be occurring beneath southern Tibet. The lower crustal flow can then accommodate the on-going east-west extension on the plateau and maintain a flat but highly dynamic plateau. The lateral variations in crustal conductance described above might also be significant in this context. If regions of high conductance are due to the highest fluid content or best fluid connection, then they might also represent the zones of most active crustal deformation, since they will be the weakest owing to the enhanced fluid content.

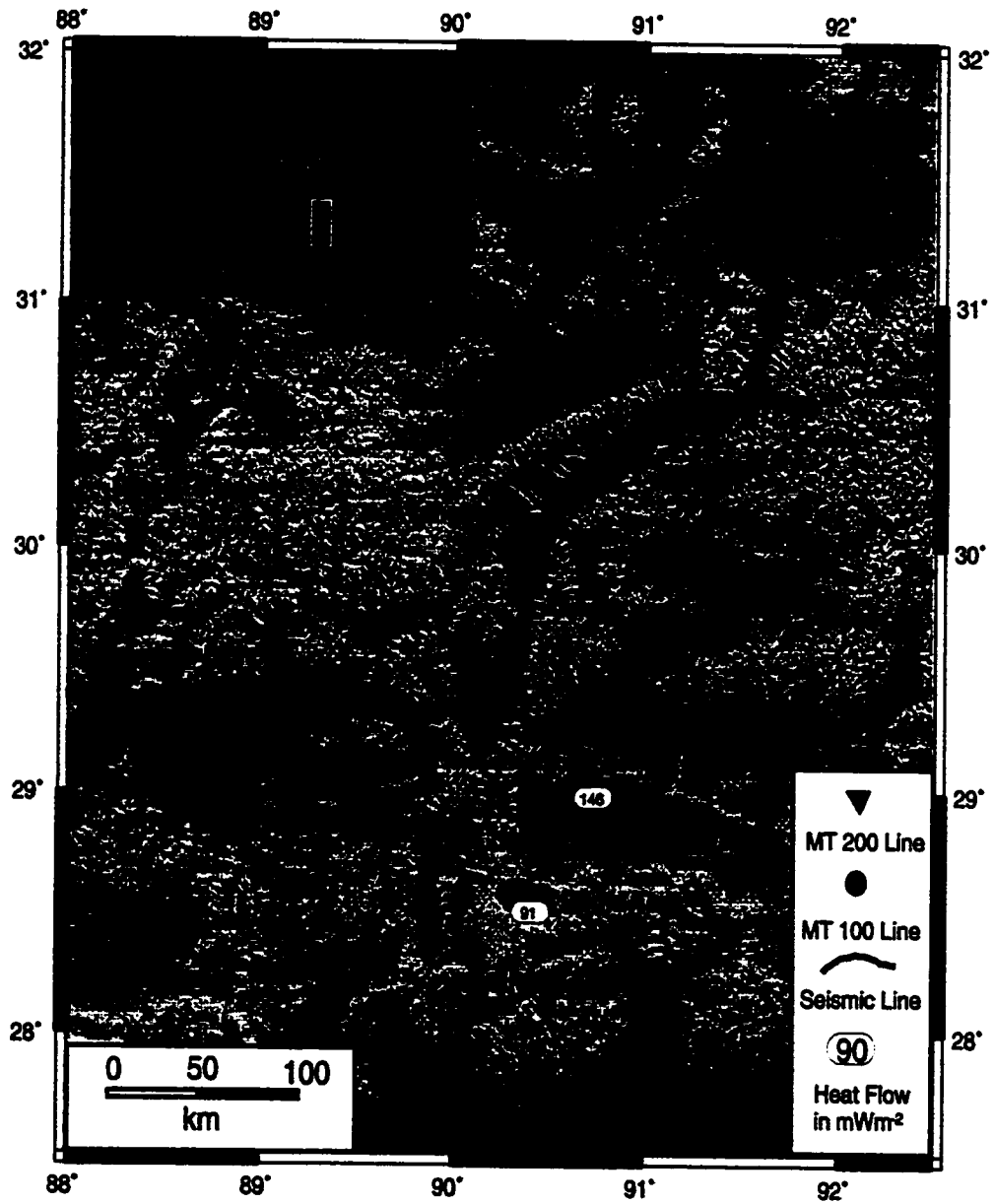


Figure 4.1 Location map of Tibet 200 Line.
INDEPTH seismic profile and heat flow data are also shown.

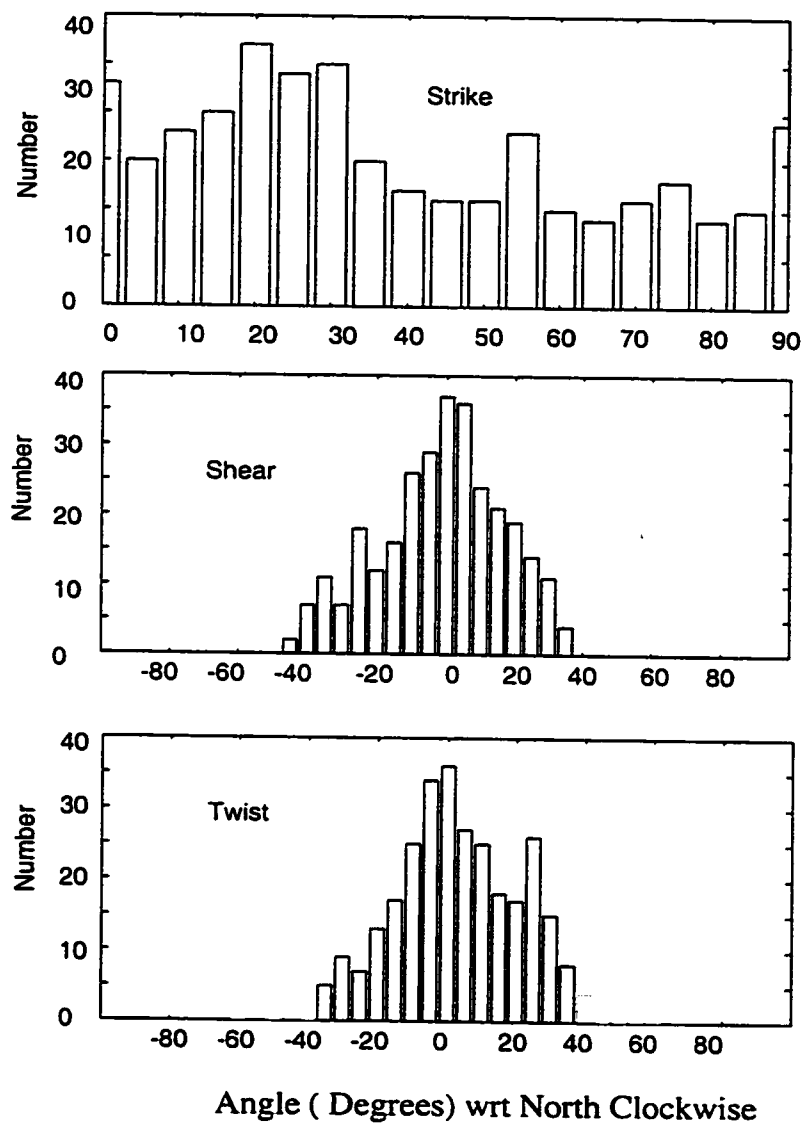


Figure 4.2 Histograms of Strike, Shear and Twist for single site, single frequency data analysis

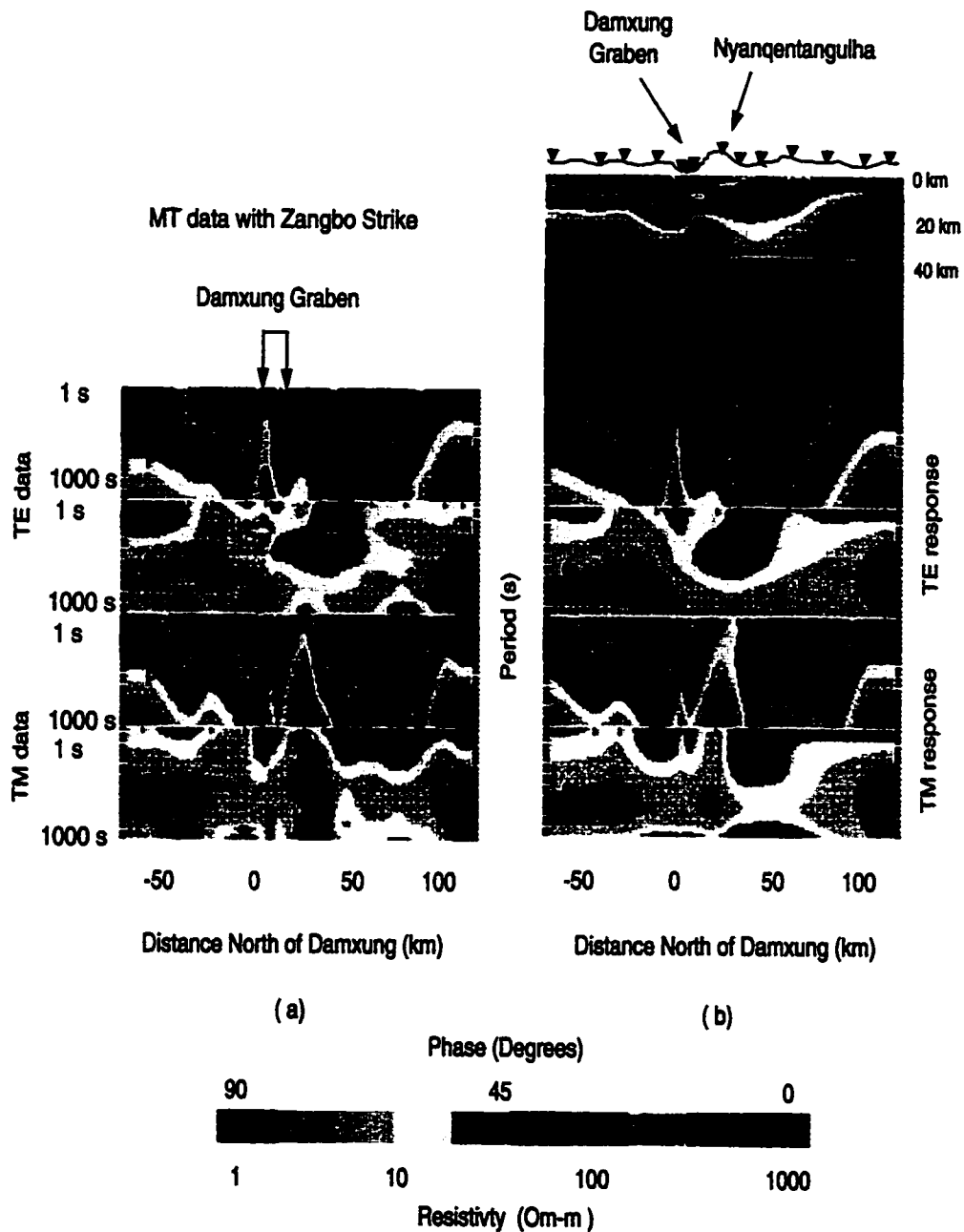


Figure 4.3 (a) 200 line MT data in Pseudosection form. Also shown are the MT responses of the inversion model (b) with EW strike.

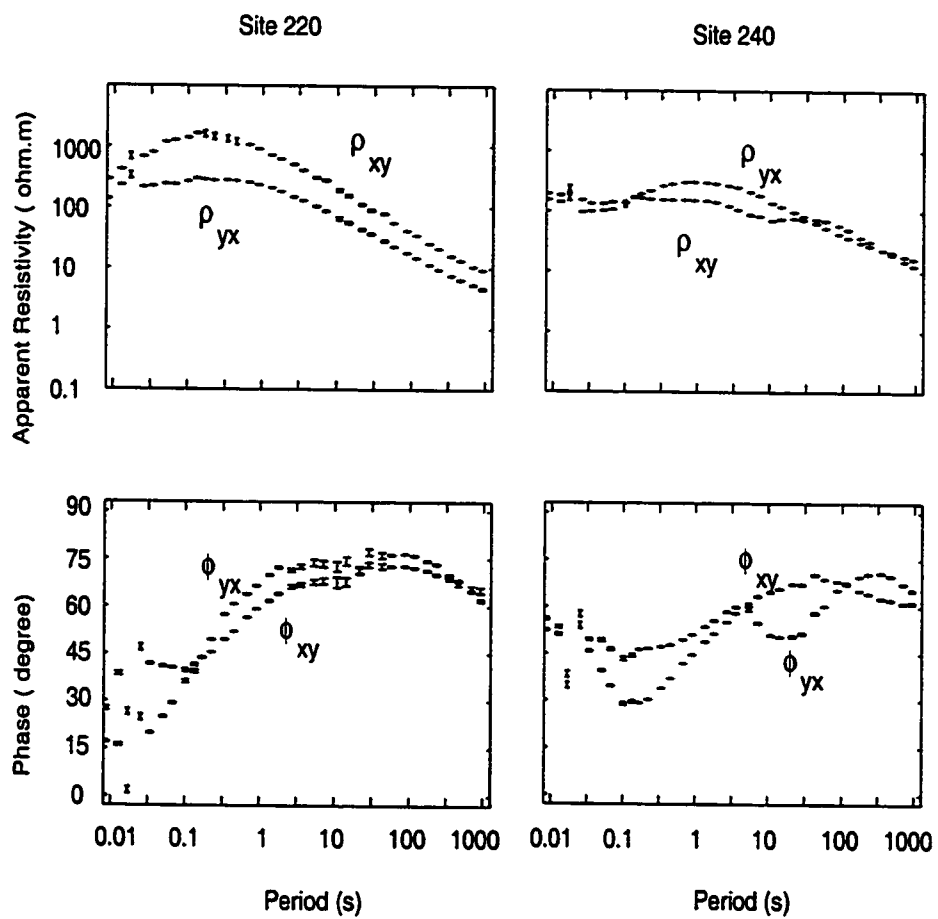


Figure 4.4 Measured MT data at site 220 and 240.
Data are shown in measured coordinate.

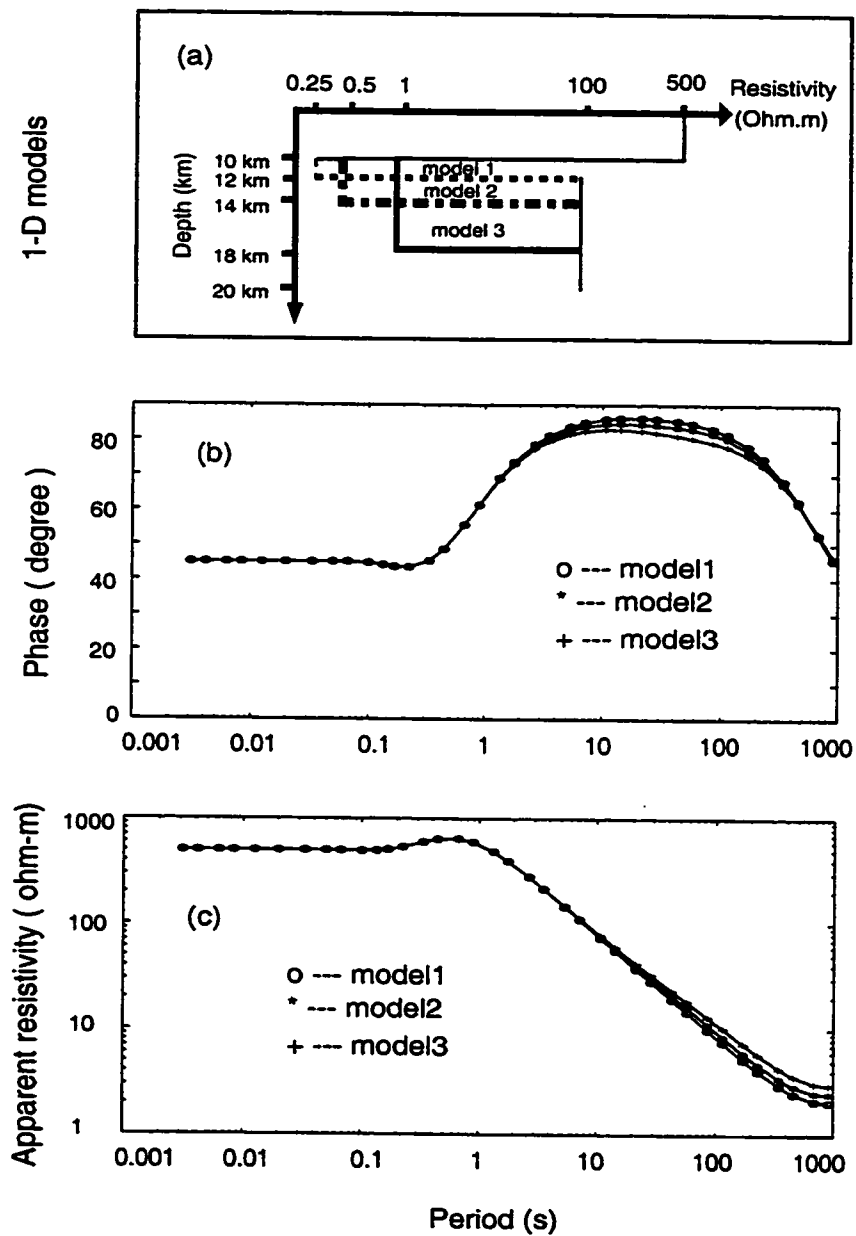


Figure 4.5 1-D models and their MT responses.
 (a) Three 1-D models with 8000 S conductance.
 (b) Phase responses of the three models.
 (c) Apparent resistivity responses of these models.

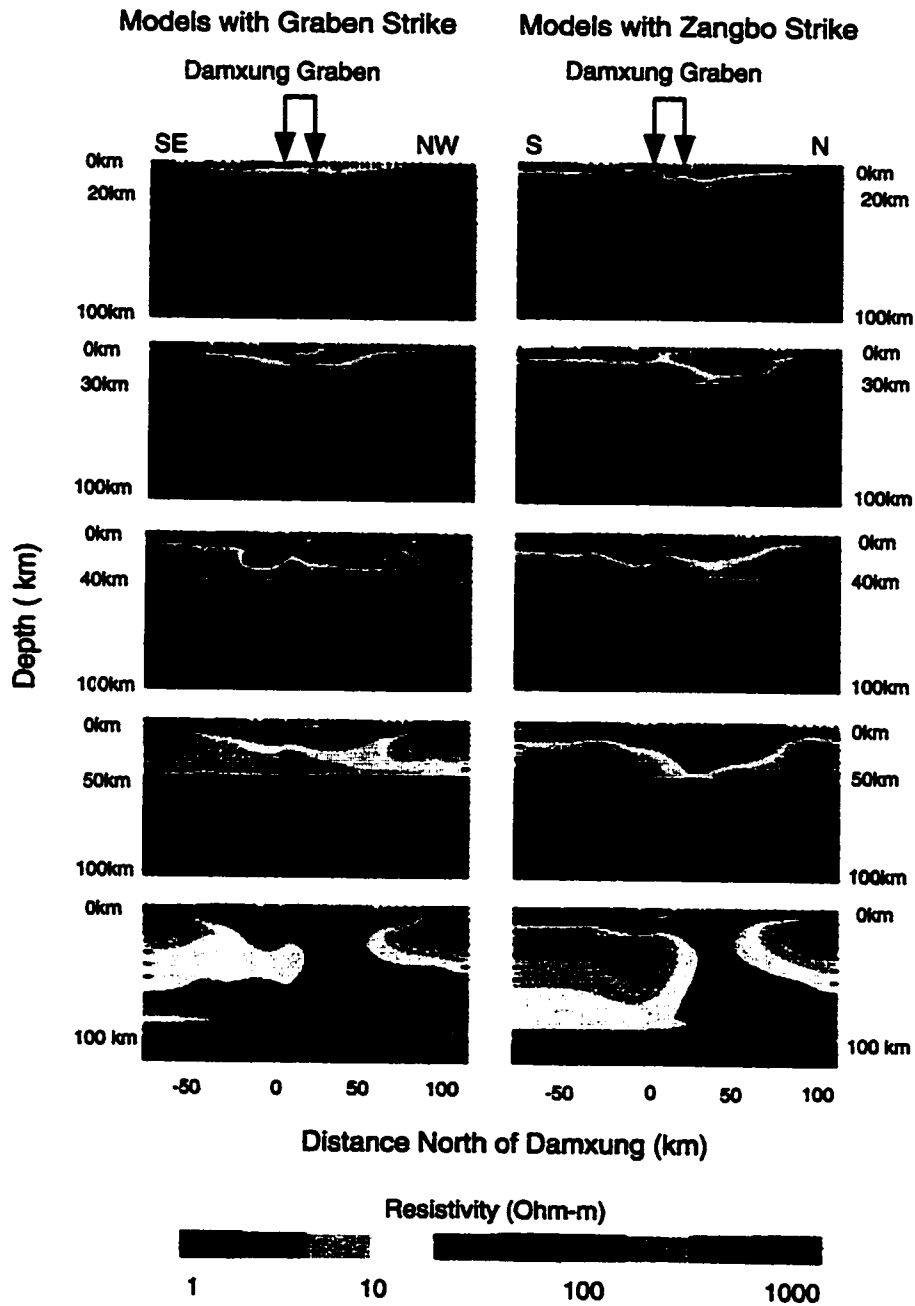


Figure 4.6 Conductivity models inverted from 200 line data. Models on the right are using EW strike and models on the left are from graben strike.

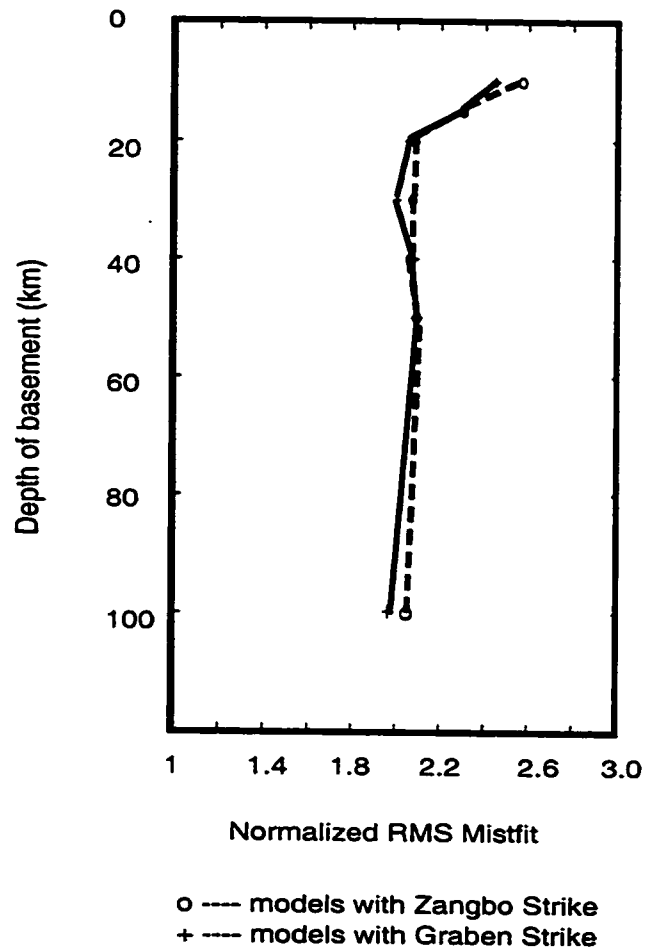


Figure 4.7 Data misfit of constrained inversion. Depth of the basement indicates the depth below which the model becomes fixed during inversion.

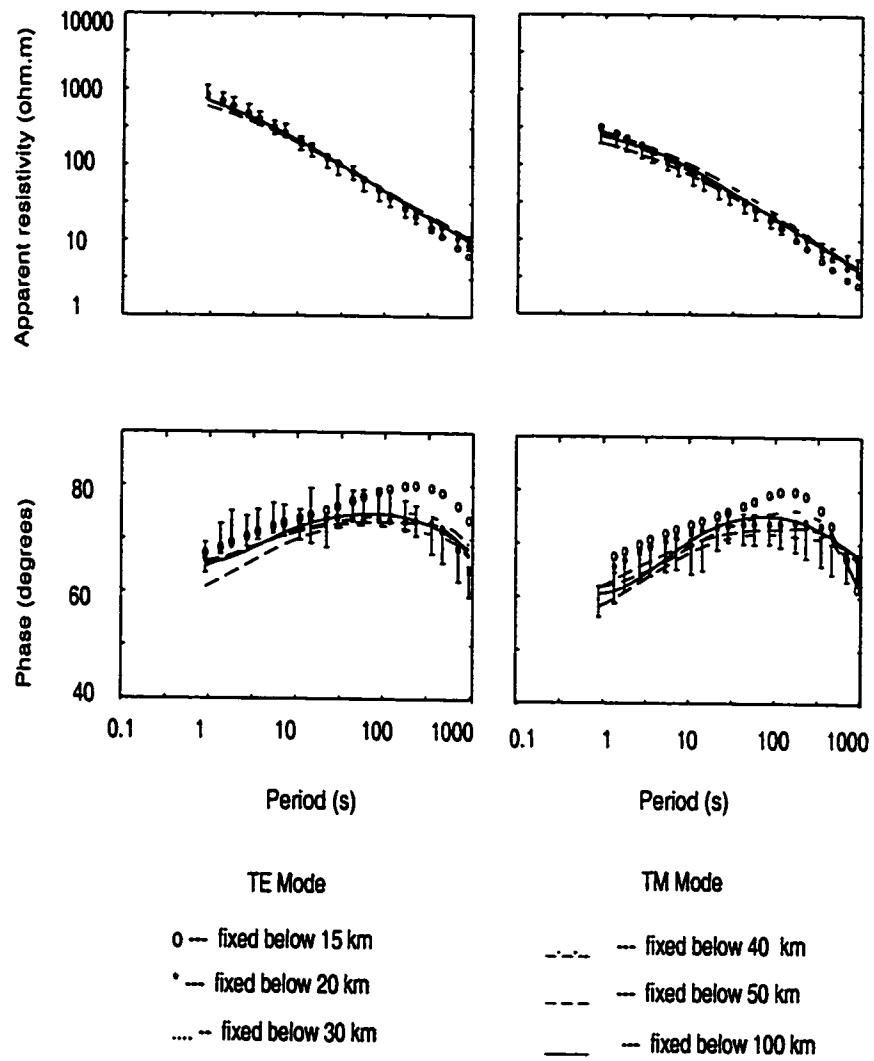


Figure 4.8. TE and TM responses of a set of models with EW strike and observed data at site 220.

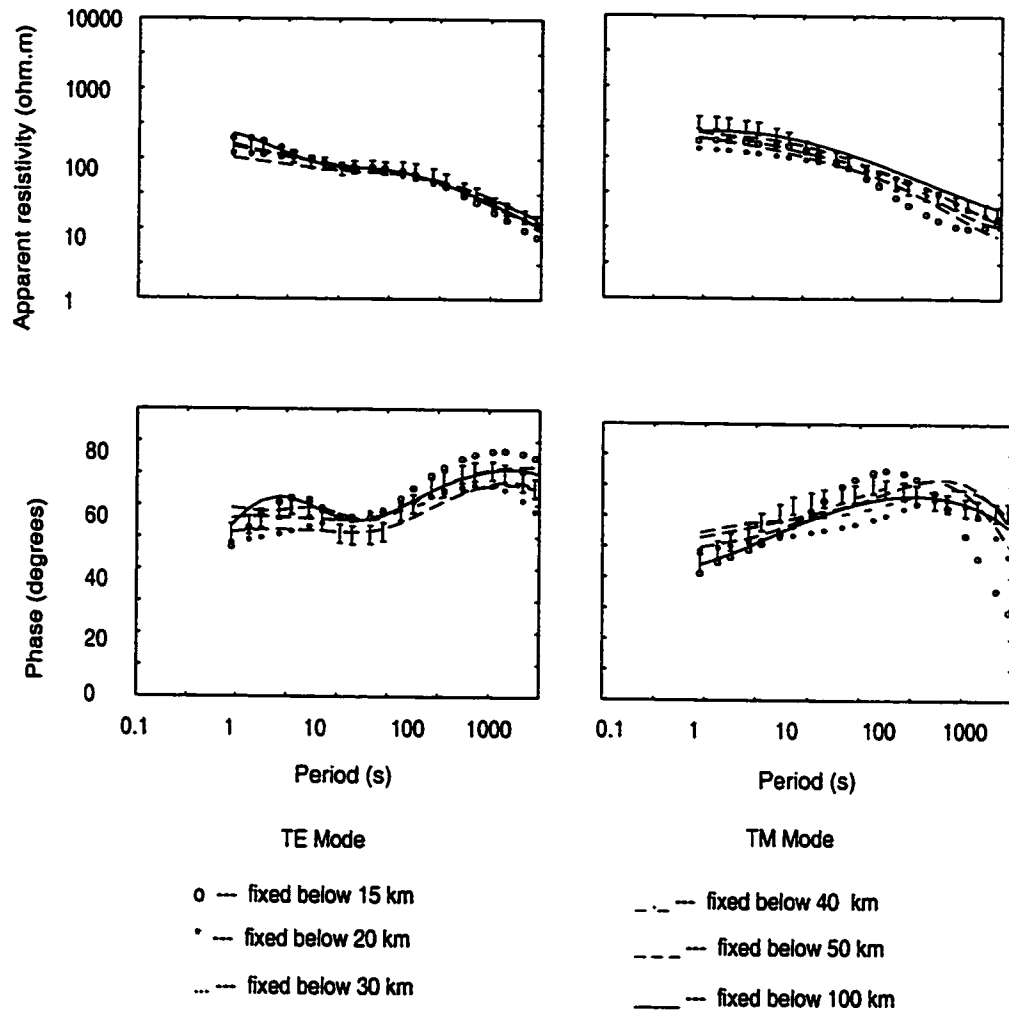


Figure 4.9. TE and TM responses of a set of models with EW strike and observed data at site 240.

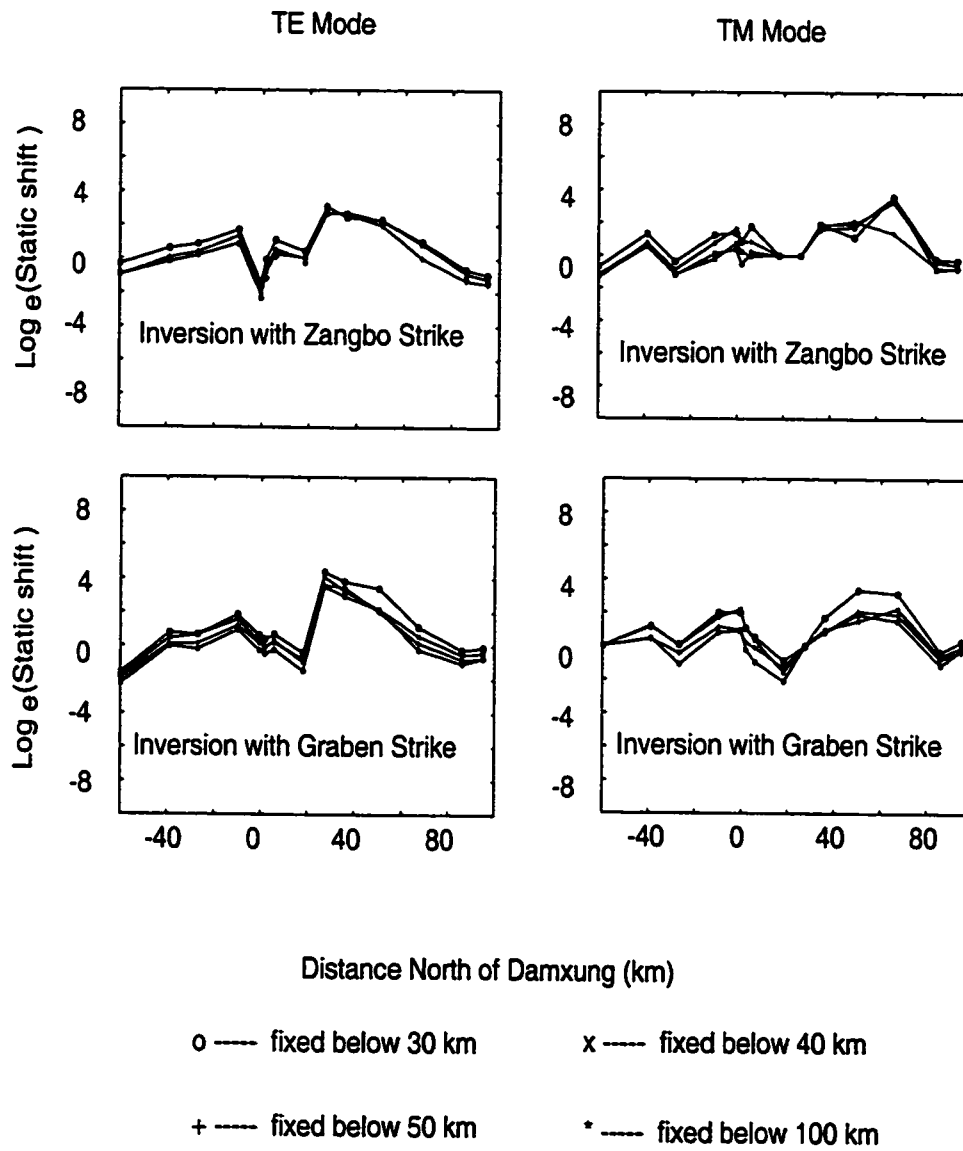


Figure 4.10 Static shift coefficients for 200 line data

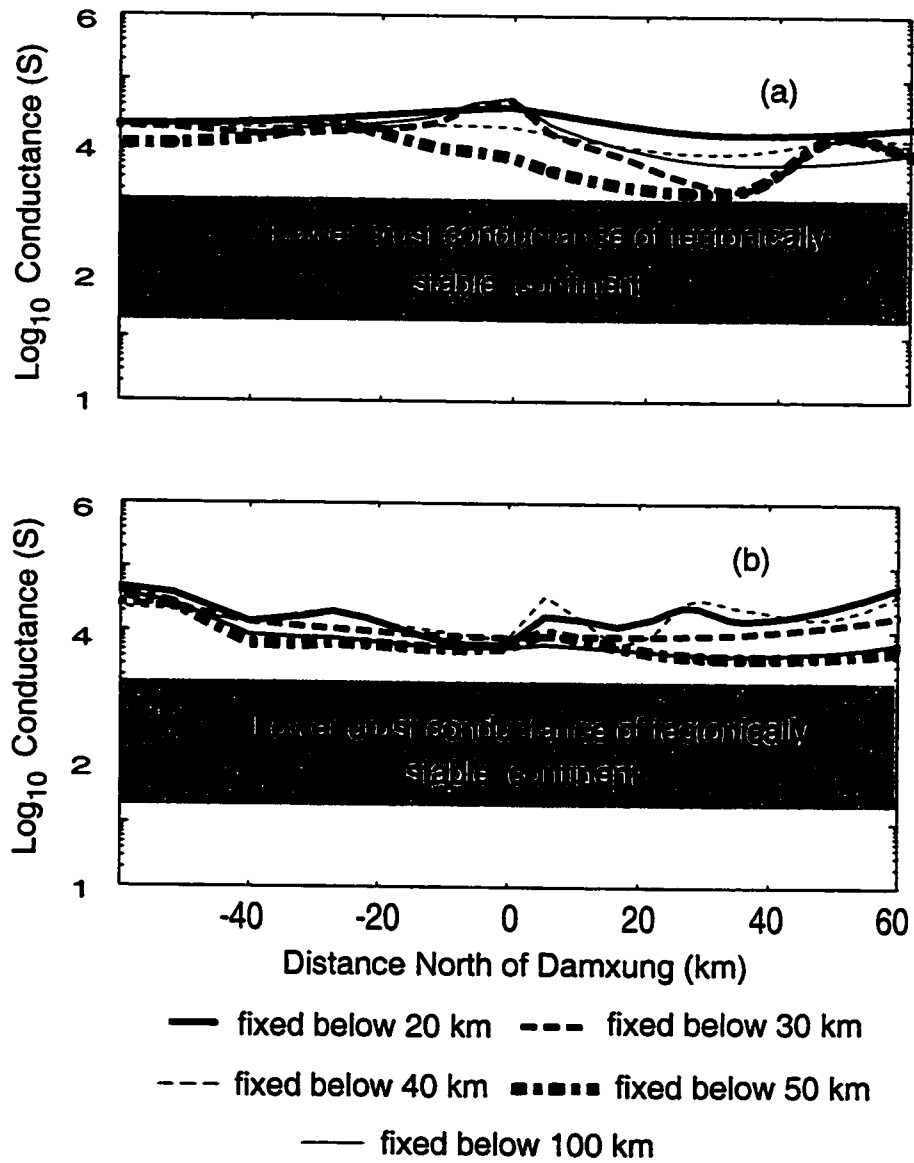


Figure 4.11 Model conductance for Tibet 200 line.
 (a) Conductance are shown for models with EW strike
 (b) Conductance are shown for models with graben strike

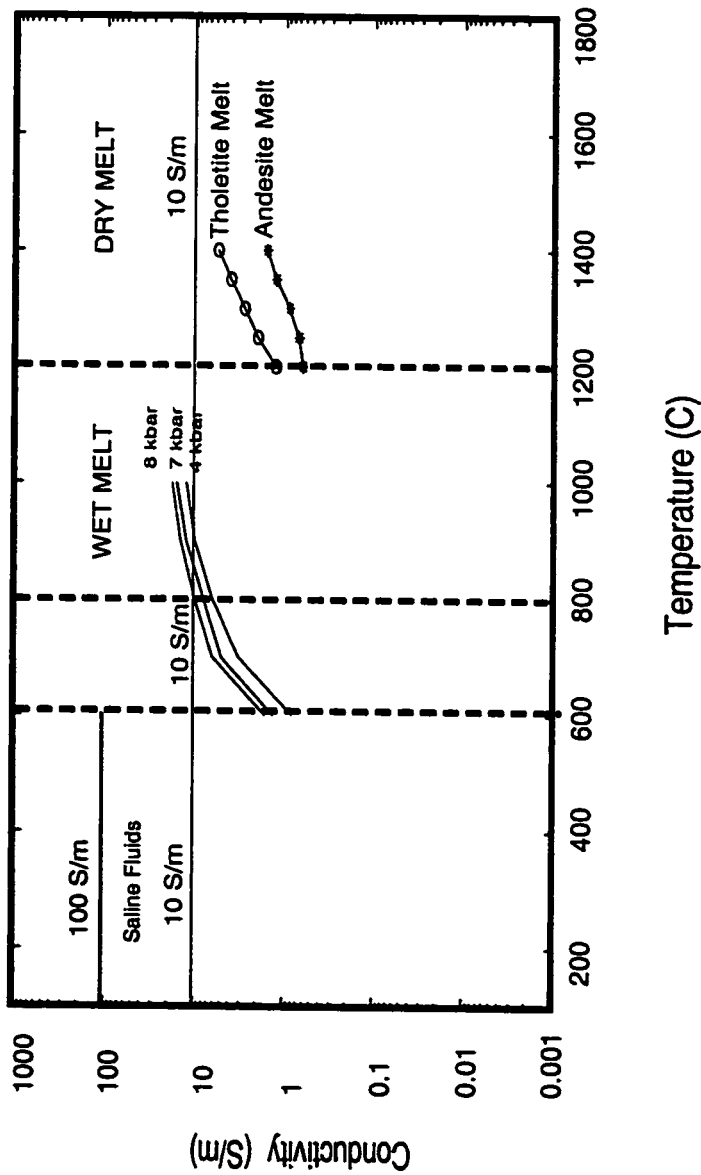


Figure 4.12. Electrical conductivity of melts and saline fluid
 Wet melt data are from Lebedev et al.[1964] Dry melt data are from Tyburczy et al. [1983]
 The maximum conductivity for saturated saline fluid is 100 S/m and maximum conductivity
 for melt in southern Tibet is 10 S/m with a temperature of 800° C.

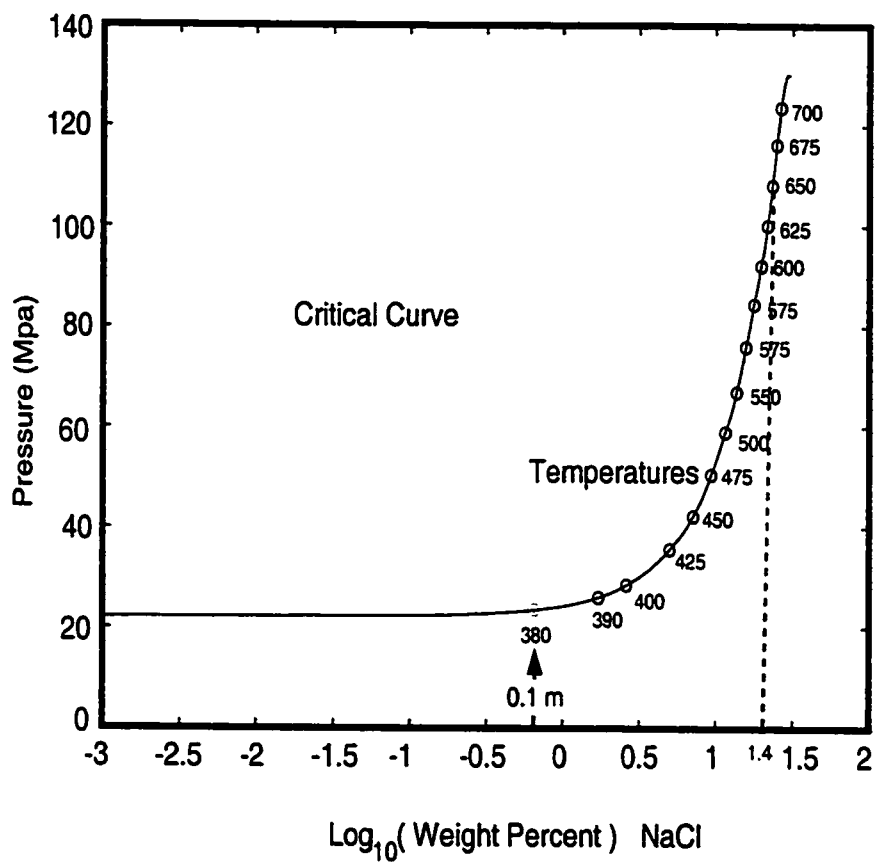


Figure 4.13 The Pressure-temperature and salinity critical curve for NaCl. (after Olhoeft, 1981)

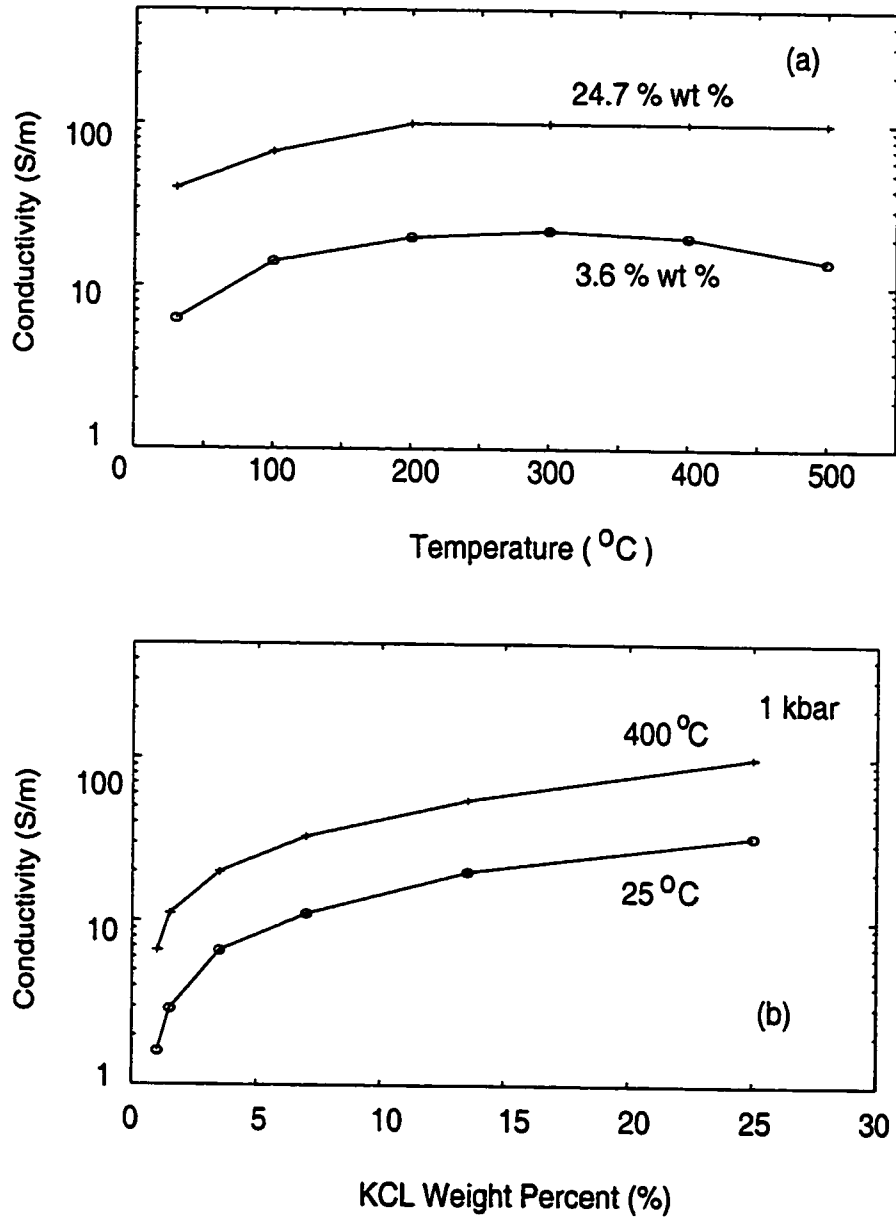


Figure 4.14 Conductivity of KCl solution as function of temperature and weight percentage.

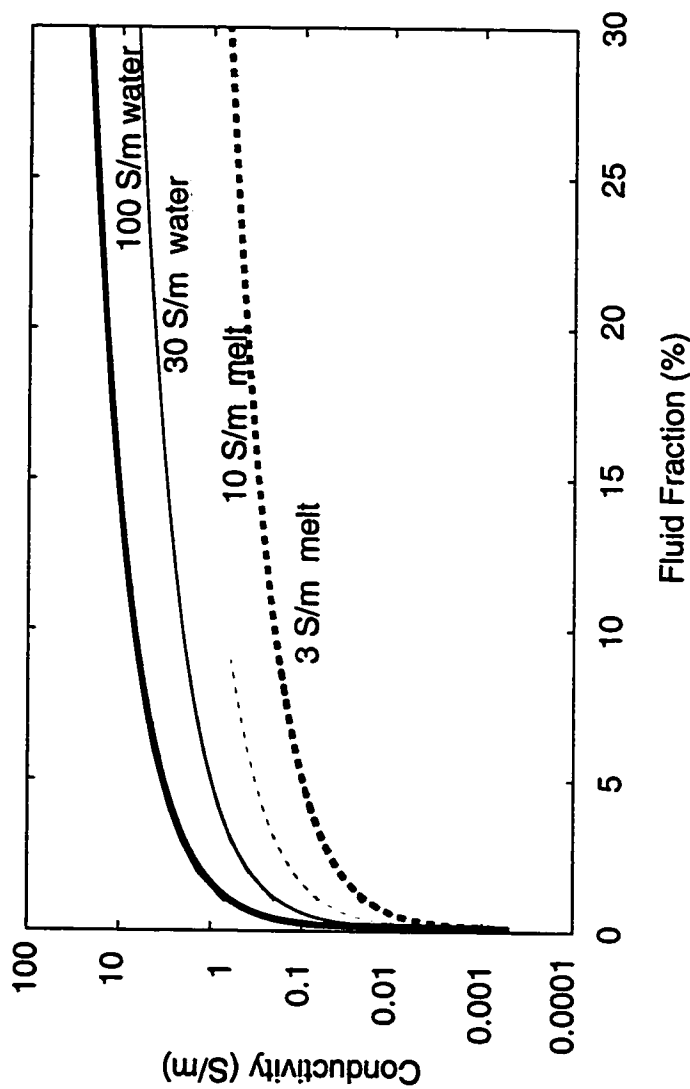


Figure 4.15 Bulk conductivity of fluid bearing rocks. Curves are calculated from Hashin-Strikman upper bound and solid rock conductivity is 0.0005 S/m. The conductivity of saline fluid are 100 S/m, 30 S/m and melt are 10 S/m and 30 S/m

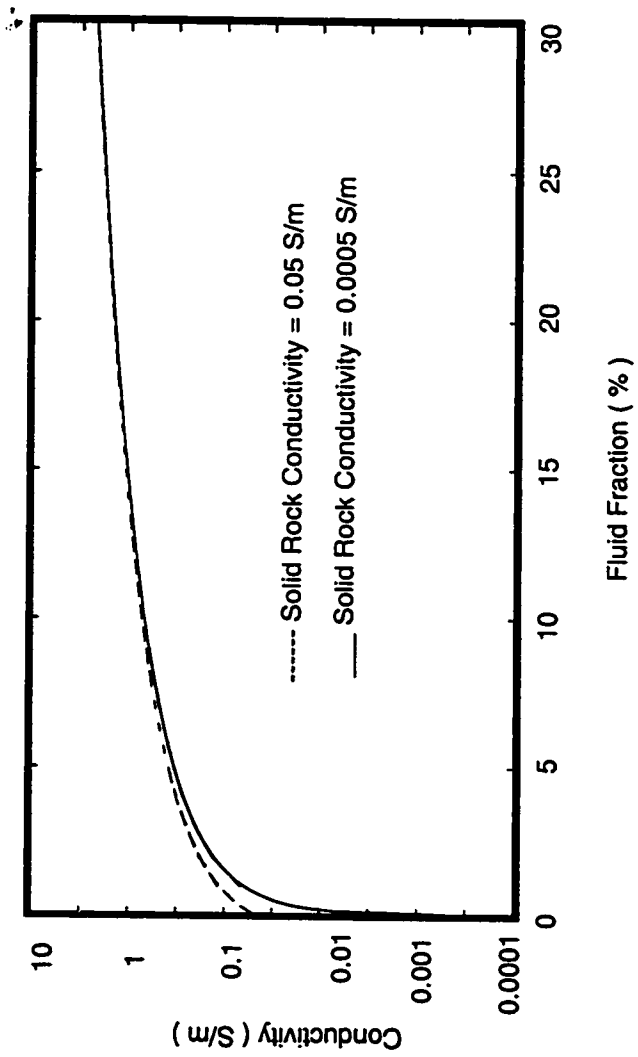


Figure 4.16 Effect of solid rock conductivity on bulk conductivity

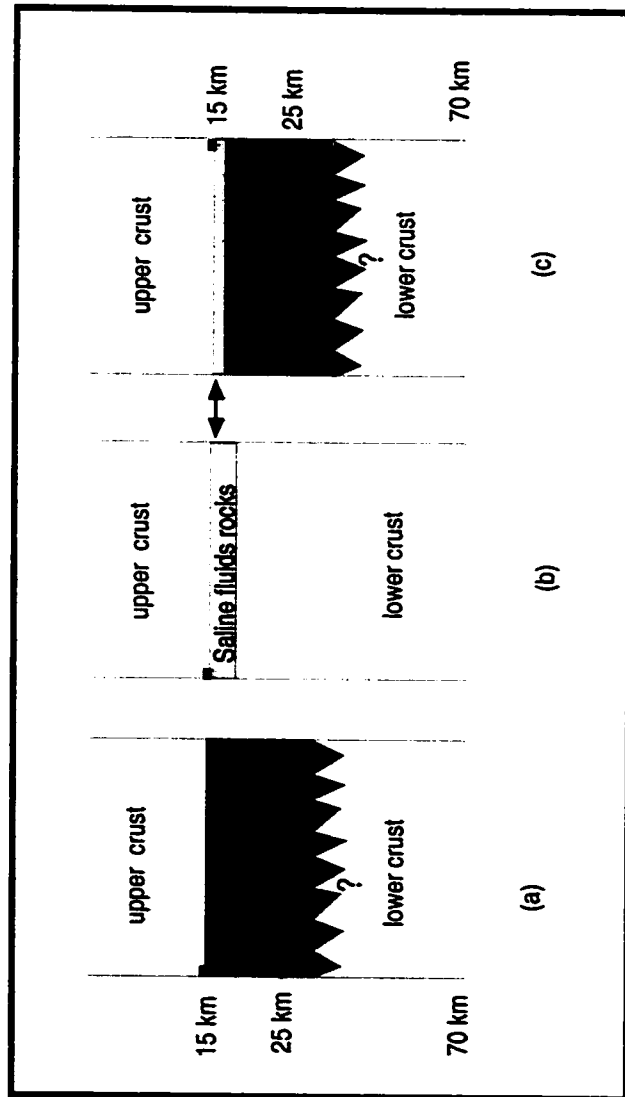


Figure 4.17 Three schematic models for southern Tibet.

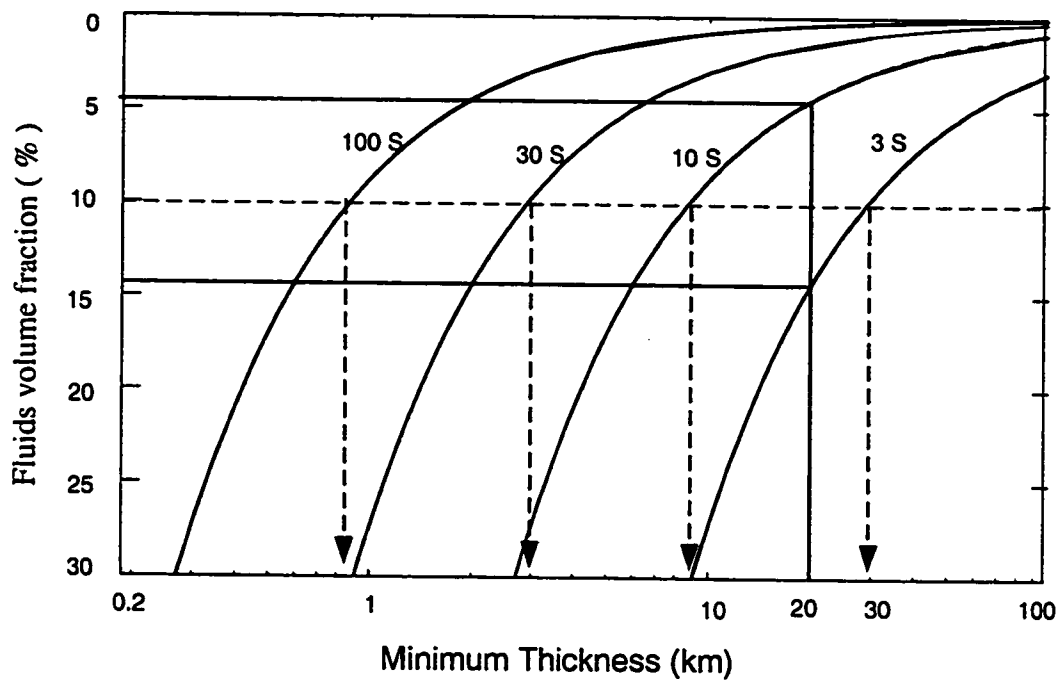


Figure 4.18 Thickness as function of fluid volume fraction and fluid conductivity.

Many combinations of thickness, fluid fraction and fluid conductivity can produce the 6,000 S conductance required by MT data. Given a range of fluid conductivities (3S - 100 S) and 10 % fluid fraction, the thickness required by MT data can vary from 0.9 km to 30 km.

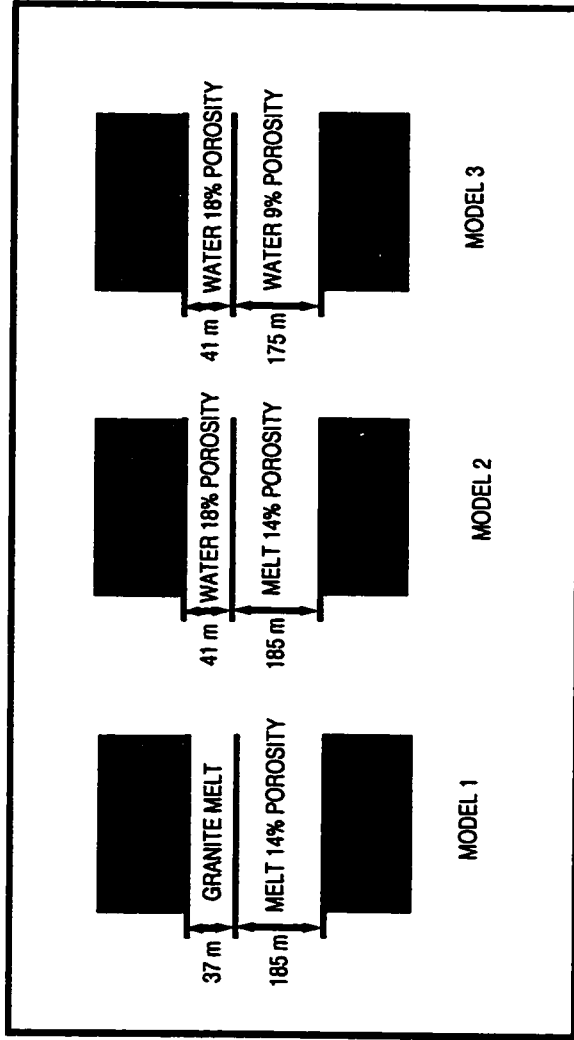


Figure 4.19 Possible models for Damxung Bright Spots.
 (a) all melt model (b) all water model (c) mixed mode.
 (Modified from Ross et al., 2000)

CHAPTER 5

RESISTIVITY STRUCTURE OF CENTRAL TIBET AND ITS TECTONIC IMPLICATIONS

5.1 Introduction

As the largest and highest plateau on the earth, the Tibetan Plateau has been a key location for understanding the processes of mountain building, plateau formation and global climate change. While it is well accepted that the Tibetan Plateau is the consequence of the continent collision between India and Asia, many of the first order questions are still under debate. For example, is the plateau uplifted uniformly and what mechanisms thickened the Tibetan crust? In the past two decades, our understanding of this gigantic plateau has been significantly improved through numerous scientific expeditions to Tibet. Although the data collected on the plateau are still very limited relative to the size of the plateau, some large-scale lithospheric structures have been revealed. Seismic studies [Molnar, 1988; McNamara et al., 1995] indicate the Tibetan crust is ~70 km thick and the thickness decreases from south to north. While there are no strong constraints north of the Zangbo suture, seismic imaging clearly shows that the Indian lithosphere is underthrusting southern Tibet [Zhao et al., 1993]. Numerous studies [Ni and Barazangi, 1983; Holt and Wallace, 1990; McNamara et al., 1995] suggest that an abnormal mantle exists beneath northern Tibet and it may relate to the convective removal of the mantle lithosphere [Molnar et al. 1993]. Never-the-less, despite recent understanding of the Tibetan lithosphere, none of the proposed geodynamic models for the uplift of the plateau can

be totally eliminated [Argand, 1924; Dewey and Burke, 1973; Zhao and Morgan, 1987; Willet and Beaumont, 1994] and it is quite possibly that multiple mechanisms may have worked in tandem in the formation of the plateau [Chen, 1999].

Recent studies [Jin et al., 1994; Royden et al., 1997 and Alsdorf, et al., 1999] suggest that a low viscosity lower crust may be pervasive underneath the Tibetan Plateau. This fluid-like lower crust, if present, provides strong support for geodynamic models that require lower crustal flow. Additionally, partial melt has been proposed to be present in the crust of Tibet [Nelson et al., 1996]. The existence of pervasive partial melt in the Tibetan crust has profound implications, not only for current tectonics on the plateau, but also for its past uplift. A widespread lower crustal partial melt layer can decouple the mantle from the upper crust and thus accommodate the on-going E-W extension on the plateau. A fluid-like lower crust can also absorb the advancing Indian lithosphere through thickening, and hence, uplift the Tibetan Plateau too [Zhao and Morgan, 1987]. So, in this context, identifying the presence and extent of partial melt beneath the entire plateau is very significant.

The INDEPTH (International Deep Profiling of Tibet and the Himalayas) project was initiated in 1992 to improve our knowledge of the geological structures and evolution of the Tibetan Plateau. To date, the main INDEPTH profile extends from the crest of the high Himalayas to the central Qiangtang Terrane, covering a distance of ~800 km. Along this profile, seismic (seismic reflection and broadband earthquake), magnetotelluric (MT) and surface geological data have been collected.

Beyond the INDEPTH main profile, the INDEPTH MT profile extends across the northern Tibet into the Qaidam Basin. In southern Tibet, the INDEPTH team has identified an abnormal middle crustal layer [Nelson et al., 1996, Brown et al., 1996, Kind et al., 1996; Chen et al., 1996]. The high seismic reflectivity and high electrical conductivity of this layer strongly suggest the existence of fluids in the crust. Combining seismic and MT data, the analysis in Chapter 5 suggests that this abnormal mid-crustal layer represents a thin layer (~200 m) of saline fluids overlaying a thick (>10 km) partially molten system. This chapter extends investigation to the north.

In this study, we present a detailed analysis of INDEPTH MT 500 line data that span both the Lhasa and Qiangtang Terranes and address the question of whether partial melt exists beneath the Qiangtang Terrane. In the following discussion we first provide some geological background about the region of study, and then present detailed analyses of the MT data. In the light of other geophysical and geological constraints, we present a detailed discussion of our results and their tectonic implications.

5.2 Regional geology and previous work.

The Tibetan Plateau has a long history of continental collisions, and a series of continental fragments have been identified within the plateau [Chang and Zheng, 1973; Sengor, 1981]. The Lhasa and Qiangtang Terranes are two continental fragments accreted onto the southern margin of Asia. The Qiangtang Terrane is bounded by the Bangong-Nujiang Suture (BNS) in the south and the Jinsha Suture in

the north and was added to Asia in Triassic and early Jurassic [Yin et al., 2000] (Figure 5.1). Between the Bangong-Nujiang Suture (BNS) and the Zangbo Suture lies the Lhasa Terrane which collided with the Qiangtang Terrane in the late Jurassic [Dewey et al., 1988].

In the central Qiangtang Terrane, Triassic-Jurassic shallow marine carbonate rocks are dominant at the surface [Liu, 1988]. First reported by Henning [1915], blueschist-bearing metamorphic complexes have been identified in the Qiangtang Terrane [Kapp et al. 2000]. The study of these complexes indicate that these rocks may represent the lower crust composition of the Qiangtang Terrane [Kapp et al. 2000]. Crossing the BNS into the Lhasa Terrane, scattered Ophiolites and a thrust system have been identified [Yin et al. 2000, see Figure 5.2]. Although the BNS separates the Lhasa and Qiangtang terranes and was formed in Mesozoic times, Yin et al. [2000] argue that it has been reactivated because it is associated with a thrust system that cuts Tertiary strata. While the magnitude of this thrusting is not well constrained, this system may have formed a crustal-scale ramp that extends into the Qiangtang lower crust. The bedrock in the Lhasa terrane is formed by a supracrustal sequence of limestone, shale and arenites of Paleozoic through Paleogene age [Burg and Chen, 1984 and Kidd et al., 1988]. These sequences were probably formed in shallow marine environment in Late Paleozoic and Mesozoic time [Tapponnier et al., 1981]. In the southern part of the Lhasa Terrane, Linzizong volcanic rocks and Gandese batholith rocks are well exposed (see Figure 5.2).

Numerous studies crossing the BNS have concluded that the Qiangtang lithosphere is different from the Lhasa Terrane in its physical properties. Seismic studies [Ni and Barazangi, 1983, Holt and Wallace, 1990; McNamara et al., 1995] indicate a difference in Pn velocity and Sn propagation efficiency and suggest a change in mantle structures from the Lhasa to Qiangtang Terrane. Based on seismicity and geological observations, Molnar et al. [1993] estimated that the temperature under northern Tibet could be $\sim 500^{\circ}$ C higher than southern Tibet at mantle depth and they propose that this temperature variation is a consequence of the convective removal of mantle lithosphere. The BNS has also been suggested as the location where the Indian lithosphere stops underthrusting Tibet [Beghoul et al, 1993, Jin et al., 1996]. More recently, INDEPTH seismic data [Huang et al., 2000] show the onset of strong shear wave splitting just ~ 40 km south of the surface expression of the BNS and suggest that the crust may have contributed to this sharp change in seismic properties.

All these lines of evidence indicate changes of seismic properties across the BNS, but the resistivity structure of this region is not well resolved. With advanced instrumentation and a densely spaced profile, the INDEPTH MT 500 Line provides an excellent opportunity to investigate the lateral variation of resistivity structures across the BNS and investigate whether partial melt exists beneath the Qiangtang Terrane.

5.3 The 500-Line magnetotelluric data

The INDEPTH III magnetotelluric (MT) data were collected along a ~ 400 km profile in the summer of 1998. This profile starts near Nam Tso, crosses the Bangong-

Nujiang Suture (BNS) and ends near Longwei Tso (Figure 5.1). Tectonically, the 500 Line transverses both the Lhasa and Qiangtang Terranes and provides an opportunity to investigate changes in crustal properties between the two different tectonic units.

Two types of MT system were employed in the survey. Long period MT data (20-20,000 s) were collected with 15 Long period Recording MT Systems (LRMT) of Phoenix Geophysics (based on the design of LiMS from Geological Survey of Canada). Broadband MT data (from 1000 Hz to 1000 s) were collected using two EMI MT-24 systems. The INDEPTH 500 Line is the one of the most densely spaced MT profiles on the plateau. Along the ~400 km profile, there are a total of 58 MT-24 sites with an average site spacing of ~7 km and 26 LRMT sites with an average site spacing of ~15 km. Both LRMT and MT-24 sites are remotely referenced. The LRMT sites were usually occupied for two weeks and the MT-24 systems recorded for about 24 hours. MT impedance tensors were estimated from time series using the robust methods reviewed by Jones et al. [1989].

Although in-depth analyses are needed to extract detailed information from a data set, the first order features of the raw data can be readily seen. The observed data in pseudosection form are shown in Figure 5.3. To first order, the short period data are resistive (indicated by cold colors) indicating a resistive upper crust. The longer period data are conductive (indicated by warm colors) suggesting a conductive mid-to-lower crust. Crossing the plateau, a similar pattern has been observed for all the MT data [Wei et al., 2000].

Typically, apparent resistivity data are more susceptible to near-surface distortions than phase data. These near-surface distortions can displace the apparent resistivity curves by a frequency-independent constant known as static shift [Jones, 1988]. However, the phase data are unaffected. So, the information obtained from phase data are more reliable than apparent resistivity data.

While pseudosections show the overall characteristics of the data set, sounding curves present more detailed features of the data. Figure 5.4 shows sounding curves of five MT sites along the profile. The locations of these sites are labeled in Figure 5.12. All of these curves have down-going tails in apparent resistivity and rising tails in phase at periods longer than 10s. These trends indicate that the mid-to-lower crust beneath this profile is more conductive than the upper crust. The less conductive upper crust can be seen from the low phase value and high apparent resistivity at short (<1 s) periods.

To investigate the dimensionality and distortion of the data set, we applied the tensor decomposition technique of Smith [1997] to our data. To illustrate how the electrical strike varies with period, we divide the data into three sub-bands and plot them on a regional map (Figure 5.5). Although there are variations along the profile, the strike direction is dominantly ~E-W (or 90° from E-W) and this pattern persists at longer periods. At the northern end, there is a consistent deviation from E-W and this deviation may be due to strike variation along the profile or a 3-D effect. To avoid this complication, we will not use the northern 11 sites in our 2-D inversion. Overall,

the geoelectrical strike of the 500 Line is $\sim E10^{\circ}S$, close to the dominant E-W geological strike. So, we use the E-W strike in our analysis.

Independently, the dimensionality of the data set can be investigated by examining Parkinson's vector [Parkinson, 1959] which is a graphic representation of the complex transfer function between vertical and horizontal magnetic field variations. It is well accepted that the reversed real Parkinson arrows point toward current concentrations and thus toward regions of high internal electrical conductivity. In an ideal 2-D case, the Parkinson vectors far away from a current concentration should point perpendicular to its strike while these vectors become smaller and unstable over the current. Figure 5.6 shows reversed real Parkinson arrows along the 500 line at four different periods (10 s, 100 s, 1000 s and 2000 s) on regional maps. Although there are variations, the dominant vectors direction is N-S and support the regional E-W strike. The Parkinson vectors at sites near Nam Tso clearly point to the lake and indicate that either the lake or perhaps highly conductive sediments associated with it have a strong effect on the nearby sites.

With a geoelectric strike, MT data can be presented in two separate modes. The transverse magnetic (TM) mode has electrical currents flowing across the strike while electrical currents flow along the strike in the transverse electric (TE) mode. For the Tibet 500 line, the TM mode has current flowing along the profile and TE mode current flows perpendicular to the profile. Thus, TE current can be affected by the unsampled structure (such as Nam Tso) off the profile.

5.4 Inversion of the 500 Line MT data.

Both the Rapid Relaxation Inversion (RRI) algorithm of Smith and Booker [1991] and Non-linear Conjugate Gradient (NLCG) inversion of Rodi and Mackie [2001] were used to invert the data. RRI can fit the observed data as well as NLCG, but the RRI models tend to be rougher than the NLCG models. This difference in inversion model can be attributed to the large site spacing and different inversion algorithms. RRI becomes a fully 2-D inversion only at convergence, uses approximate sensitivities and has degrees of freedom only beneath sites. When MT sites are widely spaced, RRI may not be able to find the correct structure between these sites. Then forcing the data misfit below what is permissible for RRI's ability to parameterize the structure can make the model too rough even though the achieved misfit does not suggest over-fitting of the data. NLCG, on the other hand, can directly update structure between the sites. Like RRI, NLCG makes the inversion unique by minimizing an objective function that is a weighted combination of a structure penalty and the data misfit. There is a parameter called tau which controls whether the structure penalty or data misfit is more important. What one needs to do is find the tau that results in a desired level of misfit when the total objective function is minimized. However, as implemented, NLCG requires the user to specify tau. One has to do a series of inversions to find the tau that gives the desired misfit. An additional complexity of the NLCG version that I used is that there are four different choices of structure penalty. two minimize the mean square Laplacian and two minimize the

mean square Biharmonic operator of the model. For each structure operator there are two choices of how the length in the derivatives scale with depth. The one called "uniform grid" use the model block size to scale the derivatives and has the effect of suppressing horizontal and vertical variations where the block size is large. The other choice (called "non-uniform grid") compensates for block size in such a way that the derivative scale is the same everywhere in the model. This choice permits more rapid model gradients at depth and in general leads to a rougher looking model for a given misfit. We experimented with all these choices but the results to be presented use the uniform grid Laplacian operator. This choice produced a noticeably smoother looking model, especially at depth, while still permitting acceptable misfit to be achieved.

I present inversions of TM data alone and TE+TM data. For TM, the static shifts were fixed at 0 but the resistivity data were down weighted with an error floor of 50%. The error floor for phase was set at only 1 degree (equivalent to 3% in resistivity). This, in effect, allows small static shifts while keeping the median static close to zero. When inverting TE+TM data, I set the error floor for the resistivity to 20% and for phase to 1.43 degrees (equivalent to 5% in resistivity) and I allowed the static shifts to be computed. However the static shifts were heavily damped in early iterations to make the inversion try to fit the resistivity with structure before resorting to a static shift.

Initial inversions start from a 100 Ω .m half space and first invert TM and TE separately and then simultaneously. Usually, inverting TE or TM data alone will be

easier than inverting them together. This is true because TE and TM data see different aspects of the structure and may not be consistent due to off-profile structure, local distortion or a wrong choice of strike direction. Vertical magnetic field (Hz) data were also inverted along with TE and TM data, but we were unable to find a model that can adequately fit all three sets of data. One reason may be that the Hz responses are so weak that they contain no consistent information. Another is that the Hz reacts to 3-D complications differently than TE or TM.

The TM and TE+TM models are shown in Figure 5.7. The upper model in Figure 5.7 is for TM data alone and has an overall normalized misfit to the data of 1.4. Normalized rms misfit is the square root of the sum of the actual misfits divided by their estimated errors (modified by the error floors discussed above). The lower model is for the simultaneous inversion of TE and TM. Its normalized rms misfit is 1.7. The model responses, observed data and normalized residuals for the TM model are shown in Figure 5.8 and the data and model responses for the TE+TM model is shown in Figure 5.9. We can see that the model responses match the data quite well and the normalized residuals are generally close to zero across the full bandwidth. To show the detail of the fit to the data, sounding curves at a few typical sites are shown in Figure 5.4. The data uncertainties shown are after the error floors are applied. The solid curves are the calculated model responses. Again, these curves show that the model fits the features of the observed data to a satisfactory level.

To constrain the conductance required by the MT 500 line data, we inverted our TM data using the constrained inversion technique described in chapter 4. We used only TM data because, as we shall discuss in the next section, there is strong evidence that the saline lake Nam Tso at east of the southern 500 line significantly distorted the TE data in a way that can not be simply removed using static shifts. The TM only model shown in Figure 5.7 (a), modified by a 1000 Ω .m basement below certain depth, was used as the starting model for each inversion. The resistive basement was held fixed during inversion. The initial misfit is significantly smaller than starting from a 100 Ω .m half space and the inversion quickly converges. This process was repeated with the resistive basement fixed below 100 km, 60 km, 50 km, 40 km and 30 km. When the basement was moved up to 20 km, the inversion algorithm did not decrease its misfit indicating that the data can not tolerate a basement as shallow as 20 km. So, in the following discussion, we only consider models with a resistive basement deeper than 20 km. Three of the inversions are shown in Figure 5.10. It is worth noting that they have almost identical shallow structure. We conclude that the shallow structure interpretation is independent of the thickness of the deeper conductor.

The conductance above the basement for each model in Figure 5.10 is shown in Figure 5.11. The model conductance along the profile is fairly stable and decreases as the basement is made shallower. The model with the resistive basement fixed at 30 km has the minimum conductance. The absolute minimum value is 1,600 S. This is

much less than the 6,000 S found for the 200 line. While the regional conductance beneath central Tibet is much lower than that of southern Tibet, it is still high relative to typical continental crust and thus mechanisms that can cause high conductivity in the deep crust need to be investigated.

5.5 Discussion.

5.5.1 The resistivity structure of the northern Lhasa Terrane.

The MT 500 line starts near the southwest end of Nam Tso and overlaps with the MT 200 line for about ~80 km, but separated by Nam Tso (see Figure 5.1). This deployment not only provides a continuous view of the resistivity structures north of the MT 200 line, it gives us a chance to compare the resistivity structures from these two different profiles where they overlap. The 200 line resistivity model from Chen et al. [1996] has a conductive mid-lower crust and the conductive crust extends at least ~50 km outside the Damxung Graben. In chapter 4, I present detailed analysis of the MT 200 line data and conclude that the seismic bright spot in the Damxung Graben is due to a thin layer of rocks with saline pore fluid overlaying a thick layer of partial melt. Outside the Graben, no seismic data have been collected along the 200 line. Thus the existence of the saline fluid is not well constrained, but the continuation of the highly conductive structure outside the graben indicates that the partial melt system and perhaps its saline cap extends outside the graben.

Both the MT 200 line and TE+TM 500 line models are shown in Figure 5.12. The 500 line model is quite different from the 200 line model in the overlapped section.

While the 200 line model is conductive ($< 30 \Omega.m$) below 20 km, the 500 line TE+TM model has a resistive ($100 \Omega.m$) upper to middle crust (<40 km) with a deep resistive root reaching 100 km depth. Given the short distance (~ 50 km) between these two profiles and the long period (> 1000 s) data used in both studies, such a sharp change in resistivity structure is unexpected. What can cause such a sharp lateral change in resistivity? If the real resistivity structure varies this rapidly off the profiles, our 2-D analysis is invalid. So the source of this change needs to be investigated.

To understand the difference between these models, a comparison of the TM model and TE+TM model is very instructive. As seen in Figure 5.7, the TM model has a resistive upper crust (<20 km) and a conductive mid-lower crust at the south end of the 500 line. This structure is nearly identical to the structure of the 200 line. On the other hand, the TE+TM model requires a resistive ($> 100 \Omega.m$) mid-upper (<40 km) which is different from the TM model and the 200 line model. TE data depends on off-profile structure much more than TM data [Wannamaker et al., 1984]. An obvious off-profile structure to be considered is the saline lake Nam Tso.

The first thing to note is that the deep resistive root is exactly coincided with the sites adjacent to the Nam Tso (see Figure 5.12). Furthermore, note that the resistive upper crust is significantly thicker on the 200 line model under the sites nearest to Nam Tso. So, both profiles may suffer from a similar distortion although it is stronger along the 500 line where the lake is wider.

Electric current flowing from a salt-water body into land must be conserved. Since the land has a lower conductivity than salt water, the electric field on the land will be higher than in the water. Because the resistivity is proportional to the square of the electric field, MT sites deployed along the lakeshore will produce higher resistivity data than they would in the absence of the lake. If this is purely a electric field effect then it can be removed using static shifts, We tried a variety of strategies to find a TE+TM model that fit the data and had a conductive structure like the TM alone model. One was to start from the TM model and eliminate the TE resistivity from the joint inversion. The result was a model almost identical to the TE+TM model of Figure 5.7 (b). Thus the deep resistive zone is constrained by information in the TE phase and can not be eliminated using static shifts. This suggest that Nam Tso is a strong enough distorter that it distorts the magnetic as well as the electric field. Unlike electric distortion, magnetic distortion does affect phase. We have already seen in Figure 5.6 that Nam Tso has perturbed the vertical magnetic field and it should not be surprising that it has also affected the horizontal magnetic field.

While the deep resistive structure near the south end of the 500 line may be due to the lake effect, the large scale, shallow resistive structure just to its north is real and can be related to the exposed Bange Granite Unit. Both the TM model and TE+TM model in Figure 5.7 show this resistive structure although the scale of the structure in the TM model is smaller than in the TE+TM model. TM data are more

sensitive to resistors than TE data, so the difference in the scale may also be caused by the nearby lake.

Since the deep resistive structure in the TE+TM model seems likely to be a 3D effect, we conclude that overall, the resistivity structure in central Tibet is similar to other parts of the Tibetan Plateau: a resistive upper crust overlays a conductive mid-lower crust.

5.5.2 The resistivity structure near the BNS.

While a suture has important tectonic implications, it does not necessarily have different resistivity from its surroundings. A conductive suture zone can be due to the existence of fluids or conductive minerals, but a suture with a few million years of age may not contain any conductive material and thus show no significant resistivity contrast from adjacent units. Beneath the BNS (Figure 12), the earth is resistive ($>300 \Omega.m$) in the upper crust (< 20 km) and the middle to lower crust has a laterally uniform resistivity of $\sim 10 \Omega.m$. On the Tibetan Plateau, MT data crossing three sutures (see Figure 5.1) show no clear resistivity expressions of these sutures. Chen et al. [1996] pointed out that the Zangbo suture on the 100 line model evident in the uppermost few kilometers has no electrical expression below 15 km. On the MT 600 line, initial analysis [Wei et al., 2000] also shows no resistivity expression for the Jinsha suture.

While there is no clear structure related to the mapped surface trace of the BNS, there is a conductive structure about ~ 50 km south. This north dipping

conductive structure has a resistivity of $<30 \Omega.m$ and is required by both the TM and TE data (Figure 5.7). This structure reaches the surface in the vicinity of two sedimentary basins (Duba Basin and Lumpola Basin) and appears to connect the surface basins to the conductive structure in the deeper crust. At the same place where this conductive structure is exposed at the surface, there is a sharp northward increase in shear wave splitting. Huang et al. [2000] argue that this lateral change in shear wave splitting is so sharp that it must have a shallow crustal component despite prevailing opinion that large shear wave splitting can only be in the mantle. It is too early to relate the shear wave splitting to our dipping conductor. However one tentative conclusion that both the seismic and MT data support is that the true BNS may be ~ 50 km south of its previously accepted location.

5.5.3 Partial melt in the Central Tibet?

We have concluded that the 500 line data indicate a conductive mid-lower crust as that has been observed across the entire plateau. From the constrained inversion, we find the minimum conductance for the Tibet 500 line to be 1600 S. Compared to the minimum conductance of the 200 line, the conductance required by the 500 line is $\sim 4,000$ S lower but still high relative to the typical conductance of continental crust (20-2,000 S). Also note that the 1600 S is an absolute minimum conductance and much higher true value is possible. So, mechanisms that can cause high conductivity in the deep crust need to be investigated.

The high electrical conductivities observed in the deep continental crust can be explained by several candidates: graphite, ore minerals, saline fluid and partial melt [Jones, 1992]. Graphite has been reported at mid-crustal depths [Frost *et al.*, 1989a] but it may be difficult to maintain electrical connection in tectonically active areas such as the Tibetan Plateau. Ore minerals found in the Earth may play an important role in enhancing crustal conductivity, but the large spatial dimensions observed in this study make ore minerals an unlikely candidate. Thus, fluids are the most likely cause for the elevated conductivities. Both aqueous fluids and partial melt have been identified in the continental lower crust [Hydman *et al.*, 1989; Shankland *et al.*, 1981] and they can equally explain the high conductance we observe in the Qiangtang Terrane. Even though both saline fluid and partial melt can enhance lower crust conductivity, they have different thermal regimes. Free fluids can exist in the deep crust only if the temperature is lower than the wet granite melting temperature (650 °C). When the temperature is higher, rocks with free fluids start to melt.

Many studies on the plateau indicate that the Lhasa Terrane has a colder lower crust than the Qiangtang Terrane. In southern Tibet, sub-crustal earthquakes [Chen and Molnar, 1983; Zhu and Helmberger, 1996] indicate a cold mantle lid with an estimated temperature of ~800 °C and thus the lower crust temperature should be cooler. Based on the Pn variations across the Tibetan Plateau and other geological observations, Molnar *et al.* [1993] estimate the temperature of the upper mantle beneath northern Tibet is ~500° C warmer than southern Tibet, therefore the

temperature in the upper mantle of the Qiangtang Terrane can be as high as 1300 °C. Given the high upper mantle temperature, a high temperature in the lower crust in Qiangtang Terrane may be expected. Deep crustal xenoliths discovered in the Qiangtang Terrane [Haker et al., 2000] indicate that the temperature at 30 km reaches 800 °C and the temperature is higher in the lower crust (1000 °C at ~50 km). Given such high temperatures in the Qiantang lower crust, the conductive crust is most likely due to partial melt. Aqueous fluids at such a high temperature must produce melts.

The wide-angle seismic data [Zhao et al., 2000] collected along the 500 line profile support low fraction partial melt. The Vp velocity contours of Zhao et al. [2000] are overlaid on the 500 line model in Figure 12. While there are small changes in the Vp velocity, no clear low seismic velocity zone can be identified. So, the low velocity layer in southern Tibet [Kind et al., 1996] does not extend to central Tibet. This argues for lower melt porosity along the 500 line. Using the results from chapter 4 and the upper bound of 10 S/m conductivity for melt, the observed minimum conductance of 1600 S requires a minimum thickness of ~30 km for a 1% partial melt layer and ~5 km thick for a 5% partial melt layer. Since our constrained inversion implied a conducting zone with a bottom deeper than 20 km and thus thicker than 5km, we can conclude that the partial melt is probably below 5 %.

5.6 Conclusions and implications

The MT data collected in Tibet provide strong evidence for the existence of partial melt in the crust. In the southern Lhasa Terrane, the 200 line data indicate that a fairly high percentage (>10%) partial melt exists. This melt appears to be associated with significant aqueous fluid at a temperature below 800 °C. Analysis of the 500 Line data suggest that partial melt also exists beneath the Qiangtang Terrane but at substantially lower percentage and higher temperature. Since the higher temperature precludes free aqueous fluid, the lower observed conductance of Qiangtang Terrane relative to the Lhasa Terrane may simply be a direct consequence of the absence of a saline fluid cap on the partially molten layer. North of the Qiantang Terrane, the initial analysis of INDEPTH 600 Line data [Wei et al., 2001] suggests the existence of partial melt beneath the northern part of the plateau too. So, data from the INDEPTH MT experiment that traverses the entire plateau support a widespread mid-lower crustal partial melting layer.

The widespread distribution of partial melt in the Tibetan crust has important implications. The existence of partial melt in host rock can dramatically alter the rheology, enhancing creep rate and lowering effective viscosity [Cooper and Kohlstedt, 1986]. Thus the MT data support the idea that the upper 15 km of the Tibetan crust is separated and probably decoupled from the lower crust and mantle by a deformable layer. While the detected conductance in the layer varies across the plateau, its existence and mechanical weakness may not. This explains why the

Plateau is essentially flat despite the thickness of crust decreasing from ~80 km in the south to ~ 60 km in the north. It also explains why the East –West extension expressed by large scale North-South rift systems [Armijo et al., 1984] have no deep cutting canyons and seem to be unrelated to deep regional structure. Finally, the MT data lend support to all the various uplift and deformation models that require a fluid middle crust [Zhao and Morgan, 1987, Royden et al., 1997].

The MT study in central Tibet reveals lateral resistivity variations from the Lhasa Terrane to the Qiangtang Terrane. Although the deep resistive structure of the south end of the 500 line is likely a distortion caused by the nearby Nam Tso, the northern Lhasa Terrane and southern Qiangtang Terrane are significantly less conductive than the southern Lhasa Terrane. At shallower depth, the resistive Bange Granite unit of the northern Lhasa Terrane extends down to ~20 km and has a scale of ~50 km horizontally. Beneath the mapped surface trace of the BNS, no electrical or seismic expressions of the suture have been identified. On the other hand, both seismic and electrical properties of the crust change at ~ 50 km south of the BNS. The MT data require a north dipping conductive structure whose shallow part is well correlated to the exposed sedimentary basins at the surface but which extends down into the conductive middle crust. At the same location, seismic data show a sharp increase in shear wave splitting. So, we suggest that the real suture could be ~ 50 km south of the mapped surface trace of the BNS.

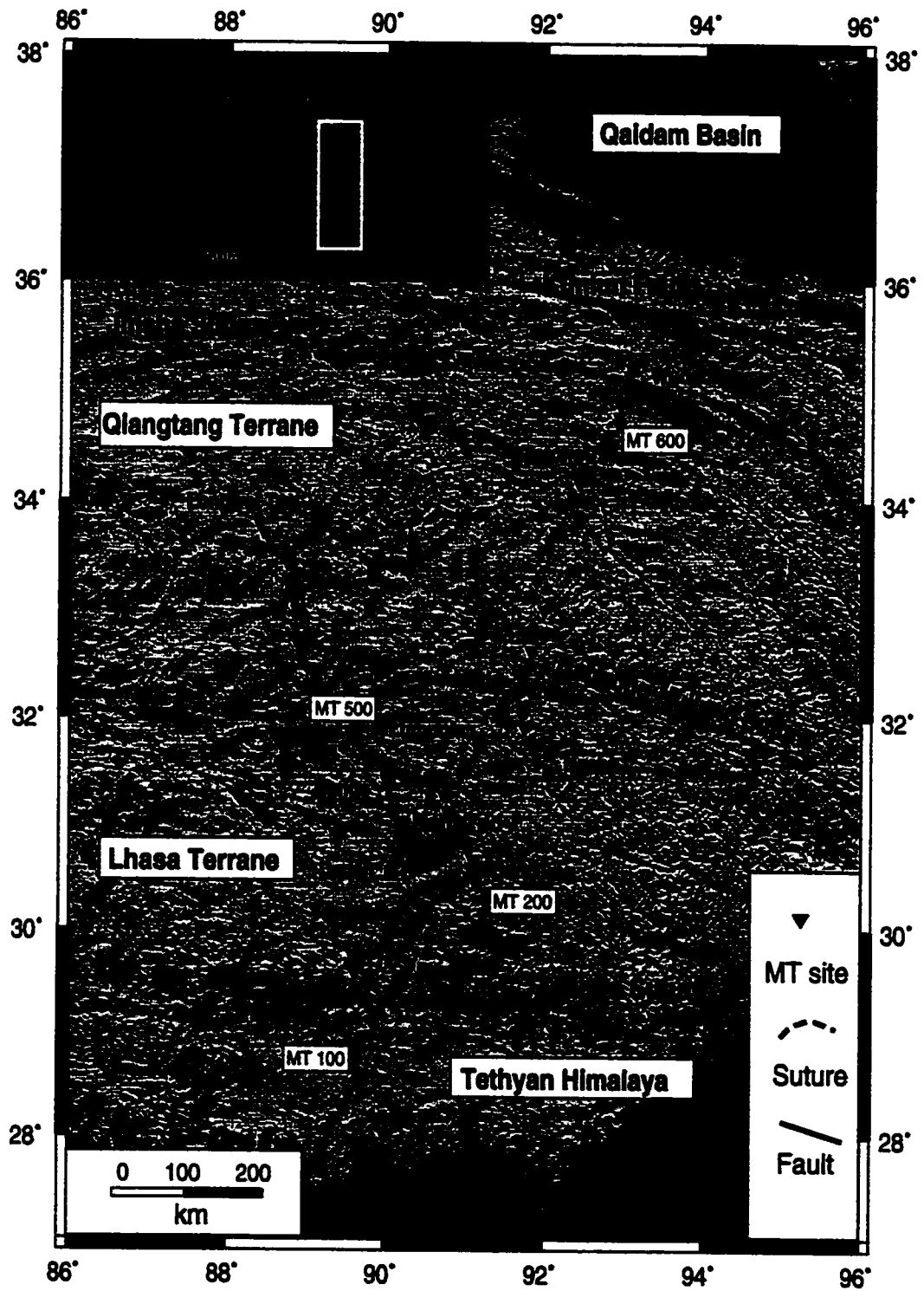


Figure 5.1 Location map of the INDEPTH MT surveys on Tibetan Plateau

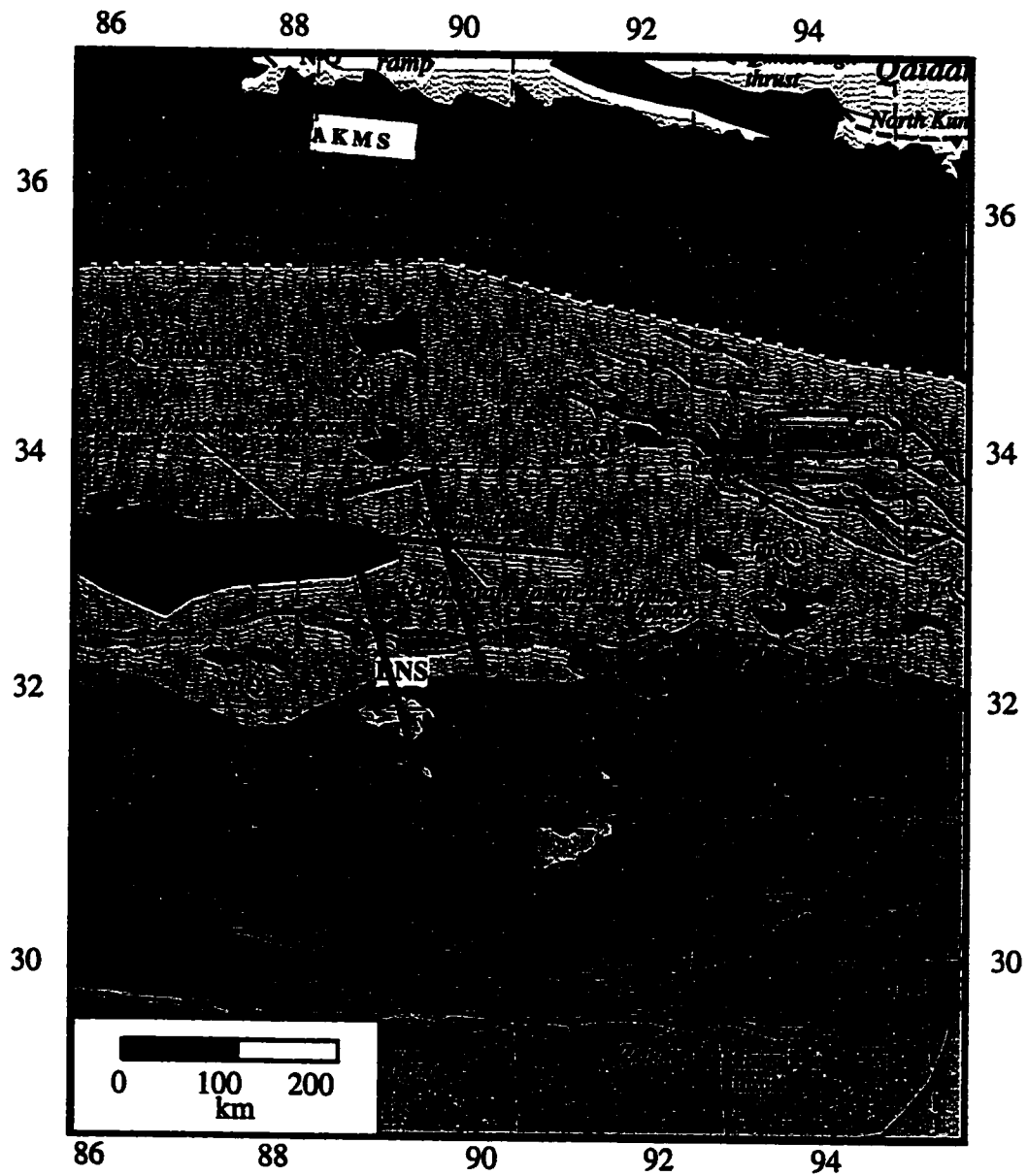


Figure 5.2 Simplified tectonic map of central Tibet
(modified from Yin et al., 2000)

The blue box indicates the area of 500 line study and some of the keys are list below. K-Tg: Gandese plutonic rocks. Tv(lz):early Tertiary Linzizong volcanic rocks. Oph: Ophilitite. gnAM: Amdo gneiss. Gr(Q): Mesozoic plutonic rocks. Ts: Tertiary sedimentary rocks. BNS: Bangon-Nujing Suture. AKMS: Ayimaqin-Kunlun-Mutztagh Suture.

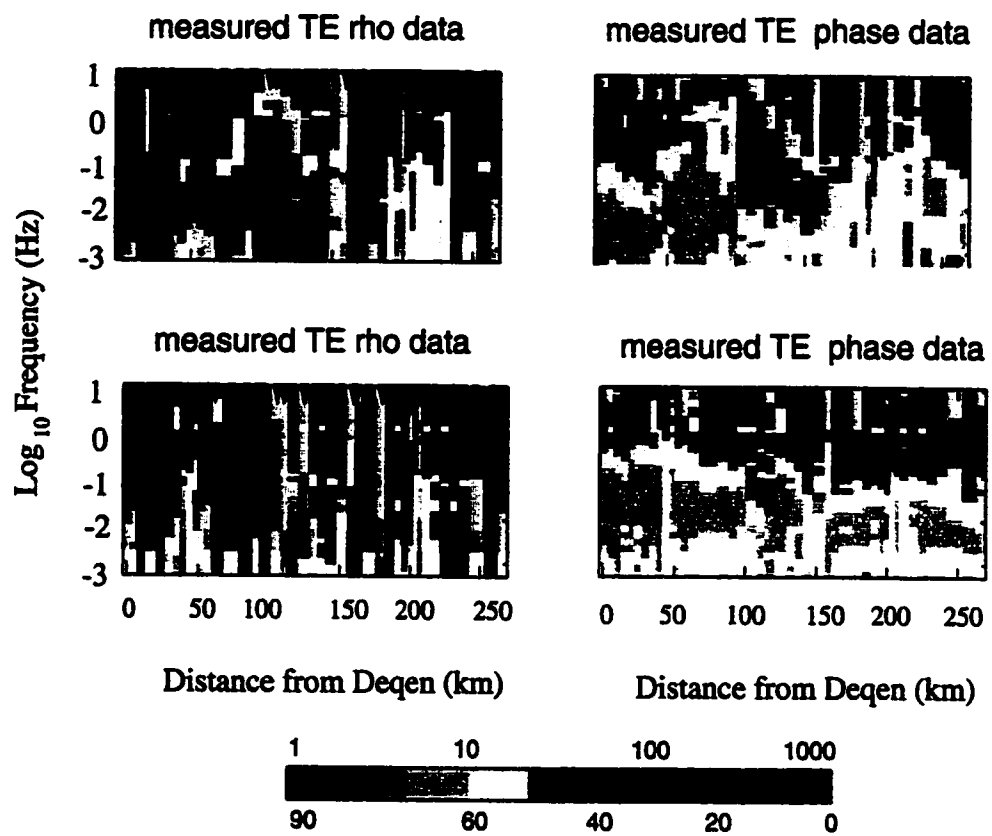


Figure 5.3 Pseudosections of Tibet 500 line data

Note the blank space indicates excluded bad data

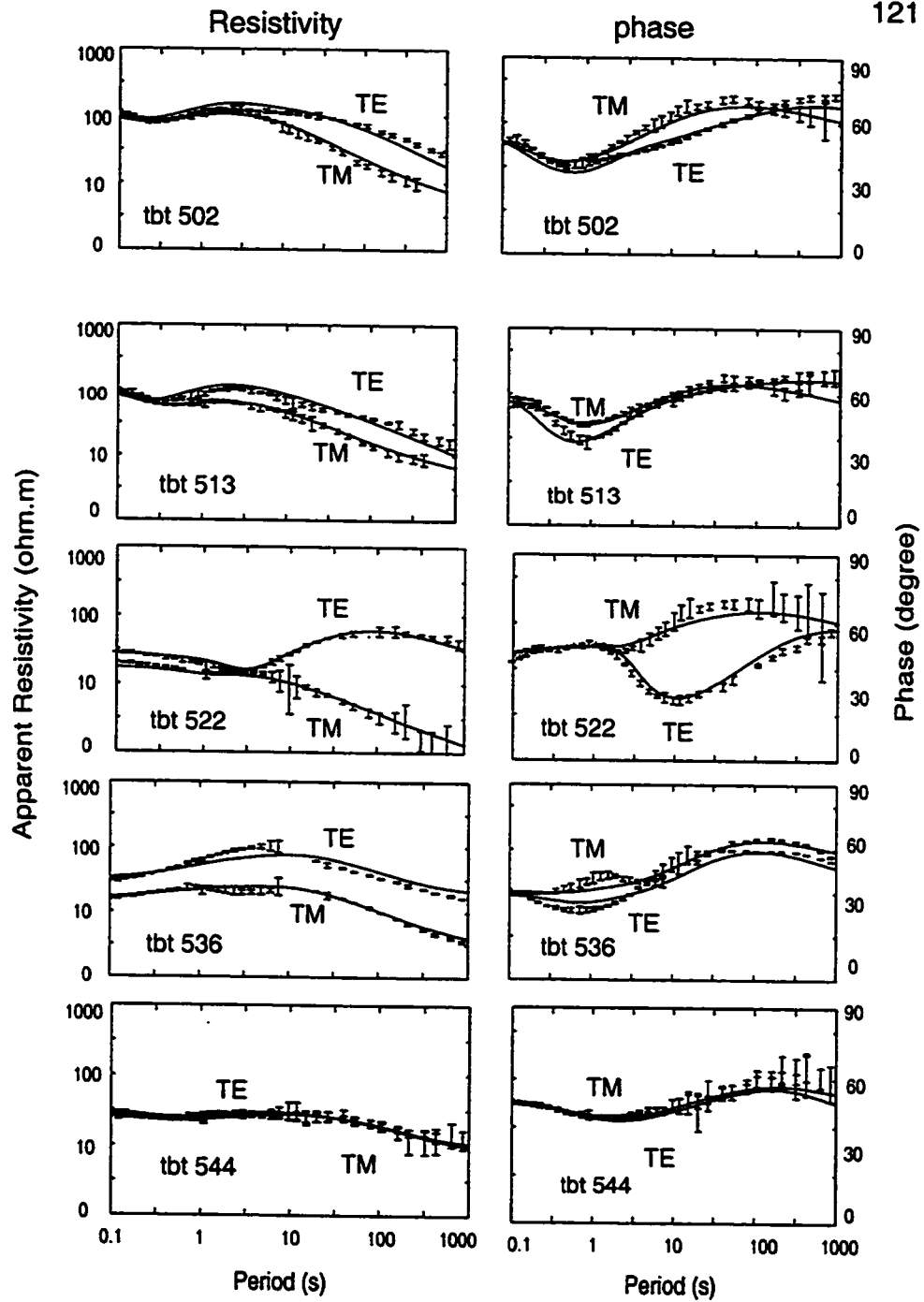
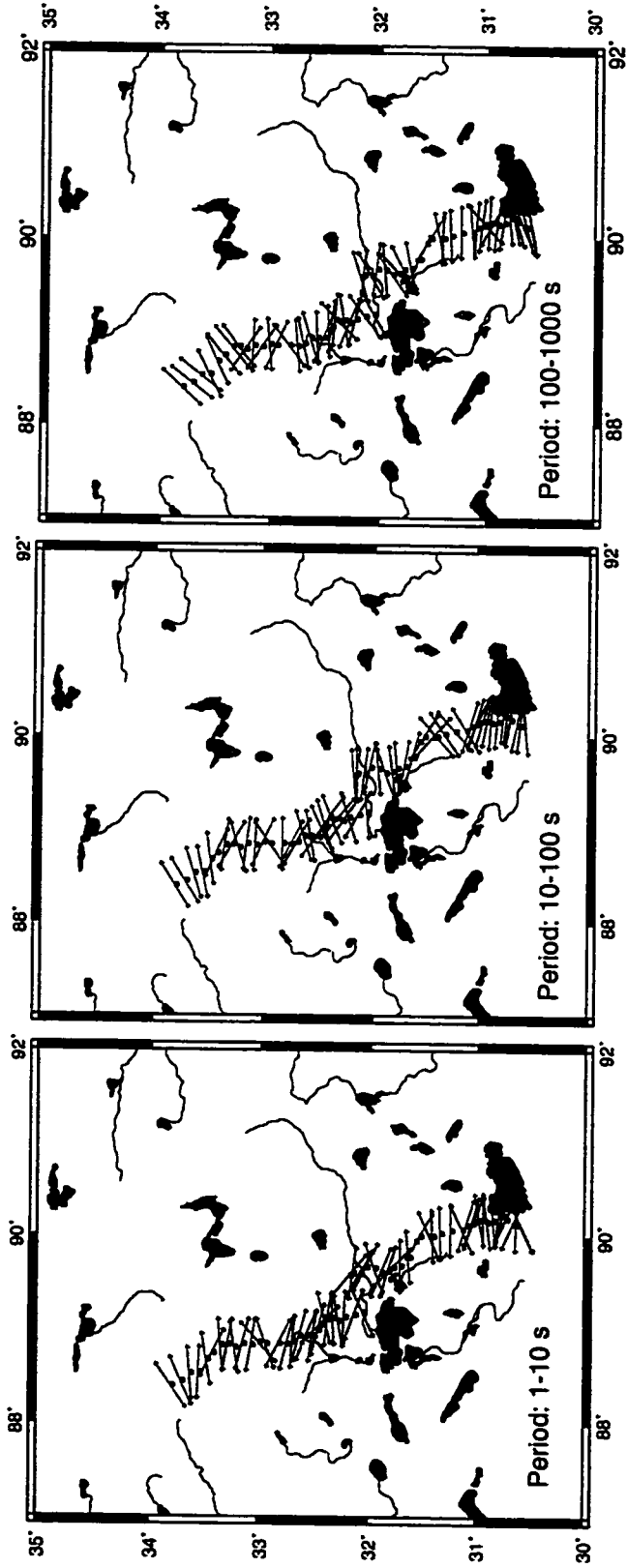


Figure 5.4 Observed data and model responses
 Data are shown with uniform error floors used in inversion
 and the solid lines are the MT responses from the model
 shown in Figure 5.7 (b).



Period: 1s - 1000 s Mean Strike = $E10 S^0$

Figure 5.5 Geoelectrical strikes of INDEPTH 500 line data

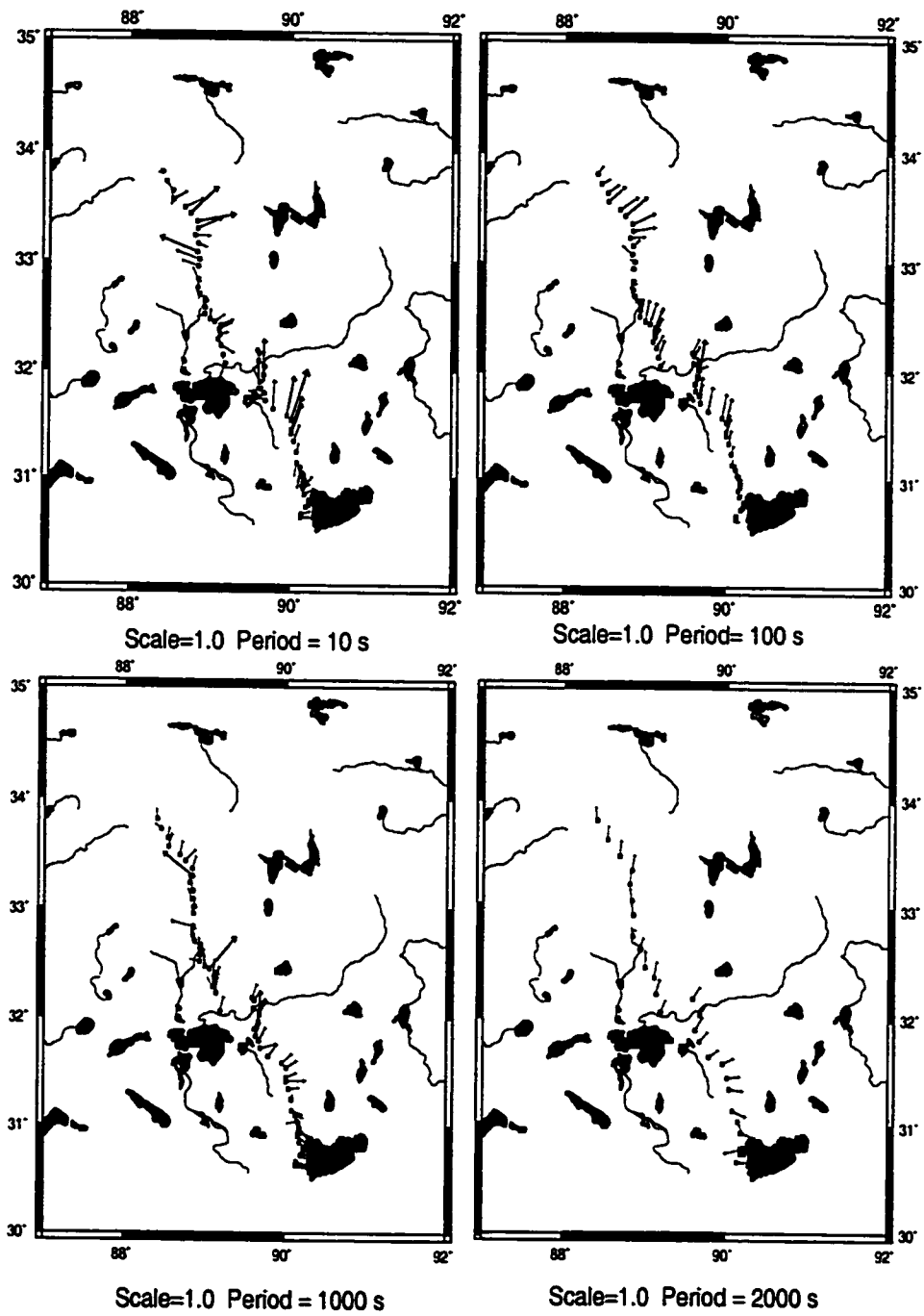


Figure 5.6 Reversed real induction vectors of INDEPTH MT 500 line

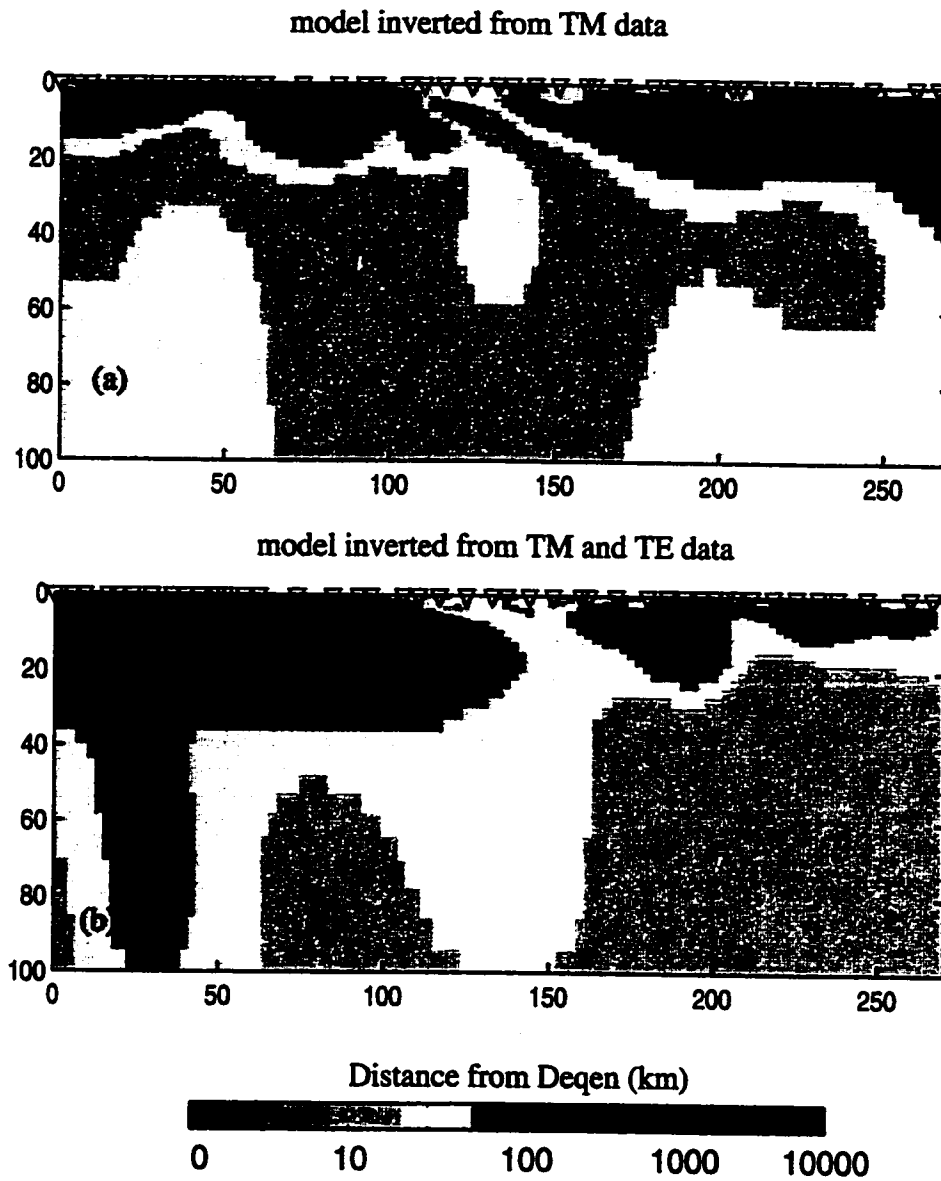


Figure 5.7 (a) Resistivity model inverted from TM data only

(b) Resistivity model inverted from TM and TE data .

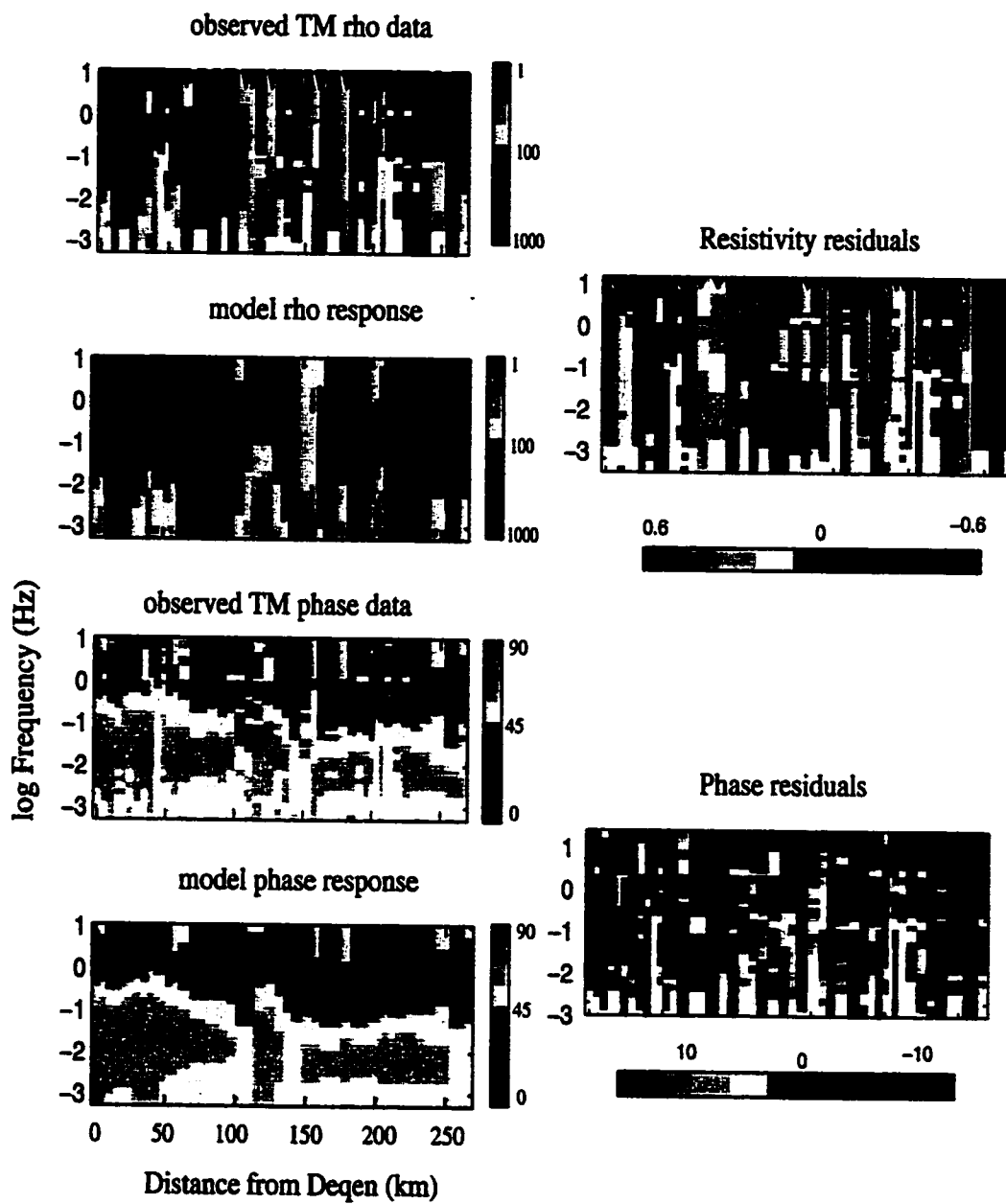


Figure 5.8 Observed TM data, MT responses from model (a) in Figure 5.7 and residuals between the observed data and model responses.

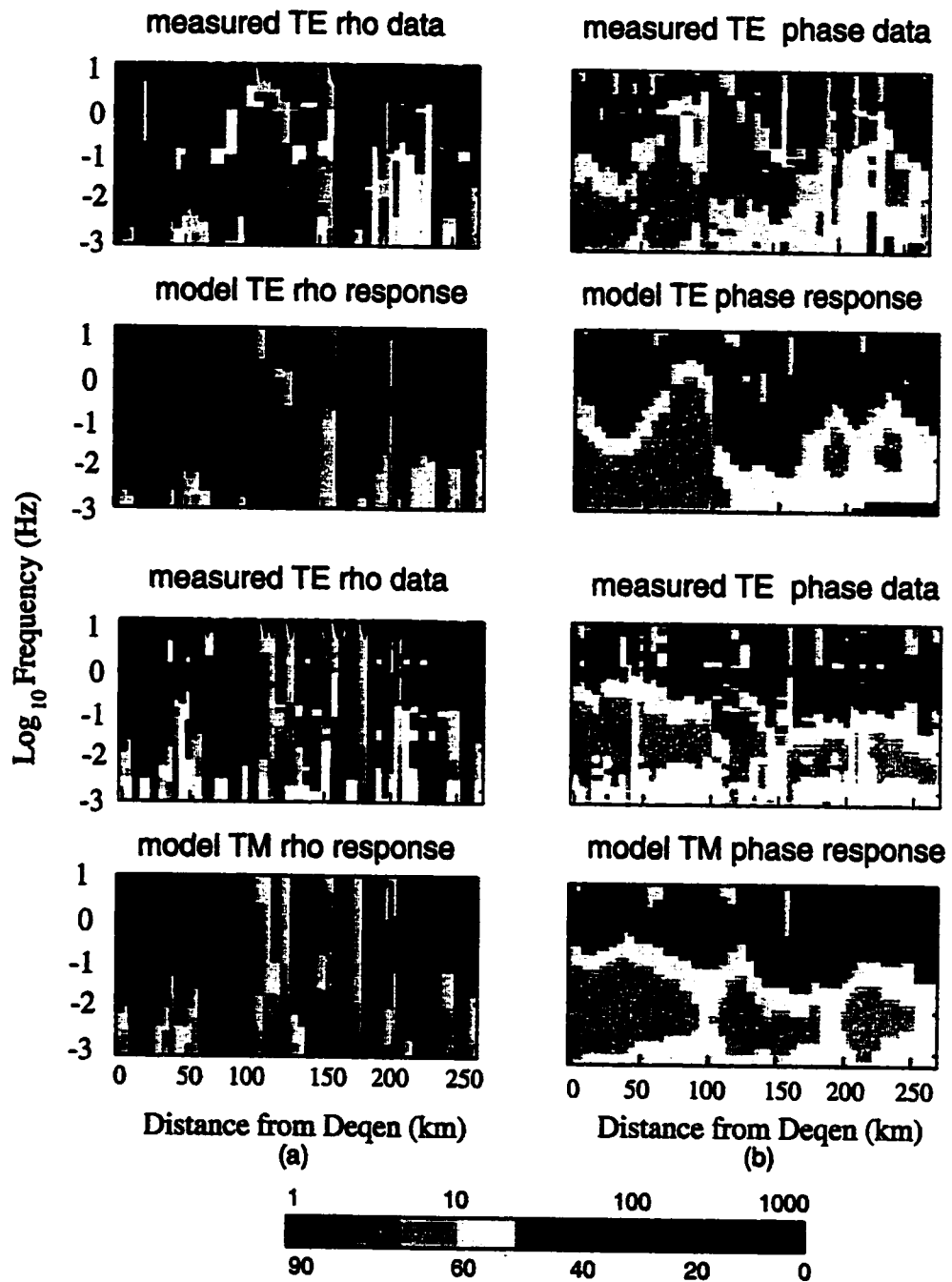


Figure 5.9 Observed data and MT responses of model (b) in Figure 5.7

Note that the blank spaces indicate excluded bad data

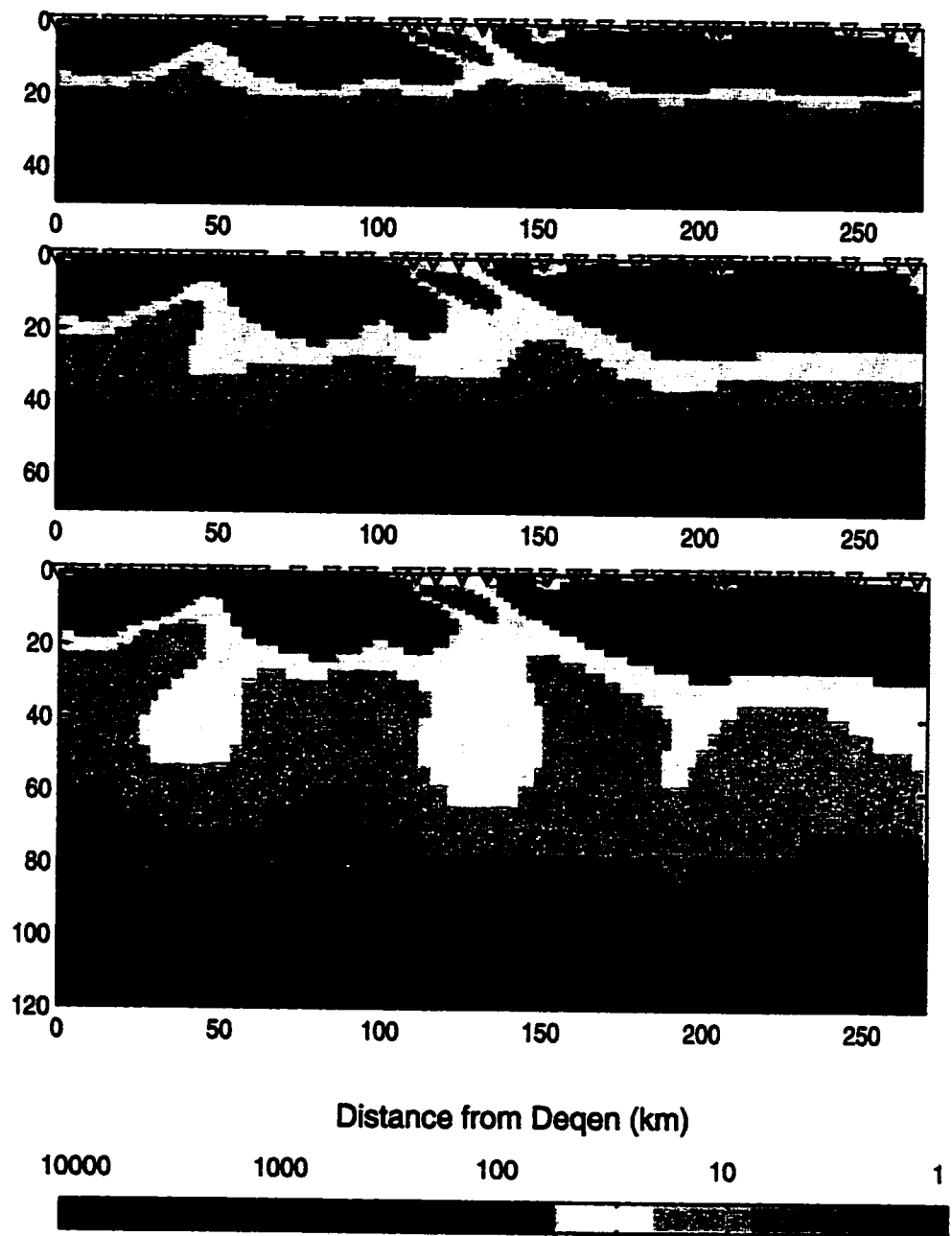
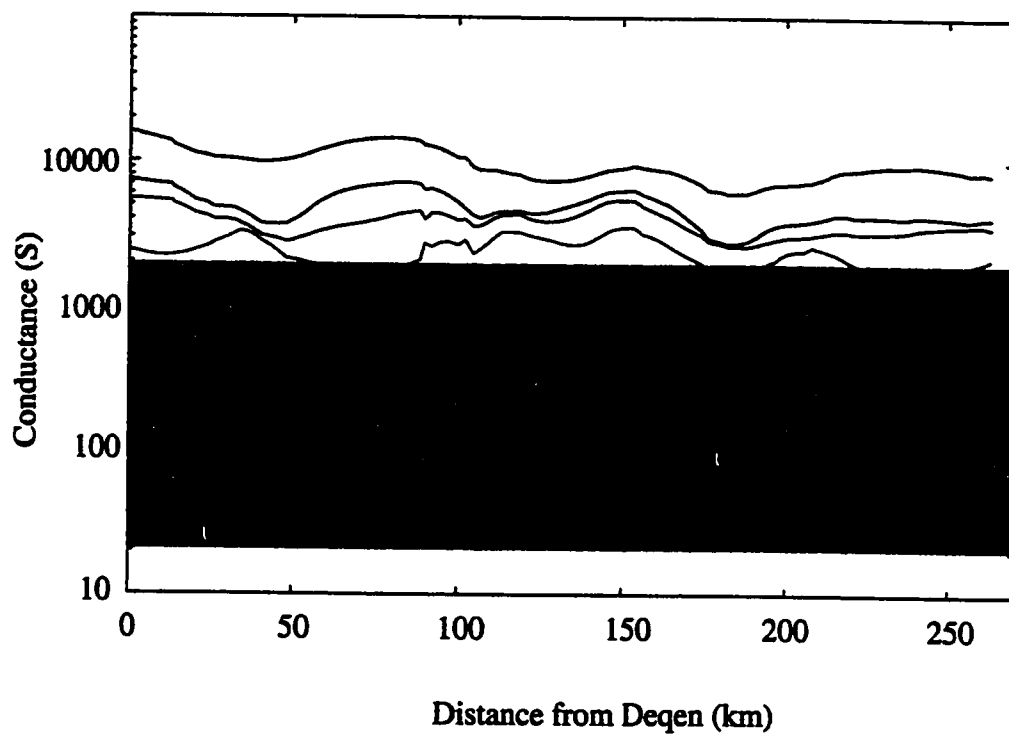


Figure 5.10 Constrained inversion of the Tibet 500 line data



— model fixed below 100 km — model fixed below 60 km
 — model fixed below 50 km — model fixed below 40 km
 — model fixed below 30 km

Figure 5.11 Integrated conductance of constrained inversion models

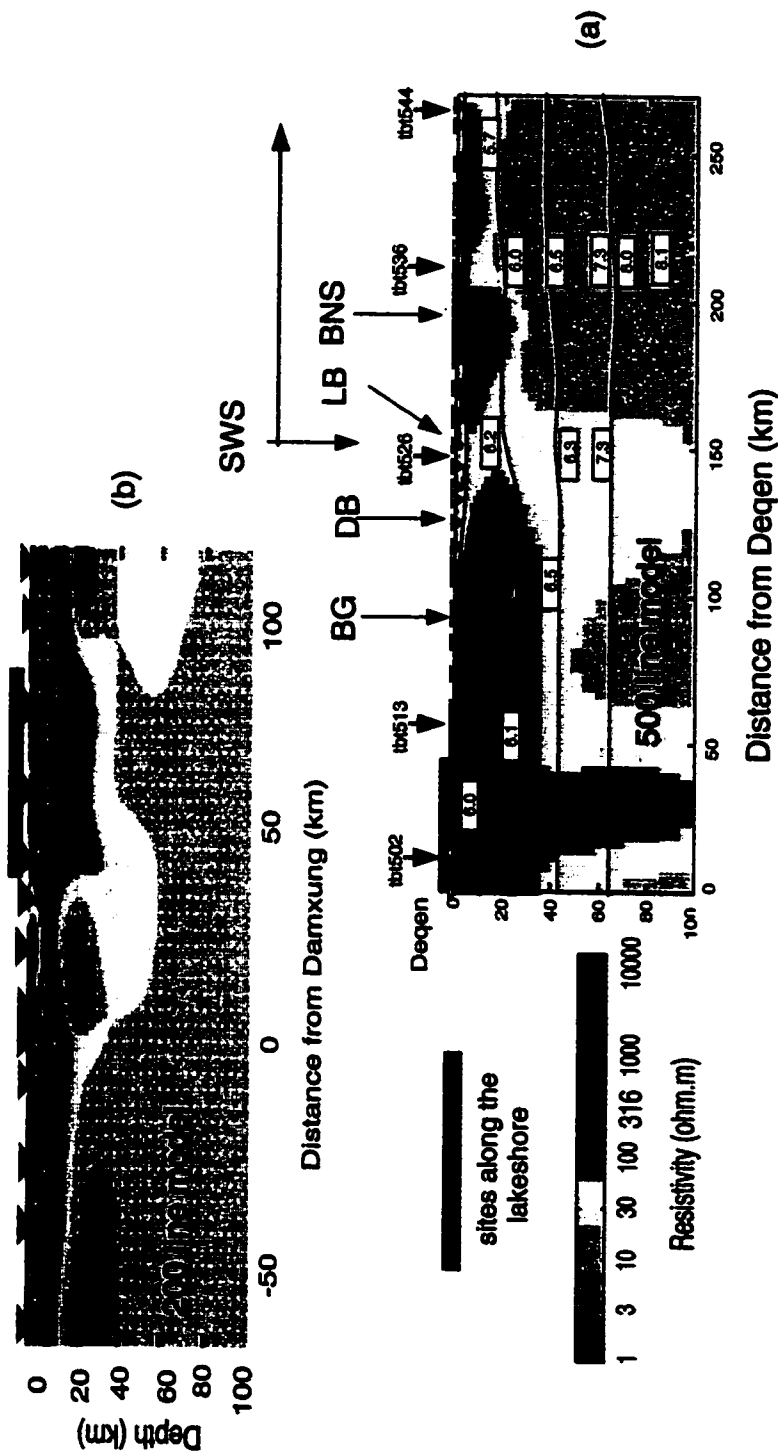


Figure 5.12 Resistivity model inverted from Tibet 500 line data (a) and model from Chen et al., 1996 (b)

The reversed triangles are MT sites and the read bar indicate where sites are near the lake.

The Vp seismic velocity contour shown on model (a) are from Zhao et al., 2001

SWS ---- onset of strong Shear Wave Splitting (Huang et al., 2000) GB --- Bange Granite

DB --- Buba Basin LB --- Lumpola Basin BNS ---Bangong Nujiang Suture.

CHAPTER 6

CONCLUSIONS

We have developed a new MT inversion algorithm that can invert MT data in the presence of strong topographic and bathymetric distortions. Several synthetic examples were presented to demonstrate that the new algorithm can recover conductivity structures in the presence of strong topography and bathymetry. In this dissertation, I have concentrated on the MT data from central Tibet where the topographic effect can be ignored and this inversion algorithm has not been tested on field data.

The analysis of the Tibet 200 line data shows that a minimum conductance of 6,000 S is required near Damxung where seismic bright spots have been identified. Many combinations of thickness and fluid porosity can explain the conductance. Combining the MT result with available constraints from other geophysical studies, I conclude that the seismic bright spots in southern Tibet can be best explained by a thin layer of rock with saline fluids overlying a thick partially molten system.

The analysis of the Tibet 500 line revealed the resistivity structure across the boundary of the Lhasa and Qiantang Terranes. At the south end of the profile, strong off-profile distortion by a large saline lake has biased the MT data and results in a resistive upper-middle crust. The true conductive structure at the south end of the 500

line is more shallow and conductive than our model shows. The Bange Granite is a very resistive structure that extends down to ~20 km and ~ 50 km horizontally. While the Bangong-Nujiang Suture (BNS) has been mapped at the surface, there is no electrical expression of the mapped BNS. On the other hand, both seismic and electric properties change ~ 50 km south of the surface trace of the BNS. So, it is possible that the real suture is ~50 km south of the mapped BNS. The minimum mid-crustal conductance required by the MT 500 line data is 1600 S which is ~ 4000 S lower than the minimum conductance required by the MT 200 line data but is still much higher than the typical conductance of continental crust. Based on available geophysical data, I conclude that the high conductance in central Tibet is most likely due to low porosity partial melt.

References:

- Aprea, C., Booker, J.R., Smith, J.T., 1997. The forward problem of electromagnetic induction: accurate finite-difference approximations for two-dimensional discrete boundaries with arbitrary geometry, *Geophys. J. Int.*, 129, 29-40.
- Archie, G.E., The electrical resistivity log as an aid in determining some reservoir characteristics. *Trans. Am. Inst. Min. Metall. Pet. Eng.* 146, 54-62, 1942.
- Argand, E., La tectonique de l' Asie, *Proc. 13th Int. Geol. Congr.*, 170-372 , 1924.
- Armijo, R., P. Tapponnier, J.L. Mercier and T.L. Han, Quaternary extension in southern Tibet; field observations and tectonic implications, *J. Geophys. Res.*, 91, 13,803-13,872, 1986.
- Als Dorf, D. and K.D. Nelson, Tibetan satellite magnetic low: Evidence for widespread melt in the Tibetan crust? *Geology*, 27, 943-946, 1999.
- Bahr, K., Interpretation of the magnetotelluric impedance tensor: regional inductance and local telluric distortion, *J. Geophys.* , 62, 119-127, 1988
- Beghoul, N., M. Barazangi, B. Isack. Lithospheric structure of Tibet and western North America: mechanisms of uplift and a comparative study. *J. Geophys. Res.*, 98, 1997-2016, 1993
- Brasse, H., P. Lazaeta, V. Rath, K. Schwalenburg, W. Soyer and V. Haak, The Bolivian Altiplano Conductivity Anomaly, in press, *J. Geophys. Res.*, 2000.

- Brown, L.D., W. Zhao, K.D. Nelson, M. Hauck, D. Alsdorf, A. Ross, M. Cogan, M. Clark, X. Liu and J. Che, Bright spots, structure, and magmatism in southern Tibet from INDEPTH seismic reflection profiling, *Science*, 274, 1688-1690, 1996.
- Burnham C.W and N. F. Davis, The role of H₂O in silicate melts. I, P-V-T relations in the system NaAlSi₃O₈-H₂O to 10 kilobar and 1000C, *Am. J. Sci*, 270, 54-79, 1971.
- Burnham, C.W. Water and magmas: a mixing model, *Geochim. et Cosmochim. Acta.*, 39, 1077- 1084, 1975.
- Cagniard, L., Basic theory of the magnetotelluric method of geophysical prospecting, *Geophysics*, 18, 605-635, 1953
- Chang, C. and S. Zheng, Tectonic features on the Mount Jolmo Lungma region in southern Tibet, China. *Scientica Geologica Sinica*. 1, 1-12, 1973
- Chave, A.D and J.T. Smith, On electric and magnetic galvanic distortion tensor decompositions, *J. Geophys. Res.*, 99, 4669-4682, 1994.
- Chen, L., J.R. Booker, A.G.Jones, N. Wu, M.J. Unsworth, W. Wei, H.. Tan, Electrically conductive crust in southern Tibet from INDEPTH magnetotelluric surveying. *Science*, 274, 1694-1696, 1996.
- Chen, W. and P. Molnar, Focal depths of intracontinental and intraplate earthquakes and their implications for the thermal and mechanical properties of the lithosphere. *J. Geophys. Res.*, 88, 4183-4214, 1983.
- Chen W., Was the Himalayan-Tibetan Orogen built by a single mechanism? *AGU Fall Meeting 1999*. Vol.80, NO.46, F1008, 1999/SUPPLEMENT.

- Chen, W.P. and S. Ozalaybey. Correlation between seismic anisotropy and Bouguer Gravity anomalies in Tibet and its implications for lithospheric structures. *Geophys. J. Int.* 135, 93-101, 1998.
- Chouteau, M., Bouchard, K. Two-dimensional terrain correction in magnetotelluric Surveys, *GEOPHYSICS*, 53, 854-862, 1988.
- Clark, M.K., and L. Royden, Topographic ooze : Building the eastern margin of Tibet by lower crustal flow, *Geology*, 28, 703-706, 2000.
- DeGroot-Hedlin, C and Constable, S.C, Occam's inversion to generate smooth two-dimensional models from magnetotelluric data. *Geophysics*, 55, 1613-1624, 1990.
- Cooper, R.F. and D.L. Kohlstedt, Rheology and structure of Olivine-Basalt partial melts, *J. Geophys. Res.*, 89, 9315-9323, 1986.
- Debon, F., P. Le Fort, S.M.F. Sheppard and J. Sonet, The four plutonic belts of the Transhimalaya-Himalaya; a chemical, mineralogical, isotopic, and chronological synthesis along a Tibet- Nepal section. *J. Petrol.*, 27, 219-250, 1986.
- Dewey, J.F. and Burke, K.C., Tibetan, Variscan and Pre-Cambrian basement reactivation products of continental collision, *J. Geol.*, 81, 683-692, 1973.
- Dewey, J.F, R.M Shackelton, C. Chang and Y. Sun. The tectonic evolution of the Tibetan Plateau. *Phil. Trans. R. Soc. Lond. A*, 327, 379-413, 1988.
- Echternacht, F., Tauber, S. Eisel, M., Brasse, H. Schwarz, G., Haak, V., 1997. Electromagnetic study of the active continental margin in northern Chile, *Phys. Earth Planet. Inter.* 102, 69-87.

- England, P.C. and A.B. Thompson, Pressure-temperature-time paths of regional metamorphism of continental crust, I, Heat transfer during the evolution of regions of thickened continental crust, *J. Petrol.*, 25, 894-928, 1984
- Etheridge, M.A. , V.J. Wall, and S.F. Cox, High fluid pressure during regional metamorphism and deformation: implications for mass transport and deformation mechanisms. *J. Geophys. Res.*, 89, 4344-4358, 1984.
- Evans, R.L., Tarits, P., Chave, A.D., White, A., Heinson, G. , Filloux, J.H., Toh, H., Seama, N., Utada, H. Booker, J.R., Unsworth, M.J. 1999. Asymmetric Electrical Structure in the Mantle Beneath the East Pacific Rise at 17 degree S, *Science*, 286, 752-756.
- Fielding, E. B. Isacks, M. Barazangi, C. Duncan, How flat is Tibet? *Geology*, 22, 163-167, 1994.
- Fox, R.C., Hohmann, G.W., Killpack, T.J., Rijo, L., 1980. Topographic effect in resistivity and induced-polarization surveys, *GEOPHYSICS*, 45, 75-93.
- Francheteau, J.,C. Jaupart, X.J. Shen, W.H. Kang, D.L. Lee, J.C. Bai, H..P. Wei, and H.Y. Deng, High heat flow in southern Tibet, *Nature*, 307, 32-36, 1984.
- Frost, B.R. Fyfe, W.S., Tazaki, K. and Chan, T., Grain-boundary graphite in rocks and implications for high electrical conductivity in the lower crust, *Nature*, 340, 134-136, 1989.

- Guilbert, J., G. Poupinet, M. Jiang. A study of azimuthal P residuals and shear-wave splitting across the Kunlun range (Northern Tibetan Plateau). *Phys. Earth Planet. Inter.* 95, 167-174, 1996.
- Guillot, S., P. Le Fort A. Pecher, M. R. Barman, and J. Aprahamian, Contact metamorphism and depth of emplacement of the Manaslu granite [central Nepal]. Implication for Himalayan orogenesis. *Tectonophysics*, 241, 99-119, 1995.
- Gamble, T.D, W.M. Goubau, and J. Clark, Magnetotellurics with a remote reference, *Geophysics*, 44, 53-68, 1979
- Groom, R.W and R.C Bailey. Decomposition of magnetotellurics impedance tensors in the presence of local three-dimensional galvanic distortions. *J. Geophys. Res.*, 94, 1913-1925, 1989.
- Groom, R.W and R.C Bailey. Analytic investigations of the effect of near-surface three-dimensional galvanic scatters on MT tensor decomposition..*GEOPHYSICS.*, 56, 496-518, 1991.
- Guo, X., Y. Zhang, Q. Cheng, R. Gao, Y. Pan, Magnetotelluric studies along Yadong-Golmud geosciences transect in QiangHai-Xizang plateau (in Chinese), *Bulletin of the Chinese Academy of Geological Sciences*, 21, 191-202, 1989.
- Hacker, B., E. Gnos, L. Ratschbacher, M. Grove, M. McWilliams, S. V. Sobolev, W. Jiang, Z. Wu. Hot and dry deep crustal xenoliths from Tibet. *Science*, 287, 2463-2466, 2000.

- Harrison, T.M., P. Copeland, W.S.F. Kidd, A. Yin, Raising Tibet. *Science*, 255, 1663-1670, 1992
- Harrison, T.M., P. Copeland, W.S.F. Kidd and O.M. Lovera, Activation of the Nyainqentanghla Shear Zone: implications for the uplift of the southern Tibetan Plateau. *Tectonics*, 14, 658-676, 1995.
- Hashin, Z., and S. Shtrikman, A variational approach to the theory of effective magnetic permeability of multiphase materials, *J. Appl. Phys.*, 33, 3125-3131, 1962.
- Hennig, A., Zur petrography und Geologie von Sudwest Tibet. In *Southern Tibet, Kung Boktrykeriet*, P.A. Stockholm, Norstedt, Vol 5, 220p, 1915
- Henry, P., X. Le Pichon, and B. Goffe, Kinematic, thermal and petrological model of the Himalayas: constraints related to metamorphism within the underthrust Indian crust and topographic elevation, *Tectonophysics*, 273, 31-56, 1997.
- Hirn, A., J. Lepine, G. Jobert, M. Sapin, G. Wittlinger, Z., Xu, E. Gao, X., Wang, J., Teng, S. Xiong, M.R. Pandey, J.M. Tater, Crustal structure and variability of the Himalayan border of Tibet, *Nature*, 307, 23-25, 1984
- Hirn, A., M. Jiang, M. Sapin, J. Diaz, A. Nercessian, Q.T. Lu, J.C. Lepine, D.N. Shi, M. Sachpazi, M. R. Pandey, K. Ma and J. Gallart. Seismic anisotropy as an indicator of mantle flow beneath the Himalayas and Tibet. *Nature*, 375, 571-574, 1995.
- Hirn, A., M. Sapin, J.C. Lepine, J. Diaz and M. Jiang. Increase in melt fraction along a south-north traverse below the Tibetan Plateau: evidence from seismology. *Tectonophysics*, 273, 17-30, 1997

- Hochstein, M.P. and K. Regenauer-Lieb, Heat generation associated with collision of two plates the Himalayan geothermal belt, *J. Volc Geothermal Res.*, 83, 75-92,1998
- Holcombe, H.T/, 1982, Terrain effects in resistivity and magnetotelluric surveys. Ph.D. dissertation, University of New Mexico.
- Holness, M.B. Contrasting rock permeability in the aureole of the Ballchulish igneous complex, Scottish Highlands: the influence of surface energy, *Contrib Mineral. Petrol.*, 131, 68-94,1998.
- Hoke, L., S. Lamb, D. R. Hilton, R. J. Poreda. Southern limit of mantle-derived Geothermal helium emissions in Tibet: implications for lithospheric structure. *Earth Planet. Sci. Lett.*, 180, 297-308, 2000.
- Holt, W.E. and T.C. Wallace, Crustal thickness and upper mantle velocities in the Tibetan Plateau region from the inversion of regional Pnl waveforms: Evidence for a thick upper mantle lid beneath southern Tibet, *J. Geophys. Res.*, 95, 12,499-12,525,1990.
- Holt, W.E. Correlated crust and mantle strain fields in Tibet. *Geology*, 28, 67-70, 2000.
- Huang, W., J. Ni, F. Tilmann, D. Nelson, J. Guo, W. Zhao, J. Mechie, R. Kind, J. Saul, R.Rapine, T. Hearn. Seismic polarization anisotropy beneath the central Tibetan Plateau. *J. Geophys. Res.*, 105, 27979-27989, 2000.
- Hyndman, R.D. and P.M. Shearer. Water in the lower continental crust: modeling

- magnetotelluric and seismic reflection results. *Geophys. J. Int.*, 98, 343-356, 1989.
- Jahns, R.H. Internal evolution of pegmatite bodies. In *Short course in granitic pegmatites in science and industry*, Edited by P.Cerny, pp 293-327. Mineralogical Association of Canada, Winnipeg, 1982.
- Jin, Y., M.K. McNutt and Y. Zhu, Evidence from gravity and topography data for folding of Tibet. *Nature*, 371, 669-674, 1994.
- Jin, Y., M.K. McNutt and Y. Zhu, Mapping the descent of Indian and Eurasian plates beneath the Tibetan Plateau from gravity anomalies. *J. Geophys. Res.* 101, 11,275-11,290, 1996.
- Jiracek, G.R., Redding, R.P., and Kojima, R.K., 1986, Application of the Rayleigh-FFT technique to magnetotelluric modeling and correction: Presented at the 8th IAGA Workshop on Electromagnetic Induction in the Earth and the Moon.
- Jones, A.G. Parkinson's pointers' potential perfidy!. *Geophys. J. R. astr. Soc.*, 87, 1215-1224, 1986.
- Jones, A.G. Static shift of magnetotelluric data and its removal in a sedimentary basin environment. *Geophysics*, 53, 967-978, 1988.
- Jones, A.G., Chave, A.D., Auld, D., Bahr, K. and Egbert, G. A Comparison of Techniques for Magnetotelluric Response Function Estimation, *J. Geophys. Res.*, 94, 14,201-14,213, 1989.
- Jones, A.G. Electrical conductivity of the continental lower crust, In *Continental lower crust*, edited by D.M. Fountain, R.Arculus and R.W.Key, pp81-143, Elsevier,

Amsterdam, 1992.

Kapp, P., A. Yin, C. Manning, M. Murphy, T.M. Harrison, M. Spurlin, L. Ding, X.

Deng, C. Wu. Blueschist-bearing metamorphic core complexes in the Qiangtang block reveal deep crustal structure of northern Tibet. *Geology*, 28, 19-22, 2000.

Kind, R., J. Ni, W. Zhao, J. Wu, X. Yuan, L. Zhao, E. Sandvol, C. Reese, J. Nabelek and T. Hearn. Evidence from earthquake data for a partially molten crustal layer in southern Tibet. *Science*, 274, 1692-1694, 1996.

Kosarev, G., R. Kind, S.V. Sobolev, X. Yuan, W. Hanka, S. Oreshin. Seismic evidence for a detached Indian lithospheric mantle beneath Tibet. *Science*, 283, 1306-1309, 1999

Kurtz, R.D., DeLaurier, J.M., and Gupta, J.C., 1986, A magnetotelluric sounding across Vancouver Island detects the subducted Juan De Fuca Plate, *Nature*, 321, 596-599.

Le Fort, P., M.Cuney, C. Deniel, C. France-lanord, S.M.F. Sheppard, B.N. Upreti and P.Vidal, Crustal generation of the Himalayan leucogranites, *Tectonophysics*, 134, 39-57, 1987.

Lebedev E.B, N.I Khitarov, Dependence on the beginning of melting of granite and the electrical conductivity of its melt on high water vapor pressure, *Geochem.Int.*, 1, 193-197, 1964.

- Li, S., M.J. Unsworth, J.R. Booker, H. Tan, W. Wei and A.G. Alan. Partial melt or aqueous fluids in the mid-crust of southern Tibet? Constraints from INDEPTH magnetotelluric data. *J. Geophys. Res.*, submitted, 2001
- Littledale, St. G.R., A journey across Tibet, from north to south, and west to Ladak. *Geogr. J.*, 7, 453-483, 1896.
- Macdonald, J.D., *Impedance spectroscopy: Emphasizing solid materials and systems*. John Wiley and Sons. New York, 1987.
- Mackie, R.L. and Madden, T.R. Three-dimensional magnetotelluric inversion using conjugate gradients, *Geophys. J. Int.*, 115, 215-229, 1993.
- Makovsky, Y. , S.L. Klemperer, L. Ratschbacher, L.D. Brown, M. Li, W. Zhao, F. Meng. INDEPTH Wide-angle reflection observation of P-wave-to-S-wave conversion from crustal bright spots in Tibet. *Science*, 274, 1690-1691, 1996.
- Makovsky, Y. and S.L. Klemperer, Measuring the seismic properties of Tibetan bright spots: free aqueous fluid in the Tibetan middle crust, *J. Geophys. Res.* 104, 10,795-10,825,1999.
- Maxwell, J.C. *A Treatise on electricity and magnetism*. 2nd ed. Clarendon, Oxford, England, 1881.
- McNamara, D.E., T.J. Owens, P.G. Silver, F.T Wu. Shear wave anisotropy beneath the Tibetan Plateau. *J. Geophys. Res.*, 99, 13,655-13,665, 1994.
- McNamara, D.E., T.J. Owens, and W.R. Walter. Observation of regional phase propagation across the Tibetan Plateau. *J. Geophys. Res.*, 100, 22,215 – 22,229,

1995

- McNamara, D.E., W.R. Walter, T.J. Owens, and C.J. Ammon. Upper mantle velocity structure beneath the Tibetan Plateau from Pn travel time tomography. *J. Geophys. Res.*, 102, 493-505, 1997.
- McNeice, G .W., A. G. Jones, Multi-site, multi-frequency tensor decomposition of magnetotelluric data. *Geophysics*, 66, 2001 [in press] .
- Mibe, K., T. Fujii and A. Yasuda. Connectivity of aqueous fluid in the Earth's upper mantle. *Geophys. Res. Lett.*, 25, 1233-1236, 1998.
- Minarik, W.G. and E.B. Watson. Interconnectivity of carbonate melt at low melt fraction. *Earth Planet. Sci. Lett.*, 133, 423-437, 1995.
- Molnar, P., A review of geophysical constraints on the deep structure of the Tibetan Plateau, the Himalaya and Karakoram, and their tectonic implications, *Trans. R. Soc. London.*, Ser A, 327, 33-88, 1988
- Molnar, P., P. England, and J. Martinod, Mantle dynamics, the uplift of the Tibetan plateau, and the Indian monsoon, *Rev. geophys.*, 31, 375-396, 1993
- Murase, T. and A.R. McBirney, Properties of some common igneous rocks and their melts at high temperature, *Geol. Soc. Am., Bull.*, 84 [11], 3563-3592, 1973.
- Murphy, M.A. A. Yin, T.M. Harrison, S.B. Durr, Z. Chen, F.J. Ryerson. W.S. F. Kidd, X. Wang, X. Zhou. Did indo-Asian collision alone create the Tibetan Plateau? *Geology*, 25, 719-722, 1997
- Navin, D.A., C. Peirce, M.C. Sinha. The RAMESSES experiment; II, Evidence for

- accumulated melt beneath a slow spreading ridge from wide-angle refraction and multichannel reflection seismic profiles. *Geophys. J. Int.*, 135, 746-772. 1998
- Nelson, K.D. and the Project INDEPTH Team. Melt in the Tibetan Crust: Where are we now? *AGU Fall Meeting 1999*. Vol.80, NO.46, F991-F992, 1999/SUPPLEMENT.
- Ngoc, P.V., 1980, Magnetotelluric survey of the Mount Meager region of the Squamish Valley (British Columbia), Geomagnetic Service of Canada, Earth Physics Branch of the Dept. of Energy, Mines and Resources Canada, OF Rep. 80-8-E .
- Ni, J., and M. Barazangi, High frequency seismic wave propagation beneath the Indian shield, Himalayan arc, Tibetan Plateau and surrounding regions: High uppermost mantle velocities and efficient propagation beneath Tibet. *Geophys. J. R. Astron. Soc.*, 72, 665-689, 1983.
- Nong, W. High resolution electromagnetic images of conductivity structure in the mid-lower crust and upper mantle. Ph.D dissertation, University of Washington, 1994.
- Norin E., Geological reconnaissance in western Tibet, Reports from the scientific expedition to the northwestern provinces of China under the leadership of Dr. Sven Hedin. Publication 29, part 3, *Geology 7*, Tryckeri Aktiebolaget, Thule, Stockholm, 1946
- Nover, G., Heikamp, S., Meurer, H.J. and D. Freund. In-situ electrical conductivity and permeability of mid-crustal rocks from the KTB drilling: consequences for high conductive layers in the Earth crust. *Surv. Geophys.*, 19, 73-85, 1998.
- Olhoeft, G. Electrical properties of granite with implications for the lower crust. *J.*

- Geophys. Res.*, 86, 931-936 1981.
- Owens, T.J. G. Zandt, Implications of crustal property variations for models of Tibetan plateau evolution, *Nature*, 387, 37-43, 1997.
- Pan, Y and W.S.F Kidd, Nyainqentanglha shear zone: A late Miocene extensional detachment in the southern Tibetan Plateau, *Geology*, 20, 775-778, 1992.
- Parker, R. L. The inverse problem of electromagnetic induction: Existence and construction of solution based upon incomplete data. *J. Geophys Res.*, 85, 4421-4428, 1980.
- Parkinson, W.D. Direction of rapid geomagnetic fluctuations. *Geophys. J. R. astr. Soc.*, 2, 1-14, 1959.
- Partzsch, G.M., F.R. Schilling and J. Arndt. The influence of partial melting on the electrical behavior of crustal rocks: laboratory examinations, model calculations and geological interpretations. *Tectonophys.*, 317, 189-203, 2000.
- Pham, V. N., D. Boyer, P. Therme, C. Yue, L., Li Y. Guo. Partial melting zones in the crust in southern Tibet from magnetotelluric results. *Nature*, 307, 310-314, 1984
- Pous, J., Munoz, J.A, Ledo, J.J., Liesa, M., Partial melting of subducted continental lower crust in the Pyrenees. *J. Geol. Soc. London* 152, 217-220, 1995
- Quist, A.S., and W.L. Marshall, Electrical conductances of aqueous sodium chloride solution from 0 to 800° at pressure to 4000 bars, *J. Phys. Chem.*, 72, 684-703, 1968.
- Redding, R.P., and Jeracek, G.B., 1984, Topographic modeling and correction in

- magnetotellurics, Presented at the 54th Ann. Internat. Mtg., Soc. Explor. Geophys., Expanded Abstracts, 44-47.
- Renner, J., B. Evans, G. Hirth, On the rheologically critical melt fraction. *Earth Planet. Sci. Lett.* 181, 585-594, 2000.
- Roberts, J.J., and J. A. Tyburczy. Partial-melt electrical conductivity: Influence of melt composition. *J. Geophys. Res.*, 104, 7055-7065, 1999.
- Rodi W and R. Mackie. Nonlinear conjugate gradient algorithm for 2-D magnetotelluric inversion. *GEOPHYSICS*, 66, 174-178, 2001
- Ross A.R., L.D. Brown, D. Alsdorf and K.D.Nelson. Deep seismic bright spots and Magmatism in southern Tibet. *J. Geophys. Res.*, 2001 [in press].
- Royden, L.H., B.C. Burchfiel, R.W. King, E. Wang, Z. Chen, F. Shen and Y. Liu, Surface deformation and lower crustal flow in eastern Tibet, *Science*, 276, 788-790, 1997
- Sandoval, E. J. Ni, R. Kind, W. Zhao. Seismic anisotropy beneath the southern Himalayas-Tibet collision zone. *J. Geophys. Res.*, 102, 17,813 –17,823,1997.
- Scaillet, B., A. Pecher, P. Rochette and M. Champenois, The Gangotri Granite [Garhwal Himalaya]; laccolithic emplacement in an extending collisional belt, *J. Geophys. Res.*, 100, 585- 607, 1995.
- Schilling, F.R., G.M. Partzsch, H. Brasse and G. Schwarz. Partial melting below the magmatic arc in the central Andes deduced from geoelectromagnetic field experiments and laboratory data. *Phys. Earth Planet. Inter.*, 103, 17-31,1997.

- Schmeling, H., Numerical models on the influence of partial melt on elastic, anelastic and electrical properties of rocks. Part I: Elasticity and anelasticity. *Phys. Earth Planet. Inter.*, 41: 105-110, 1985.
- Schmeling, H., Numerical models on the influence of partial melt on elastic, anelastic and electrical properties of rocks. Part II: Electrical conductivity. *Phys. Earth Planet. Inter.*, 43: 123-136, 1986.
- Schwartz, G., Haak, V., Martinez, E. and Bannister, J., 1984, the electrical conductivity of the Andean crust in northern Chile and southern Bolivia as inferred from magnetotelluric measurements, *J. Geophys.*, 55, 169-178.
- Sengor, A.M.C, The evolution of palaeo-tethys in the Tibetan segment of the Alpides. *Geological and Ecological studies of the Qinghai-Xizang Plateau*. Vol. 1, 51-56, Science Press, Beijing, 1981.
- Shankland, T.J., R.J. O'Connell, H.S. Waff. Geophysical constraints of partial melt in the upper mantle. *Reviews of Geophysics and Space Physics*. Vol. 19. 394-406, 1981.
- Smith, J.T., 1988, Rapid inversion of multi-dimensional magnetotelluric data, Ph.D dissertation, University of Washington, Seattle.
- Smith, J.T. and Booker, J.R., 1988, Magnetotelluric inversion for minimum structure, *GEOPHYSICS*, 53, 1565-1576.
- Smith, J.T. and J.R. Booker, Rapid inversion of two- and three-dimensional magnetotelluric data, *J. Geophys. Res.*, 96, 3905-3922, 1991

- Smith, J.T. Understanding telluric distortion matrices. *Geophys. J. Int.*, 122, 219-226, 1995
- Sourirajan, S., and G.C. Kennedy, the system H₂O-NaCl at elevated temperature and pressures, *Am. J. Sci*, 260, 115-141, 1962.
- Tapponnier P., J.L. Mercier, F. Proust, J. Andrieux, R. Armijo, J.P. Bassoullet, M. Brunel, J.P. Burg, M. Colchen, B. Dupre, J. Girardeau, J. Marcoux, G. Mascle, P. Matte, A. Nicolas, T. Li, X. Xiao, C. Chang, P. Lin, G. Li, N., Wang, G. Chen, T. Han, X. Wang, W. Den, H. Zhen, H. Sheng, Y. Cao, J. Zhou, H. Qiu, The Tibetan side of the India-Eurasia collision, *Nature*, 294, 405-410, 1981.
- Tapponnier, P., G. Peltzer, A. Le Dain, R. Armijo and P. Cobbold, Propagating extrusion tectonics of Asia, New insights from simple experiments with plasticine, *Geology*, 10, 611-616, 1982.
- Tikhonov, A.N., Determination of the electrical characteristics of the deep state of the earth's crust. *Dok. Akad. Nauk. USSR*, 73, 295-297, 1950.
- Tullis, J., R. Yund and J. Farver, Deformation-enhanced fluid distribution in feldspar aggregates and implications for ductile shear zones, *Geology*, 24, 63-66, 1996.
- Turner, S., C. Hawksworth, J. Liu, N. Rogers, S. Kelley, P. van Calsteren. Timing of the Tibetan uplift constrained by analysis of volcanic rocks. *Nature*, 364, 50-54, 1993
- Tyburczy, J.A and H.S. Waff, Electrical conductivity of molten basalt and andesite to 25 kbar pressure: Geophysical significance and implications for charge transport and melt structure. *J. Geophys. Res.*, 88, 2413-2430, 1983.

- Ucok, H. The temperature dependence of electrical resistivity of aqueous salt solutions and solution saturated rocks, Ph.D. thesis, University of Southern California. Los Angeles, 1979.
- Waff, H.S and D.F. Weill, Electrical conductivity of magmatic liquids: Effects of temperature, oxygen fugacity and composition, *Earth Planet. Sci. Lett.*, 28, 254-260, 1975.
- Wannamaker, P.E., Stodt, J.A., Rijo, L., 1986, Rapid inversion of two- and three-dimensional magnetotelluric data, *J. Geophys. Res.*, , 96, 3905-3922.
- Wannamaker, P.E. Electrical conductivity of water-undersaturated crustal melting. *J. Geophys. Res.* 91, 6321-6327, 1986
- Wannamaker, P.E., Hohmann, G.W., and S.H. Ward, Magnetotelluric responses of three-dimensional bodies in layered earths, *Geophysics*, 49, 1517-1534, 1984
- Wannamaker, P.E., J.M. Johnston, J.A. Stodt, and J.R. Booker. Anatomy of the southern, Cordilleran hingeline, Utah and Nevada, from deep electrical resistivity profiling. *Geophysics*, 62, 1069-1086, 1997
- Watanabe, T., Effect of water and melt on seismic velocities and their application to characterization of seismic reflectors. *Geophys. Res. Lett.* 20, 2933-2936, 1993.
- Watanabe, T., and K. Kurita, The relationship between electrical conductivity and melt fraction in a partially molten simple system: Archie's law behavior. *Phys. Earth Planet. Inter.*, 78, 9-17, 1993.

- Watanabe, T. and K. Kurita, Simultaneous measurements of the compressional-wave velocity and the electrical conductivity in a partially molten material. *J. Phys. Earth.*, 42: 69-87, 1994.
- Watson, E.B and Brenan, J.M., Fluids in the lithosphere, 1. Experimentally-determined wetting characteristics of CO₂-H₂O fluids and their implications for fluids transport, host-rock physical properties and fluids inclusion formation. *Earth planet. Sci. Lett.*, 85, 497-515, 1987.
- Wei, W, M, Unsworth, A. Jones, J. Booker, H. Tan, D. Nelson, L. Chen, S. Li, K. Solon, P. Bedrosian, S. Jin, M. Deng, J. Ledo, D. Kay and B. Roberts, Detection of Widespread Fluids in the Tibetan Crust by Magnetotelluric Studies. *Science*, 292, 716-718, 2001.
- Weidelt, P., Construction of conductance bounds from magnetotelluric impedances. *J. Geophys.*, 57, 191-206, 1985.
- Willett, S.D, and C. Beaumont, Subduction of Asian lithospheric mantle beneath Tibet inferred from models of continental collision, *Nature*, 369, 642-645, 1994.
- Word, S.H., 1967, Electromagnetic theory for geophysical application, in *Mining geophysics, II: Soc. Explor. Geophys.*, 13-196.
- Zandt, G., and C.J. Ammon, Continental crust composition constrained by measurement of crustal Poisson's ratio. *Nature*, 374, 152-154, 1995.

- Zhao, W.L. and W.J.P. Morgan, Injection of Indian crust into Tibetan lower crust; a two-dimensional finite element model study, *Tectonics*, 6, 489-504, 1987.
- Zhao, W., K.D., Nelson, Project INDEPTH. Deep seismic reflection evidence for continental underthrusting beneath southern Tibet, *Nature*, 366, 557-559, 1993.
- Zhao, W., J. Mechie, L.D. Brown, J. Guo, S. Haines, T. Hearn, S.L. Klemperer, Y. S. Ma, R. Meissner, K.D. Nelson, J. F. Ni, P. Pananont, R. Papine, A. Ross, J. Saul. Crustal structure of central Tibet as derived from project INDEPTH wide-angle seismic data. *Geophys. J. Int.*, 145, 486-498, 2001.
- Zhdanov, M.S. and G.V. Keller, *The Geoelectrical Methods in Geophysical Exploration*, Amsterdam, 1994.
- Zhu, L. and D.V. Helmberger, Intermediate depth earthquakes beneath the India-Tibet collision zone. *Geophys. Res. Lett.*, 23, 454-438, 1996

Vita

Shenghui Li

Born: Hebei Province, P.R. China, Sept. 18th, 1968.

Education:

09/1995-06/2001: Ph.D., Geophysics, University of Washington, Seattle.

09/1992-06/1995: M.Sc., Applied Geophysics, China University of Geosciences, Beijing, China.

09/1986-06/1990: B.A., Applied Geophysics, Changchun College of Geology, Changchun, China.

Publications:

Wei, W, M, Unsworth, A. Jones, J. Booker, H. Tan, D. Nelson, L. Chen, S. Li, K. Solon, P. Bedrosian, S. Jin, M. Deng, J. Ledo, D. Kay and B. Roberts, Detection of Widespread Fluids in the Tibetan Crust by Magnetotelluric Studies. *Science*, 292, 716-718, 2001.

Li, S., M.J. Unsworth, J.R. Booker, H. Tan, W. Wei and A.G. Alan. Partial melt or aqueous fluids in the mid-crust of southern Tibet? Constraints from INDEPTH magnetotelluric data. In preparation for *J. Geophys. Res.*, 2001

Li, S., M.J. Unsworth, P. Bedrosian, J.R. Booker, H. Tan, W. Wei and A.G. Alan. The resistivity structure in central Tibet and their geological implications. In preparation for *J. Geophys. Res.*, 2001

Li, J., W. Wei, B. Chen, S., Li. The quantitative interpretation of fixed point source sounding methods. *Geophysical and Geochemical Exploration*. 21, 3, p187-197, 1997 . Geological Press, Beijing, China. (in Chinese).

Abstracts and Presentations:

Li, S., C. Aprea and J.R. Booker. Inversion of MT data in the presence of bathymetry and topography. Poster, *American Geophysical Union Fall meeting*, San Francisco, 1998.

Li, S., M.J. Unsworth, J.R. Booker, W. Wei, H. Tan and A.G. Jones. Is the electrically conductive Tibetan crust due to partial melt or aqueous fluids? Presentation. *American Geophysical Union Fall meeting*, San Francisco, 1999.